المملكة العربية السعودية
وزارة التعليم العالي
جامعة أم القرى
كلية العلوم التطبيقية
قسم الفيزياء

مطياف العزل الكهربي للبلورات السائلة القطبية

رسالة مقدمة إلى قسم الفيزياء بكلية العلوم التطبيقية بجامعة أم القرى
كمتطلب تكميلي لبرنامج درجة الماجستير في الفيزياء

إعداد الطالبة
جازي بنت عبد الله عبد الواحد

إشراف
د. فتحي بن مصباح جودة

الفصل الدراسي الثاني

١٤٢٤ هـ/٢٠٠٣ م

بسم الله الرحمن الرحيم

وزارة التعليم العالي
جامعة أم القرى
كلية العلوم التطبيقية

نموذج رقم (٨)

إجازة أطروحة علمية في صيغتها النهائية بعد إجراء التعديلات

الاسم (رباعي) : جازي عبدالله محمد عبد الواحد كلية : العلوم التطبيقية قسم : الفيزياء ....
الأطروحة مقدمة لنيل درجة : الماجستير .... في تخصص : فيزياء الجوامد ....
عنوان الأطروحة : ((مطيافية العزل الكهربي للبلورات السائلة القطبية ....

الحمد لله رب العالمين والصلاة والسلام على أشرف الأنبياء والمرسلين وعلى آله وصحبه أجمعين وبعد :

فبناءً على توصية اللجنة المكونة لمناقشة الأطروحة المذكورة أعلاه والتي تمت مناقشتها بتاريخ / / ١٤هـ بقبولها بعد إجراء التعديلات المطلوبة، وحيث قد تم عمل اللازم ؛ فإن اللجنة توصي بإجازتها في صيغتها النهائية المرفقة للدرجة العلمية المذكورة أعلاه ...

والله الموفق ...

أعضاء اللجنة

المشرف	المناقش الداخلي	المناقش الخارجي
الاسم : د/ يحيى رضيمان الجهني	الاسم : د/ صبري أحمد أبو منصور	الاسم : د/ جمال الجارحي
التوقيع : [signature]	التوقيع : [signature]	التوقيع : [signature]

يعتمد

رئيس قسم الفيزياء

الاسم : د/ فائز بن حماد المرزبي

التوقيع : [signature] ٢/٥/١٤٢٤هـ

- يوضع هذا النموذج أمام الصفحة المقابلة لصفحة عنوان الأطروحة في كل نسخة من الرسالة .

شكر وتقدير

الحمـــد لله عـــدد خلقـــه ومداد كلماته حمداً يليق بجلال وجهه وعظيم سلطانه، أحمده ســـبحانه وتعالى أن وفقني على إتمام هذا البحث، والصلاة والسلام على سيدنا محمد النبي الأمي وعلى آله وصحبه وسلم.

يســـرني أن أتقدم بجزيل الشكر والعرفان لسعادة الدكتور فتحي جودة لإشرافه على هذه الرسالة والذي عرفني بعلم البلورات السائلة و تشجيعه المتواصل خلال فترة البحث.

ويســـرني أن أشـــكر كل من سعادة الدكتور فائز غريبي وسعادة الدكتور وليد ألطف على تعاونهما المتواصل ودعمهما لي خلال فترة رئاستهما للقسم. وإلى سعادة الدكـــتور عصـــام الأهدل وكيل الكلية للدراسات العليا جزيل الامتنان على تذليل كل الصعوبات الإدارية المتعلقة ببرنامج الماجستير.

وإذ نسيت فلا أنسى وكيلة قسم الفيزياء – في مقر الطالبات – الأستاذة فاطمة جان على عطائها وتقديم يد العون في كل وقت وإلي جميع أعضاء القسم بالمقر.

وأتقـــدم بالشكر الخاص للمهندس الشيخ هاشم على كل المساعدات الفنية التي قدمها وعمله المتواصل لإتمام البحث.

وإلـــى والـــدي و والدتـــي وزوجـــي أتقدم بجزيل الشكر والعرفان على حثهم وتشـــجيعهم ووقوفهم إلى جانبي وتحملهم المتاعب والمشاق المتوالية والسفر الطويل لكي أتمكن من إنجاز هذا البحث. لهم مني كل الشكر والامتنان.

وآخر دعوانا أن الحمد لله رب العالمين.

إهداء

إلى من أضاء لي شمعة في طريق العارفين

إلى من أشار عليَّ برأي في شعب الحائرين

إلى من همس إليّ بهمسة نصح في دروب السالكين

أهدي ثمار بحث سطر بأنفاس السنين

عنوان الرسالة:

مطياف العزل الكهربي للبلورات السائلة القطبية

ملخص البحث:

تـــم فـــي هذا البحث دراسة السماحية الكهربية بجزئيها الحقيقي والتخيلي في مـــنطقة الـــترددات من 10 Hz إلى 10 MHz عند درجات حرارة مختلفة في أطوار أربعـــة وهـــي الطور موحد الخواص (isotropic phase) والسميكتك أ* (smecticA) والسميكتك ج* (smectic C*) و الـــطور البلوري (crystal phase).

يتمـــيز طيف العزل الكهربي للطور السائل موحد الخواص بمنحنى إمتصاص يقـــع فـــي مـــنطقة MHz مـــن الطـــيف. ويعزى هذا لحركة الجزيء حول محوره العرضـــي. ورغم وجود منحنى إمتصاص آخر (عند ترددات إسترخاء أعلى من 10 MHz) للحركة الجزيئية حول المحور الطولي للجزئ إلا أننا لم نتمكن من قياس هذه الحركة الجزيئية لمحدودية جهاز مطياف الإمتصاص لمدى لا يتجاوز MHz 10. أما فـــي الطور البلوري فقد وُجِدَ أن هاتين الحركتين متوقفتين تماماً الأمر الذي يتأكد من خلال عدم وجود فرق يذكر بين قيمة السماحية الكهربية ومربع معامل الإنكسار.

مـــن دراستنا لديناميكية الجزيئات في طوري البلورات السائلة*smectic A و smectic C* وُجِدَت أنماط حركية ذات طبيعة جماعية و أخرى غير جماعية. لدراسة الحـــركة الجزيئـــية غير الجماعية، فقد تم إجراء هذه القياسات في إتجاهين مختلفين وذلك عندما يكون المجال الكهربي موازي وعمودي على المتجه ***n***. في الحالة الأولى إستخلصـــنا معلومات عن الحركة الدورانية للجزيء ككل حول محوره العرضي. أما في الحالة الثانية فقد درسنا من خلالها الحركة الدورانية للجزئ حول محوره الطولي. وهاتـــان الحركتان الدورانيتان وجد أن منحنيات إمتصاص العزل الكهربي $\varepsilon''(f)$ لها تقعـــان فـــي منطقة تتمحور حول 100 kHz و 10 MHz على التوالي. وقد لوحظ أن ترددات هاتين الحركتين تتغير مع درجة الحرارة حسب قانون أرهينيوس Arrhenius

والـــذي حســـبنا من خلاله طاقة التنشيط activation energy لكل حركة. ومن تحديد قـــيمة معلـــم التوزيع distribution parameter α إستنتجنا أن الجزيء يتحرك حول محـــوره العرضـــي كما لو كان جسم جامد بلا مرونة بينما تبين أن الحركة الجزيئية حول المحور الطولي تتميز بمرونة في الحركة الجزيئية.

وفـــيما يـــتلق بالحركة الجماعية للجزيئات، في طور سميكتك A قمنا بدراسة تراوح الجزيئات الجماعي للزاوية θ وتسمى تراوحات θ (θ - fluctuations). وتتميز هـــذه الحـــركة بأن تردد استرخائها relaxation frequency يقل كلما إقتربنا من الأنتقال الطوري من smectic A* إلى smectic C* ، ويصاحب هذا إزدياد مضطرد للسماحية الكهربية. وإجتماع هاتان الخاصيتان في حركة يُعرف بالنموذج المرن soft mode . وأصـــل هذه التسمية soft mode ناشئ من أن معامل المرونة الذي يتحكم فـــي هـــذه التراوحات ويعمل على إتزان الطور وثباته (أي يعمل على أن تكون $\hat{n}$ موازيـــة للمـــتجه $\hat{k}$) تقل قيمته كلما إقتربنا من T_c وعندما تقل قيمة k_θ تفقد المادة ثباتها وتصبح "مرنة" ضد تراوحات θ.

أمـــا فـــي طـــور سميكتك smectic C* ، فبالإضافة إلى تراوحات θ ، توجد تـــراوحات φ- φ-fluctuations وهـــذه مرتـــبطة بتراوحات المتجة $\hat{n}$ حول المحور اللولبي (أو بمعنى أوضح هي حركة جماعية متعلقة بالتركيب اللولبي لطور السميكتك C*) وهذه التراوحات تسمى كذلك بنموذج جولدستون نسبة للعالم J. Goldstone.

وفي القسم الأخير من البحث تم دراسة تأثير المجال الكهربي المتحيز bias field علـــى soft mode و Goldstone mode . وتبيـــن مـــن الدراســـة أن المجال الكهربي المتحيز يؤثر على خواص العزل الكهربي في منطقة قريبة من T_C . أما في الـــ smectic C* وجـــد أن المجال المتحيز يؤثر على Goldstone mode ويقلل من مســـاهمته للسماحية الكهربية إلى أن تخفي بالكامل مما يسهل قياس السماحية الهربية الناشئة من الـــ soft mode .

وبدراســـة مســـاهمة كل من هذه التراوحات للعزل الكهربي ومعرفة تردداتها تمكنـــنا مـــن خلال نماذج رياضية من حساب معامل اللزوجة لتراوحات θ (γ_θ) و لـــتراوحات φ (γ_φ). وهذه القيم تلعب دوراً أساسياً ومهماً التطبيقات التكنولوجية لهذه المواد.

Kingdom of Saudi Arabia
Ministry of Higher Education
Umm Al-Qura University

DIELECTRIC SPECTROSCOPY OF POLAR LIQUID CRYSTALS

By
Jazi Abdullah Abdul-Wahid

Supervised by
Associate Prof. Fathi M. Gouda

A thesis submitted in the Partial fulfilment of the requirements for the degree of Master of Science (Physics)

Physics Department, Faculty of Applied Science
Umm Al-Qura University
Holy Makkah, Saudi Arabia
1424 AH-2003 G

CONTENTS

ABSTRACT

Dielectric relaxation measurements have been carried out in the frequency range 10 Hz to 10 MHz in different phases of a liquid crystalline material. The real and imaginary parts of the complex dielectric permittivity have been investigated in the planar and homeotropic measurement geometries. In the planar orientation, the dielectric spectrum of the isotropic, the smectic A*, smectic C* and the crystalline phases have been studied in details. The isotropic phase exhibits an absorption peak related to the molecular reorientation around the long axis of molecule. The dielectric spectrum of the smectic A* and C* is characterised by two distinct peaks attributed to the collective director tilt fluctuations (the soft mode) and the phase fluctuation (the Goldstone mode). In the homeotropic orientation, the measurements have been made in the smectic A* and smectic C* phases, and the dielectric spectra exhibit an absorption peak connected with the molecular reorientation around the short axis. An extensive effort has been devoted to study the effect of bias electric field in the planar orientation. It is found that the bias field has a strong influence on the dielectric spectra in the smectic A* and smectic C* phases. In the isotropic, smectic A* and C* phases, the observed absorption peaks of collective and non-collective aspects have been analysed using single and multiple Cole-Cole functions. The molecular aspects of these

dielectric absorptions have been discussed. The temperature dependence of the dielectric contribution and relaxation frequency has been discussed in terms of the extended Landau free energy expansion. The model enables us to determine the rotational viscosity of the soft mode and the Goldstone mode in the smectic A* and C* phases, respectively.

ACKNOWLEDGMENTS

I would like to acknowledge my supervisor Dr. Fathi Gouda for introducing me to the subject of this research and for his invaluable guidance throughout the course of this work.

The help and encouragement of the head of physics department Dr. Faiez Khuraiby is highly appreciated. I would like to express my gratitude to Dr. Waleed Altaf for his support and advice. I also appreciate the help of Dr. Essam Alahdal for providing all necessary information about the Master's program. The technical assistance of Sheikh Hashem is greatly acknowledged.

I owe a lot to the members of the girls Physics department. Special thanks are due to the deputy head of the Physics department, Mrs Fatma Jan for her continuous help to solve all administrative problems.

Without the continuous support and encouragement of my parents and husband, it would not have been possible to finish this work. I feel deeply grateful for their love and care throughout my study

I would like to thank the director of the King Abdulaziz City for Science and Technology for the financial support of this work.

CHAPTER 1

INTRODUCTION

With their unusual electro-optic properties, liquid crystals technology has a major effect, not only on many areas of science and engineering, but in every day life as well. Therefore, words like "Liquid Crystals" and Liquid Crystal Displays (LCDs) became very popular. In the present chapter, a brief description of different states of matter and liquid crystal phases will be presented. An emphasis on the chiral liquid crystalline materials will be given. The relation between chirality and polar liquid crystal phases will be discussed. A motivation of investigating the paraelectric and ferroelectric liquid crystals will be given and its potential applications will be explained.

1.1 STATES OF MATTER

The degree of order in the material is directly related to the surrounding temperature and pressure which plays important role in forming the phases of matter where we will have four states instead of three states of matter that is solid, liquid crystals, liquid and gas. At low temperatures, when the material is in its solid state, the constituents (atoms, ions or molecules) cannot move about freely. Their

only movements are thermal vibrations about an equilibrium position (see figure 1.1a).

If the temperature is raised, more energy is put into the system, leading to stronger and stronger vibrations. Finally, at the transition temperature between the solid and liquid states, the *long range positional order* is broken and the constituents may move about in a random fashion (figure 1b), constantly bumping into one another and abruptly changing direction of motion. The thermal energy is still not, however, high enough to completely overcome the attractive forces between the constituents, so there is still some positional order at *short range*. Because of the remaining cohesion, the density of the liquid is constant even though, as opposed to the solid, the liquid takes the shape of its container. The liquid and solid phases are called *condensed* phases.

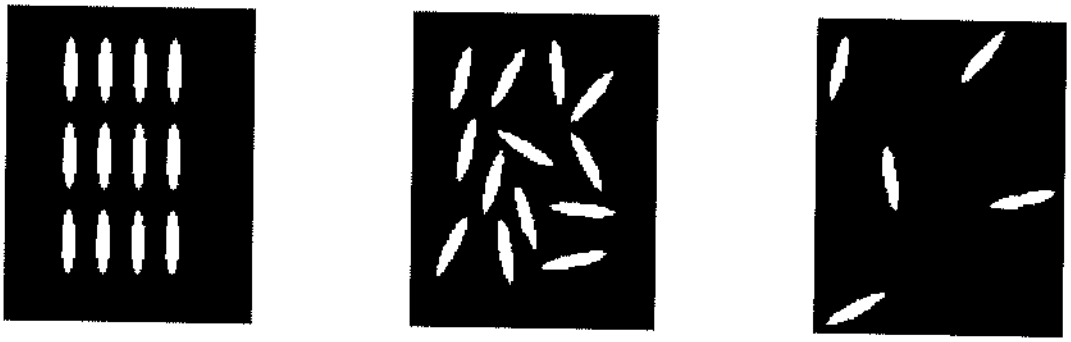

(a) (b) (c)

Figure 1.1 An illustration of the difference in positional order between the solid, liquid and vapour phases. The effect of thermal fluctuations is neglected in the sketch of the solid state. The blue colour is just a picture background.

If we keep on raising the temperature until the next phase change, the substance enters its gaseous (or vapour) state and its constituents are no longer bound to each other (figure 1c).

1.2 *LIQUID CRYSTALLINE PHASES*

(The Nematic and Smectic Phases)

Certain organic substances possess more condensed phases than the basic two [1-4]. They are referred to as liquid crystals and their constituent molecules are often called mesogens [4]. Their different extra phases, found between the solid and liquid states, are called liquid crystalline phases or sometimes mesophases [4]. The explanation to these intermediate phases lies in the fact that liquid crystal molecules have always anisotropic shape, normally having a more or less rod like shape. In the above description of the solid, liquid and vapour phases, we only took the degree of positional order into account. Because of the anisotropic shape of the liquid crystal molecules we must now also consider the orientational order in the material.

1.2.1 The Nematic Phase

By decreasing the temperature from the isotropic phase, in which the molecules are randomly positioned and oriented (see figure 1.2a), the nematic phase denoted by (N) is observed as shown in figure 1.2a. The name comes from the Greek word for thread, since in a polarizing microscope, there are often many dark lines visible in thick film samples. The orientational order in the liquid crystal phases is of course not perfect. In fact, if we were to take a snapshot of a liquid crystalline sample we would find quite large differences in orientation of different molecules (see figure 2.a). There is, however, locally a distinct *preferred* direction around which the molecules fluctuate. This average molecule orientation is described by a unit vector called the *director*, denoted by $\boldsymbol{n}$ [1-4]. It is a rather special vector as its sign is generally of no importance; $\boldsymbol{n} = -\boldsymbol{n}$. This reflects the fact that turning the director 180° is a symmetry operation, which conserves all physical properties of the liquid crystal.

Liquid crystalline mesophases are fluids which, due to partial orientational ordering of the constituent molecules, have material properties such as permittivity, refractive index, elasticity and viscosity which are anisotropic (i.e. their magnitude will *differ from one direction to another*).

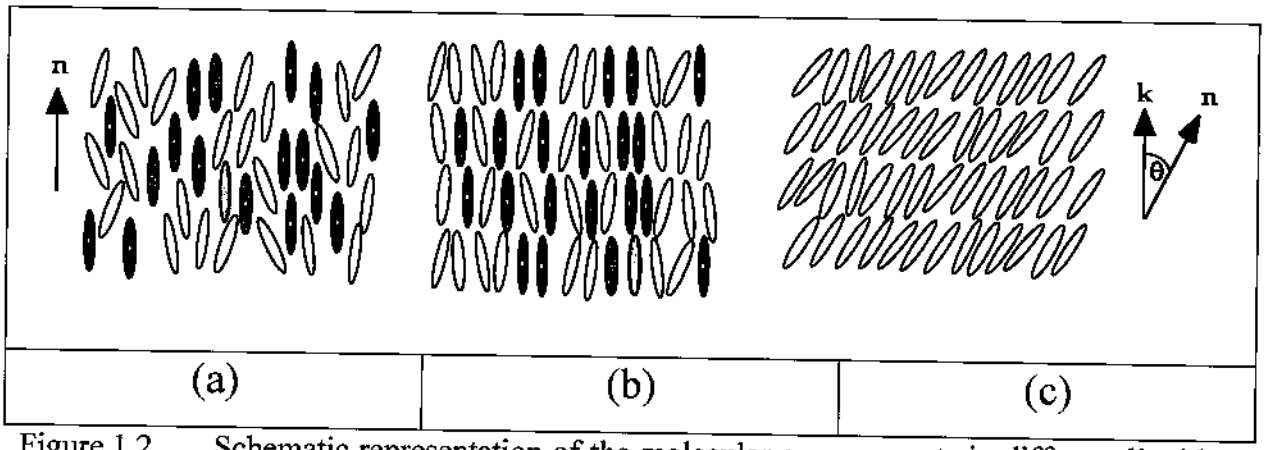

Figure 1.2 Schematic representation of the molecular arrangements in different liquid crystalline phases. The direction of net orientation is represented by a unit vector denoted ***n***. The unit vector of the layer normal in the smectic phases is denoted ***k***.

The high-degree of disorder of the phase structure means that the nematic is very fluid and thus the particles within the sample are seen to undergo intense Brownian motion.

The fluid nematic phase has a low viscosity and nematic materials can be designed so that molecular orientation can be switched by an electric field, in this fluid the molecules prefer to orient along ***n(r)***. Thus the material is anisotropic. Another important variable in nematic liquid crystals is the order parameter, which measures how well the molecules are aligned with the director. The usual measure of this order is S where ,

$$S = \frac{1}{2}\left\langle 3\cos^2\theta - 1 \right\rangle \qquad (1.1)$$

Where $\langle\ \rangle$ denotes thermal averaging and θ is the angle between each molecule and the director. If the molecules are very well aligned with the director then $S = 1$ and if the molecules are ran-

domly oriented about $\boldsymbol{n}$ i.e. isotropic; the $S = 0$. So, the higher the order parameter the more ordered the nematic liquid crystal.

1.2.2 The Smectic Phases

At certain temperatures, generally below the nematic phase, the liquid crystal material may gain an amount of positional order. When this happens the liquid crystal forms into smectic phase where the molecules, although still forming a fluid, prefer to lie on average in layers (figure 1.2(b) and 1.2(c)). Within each layer the liquid crystal is essentially a two dimensional nematic liquid crystal. This positional ordering may be described in terms of the density of the centres of mass of the molecules, thus, the basic smectic order parameter is then [2]

$$\psi = \left\langle \cos \frac{2\pi z}{d} \right\rangle \qquad (1.2)$$

where z is the coordinate parallel to the layer normal, d is the distance between layers and Ψ is the order parameter. When $|\Psi| = 0$ there is no layering and the material is nematic but if $|\Psi| > 0$ then some amount of sinusoidal layering exists and the material is smectic.

There are many types of smectic materials and figure 2 show two examples. When the nematic-like director $\boldsymbol{n}$ in each layer is

parallel to the layer normal $\boldsymbol{k}$ the material is smectic A (SmA). As shown in figure 1.2(b). If this director *tilts* away (by an angle $\boldsymbol{\theta}$) from the layer normal the smectic C (SmC) phase is formed as illustrated in figure 2(c). To fully understand the SmC order parameter it is important to introduce the azimuthal (or phase) angle φ. It can conveniently be written in complex form [3]

$$\psi = \theta e^{i\varphi} \qquad (1.3)$$

An alternative way of expressing the tilt direction is to define a unit vector along the projection of n onto the layer plane (as introduced by deGennes [3]) who called it the *C*-director, abbreviated ***c***.

There also exists higher order smectics, which form layers with positional ordering *within the layers*. For instance in smectic *B* materials the molecules in each layer for a hexagonal structure

1.3 THE CHIRAL SMECTIC PHASES

A chiral object is one which is not superposable on its mirror image, a typical example is the human hand [5]. Thus, chirality is a synonym of lacks of mirror symmetry. It is not always obvious if an object lack the mirror symmetry or not. In daily life, most people probably experience the mistake putting a wrong-handed glove on

the first hand to cover. This is due to that we do not examine thoroughly if it was left-handed or right-handed. Indeed, it is impossible to bring the gloves to coincide with each other and the lack of mirror symmetry is clear.

Some liquid crystal molecules lack mirror symmetry [4]. These molecules can exist in both left-handed and right handed forms. The left-handed molecule is a mirror image of the right - handed molecule and vice versa. Such molecules are called chiral and are sometimes marked with a star (*). A liquid crystalline phase consisting of chiral molecules is called a chiral. For instance chiral nematic phase will be designated N* and chiral smectic A and chiral smectic C will be designated A* and C*, respectively. The present work is mainly focussed on the SmA* and SmC* phases.

1.3.1 The Chiral Smectic A Phase

In the A* phase, the director, as in the A phase, is always parallel to the smectic layer normal. The star in A* designate that the medium lacks mirror symmetry. Superficially, one could be tempted to think that the chiral and non-chiral smectic A (A* and A) would be very similar or even having the same symmetry, just because they both are orthogonal smectics with the same molecular arrangement in the layers and with the same cylindrical symmetry around the layer normal. This is completely wrong due to the fact that the two phases (A* and A) have different symmetry [6]. Reflection is not a sym-

metry operation in the A* phase. However, the A phase has this symmetry operation.

One of the important consequences of chirality in the A* phase is the *tilt* that can be *induced* in the medium by the application of an electric filed (figure 1.3) in the direction perpendicular to the molecules. The tilt is around an axis which has the direction of the electric field going into the plane of the paper. This is known as the electroclinic effect, presented in 1977 by Garoff and Meyer [7]. It is also appropriately called the *soft mode* effect, because the tilt deformation is a soft mode in the A phase, the restoring torque of which softens when we approach the A to C transition where the deformation starts to ''freeze in`` to a spontaneous tilt (see figure 1.3(a). Soft mode fluctuations occur in the A phase just as in the A* phase, but only in the A* phase we can excite the tilt by an electric field. This is because a tilt fluctuation in the medium with chiral symmetry is coupled to a local polarization fluctuation resulting from the transverse dipoles being ever so slightly lined up when the tilt disturbs the cylindrical symmetry of the molecular rotation around the long molecular axis. The study of soft mode dielectric behaviour is one of the central points in the present thesis.

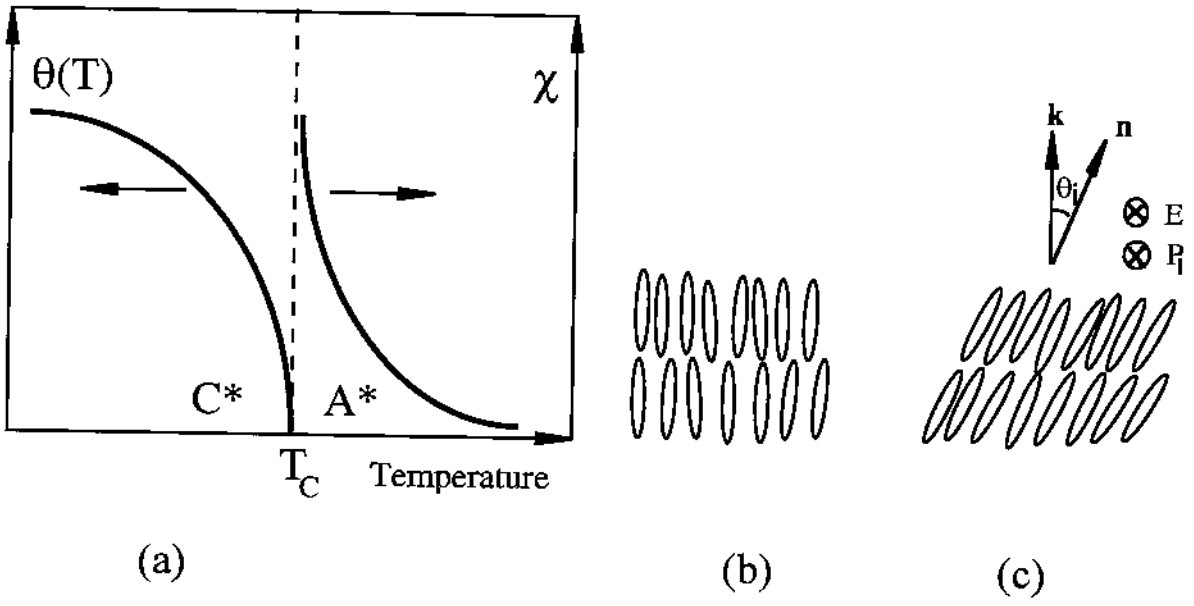

Figure 1.3 (a) In the chiral smectic A, a finite tilt can be induced by an applied electric field. At constant temperature above the smectic A* to C* transition temperature T_C, the induced tilt is proportional to the field $\theta_{ind} \sim E$. The tilt susceptibility χ ($\chi = \partial\theta/\partial E$) shows a divergence-like behaviour on approaching the transition. The C* phase is characterized by a spontaneous tilt that varies with temperature and equal to zero at T_C.(b) A smectic A* phase in the absence of any external electric field. (c) A smectic A* in the presence of applied electric field resulting in an induced tilt angle θ_{ind} between the layer normal and the director.

1.3.2 The Chiral Smectic C Phase

(Ferroelectricity in Liquid Crystals)

The smectic C phase built-up of chiral molecules is called a chiral smectic C and designated C*. It was the Harvard physicist R. B. Meyer [8] who first recognised that the symmetry properties of a chiral titled smectic would allow a spontaneous polarization directed perpendicular to the tilt plane. In order to understand this symmetry argument proposed by Meyer, let us start with a non-chiral C phase.

The C phase has a monoclinic symmetry and belongs to the point group C_{2h}: it has a mirror plane and a two fold axis perpendicular to it. The mirror plane is given by the smectic layer normal $\boldsymbol{k}$ and the smectic $\boldsymbol{c}$ director, i.e. the tilt plane. If the constituent molecules are chiral, then the chirality will break the mirror symmetry and we are left with only one symmetry axis C_2.

Keeping in mind that in all liquid crystal phases, the molecules possess a molecular rotation around both short and long axes. If we consider the molecular rotation around the long axis, due to the tilt, this rotation may become biased in time, i.e. the transverse dipole moment spends longer time in some directions than others. Now, if we have non-chiral molecules, the number of dipoles pointing inward and outward the mirror plane must be the same. In the chiral case they must not, thus a net polarization is allowed by symmetry. The argument is at least valid for one smectic layer. However, it turns out that the chirality, as in the cholesteric phase, generates in the smectic C* phase a helical structure, figure 1.4, which make the macroscopic polarization zero. In this case, the director $\boldsymbol{n}$ precesses from one layer to another, resulting in a helical structure with the helix axis parallel to $\boldsymbol{k}$. The precession of $\boldsymbol{n}$ is associated with a turn in the P_S direction (for each smectic layer) which after a full turn leads to cancellation of the bulk spontaneous polarization. In this context, as shown in figure 1.4, the pitch p in the C* phase can be defined as the shortest length in the C* phase (in a direction parallel to the helix axis) where the system has no net

spontaneous polarization. The helical pitch of smectic C* materials is found in the μm range. Applying an external electric field along the layers will unwind the helix, thus creating a macroscopically polarized medium. Another way of achieving a uniform polarization is to unwind the helix by surface actions from boundaries in the liquid crystal cell. This is the basis for the Surface Stabilized Ferroelectric Liquid Crystal (SSFLC)-principle invented by Clark and Lagerwall in 1980 [9].

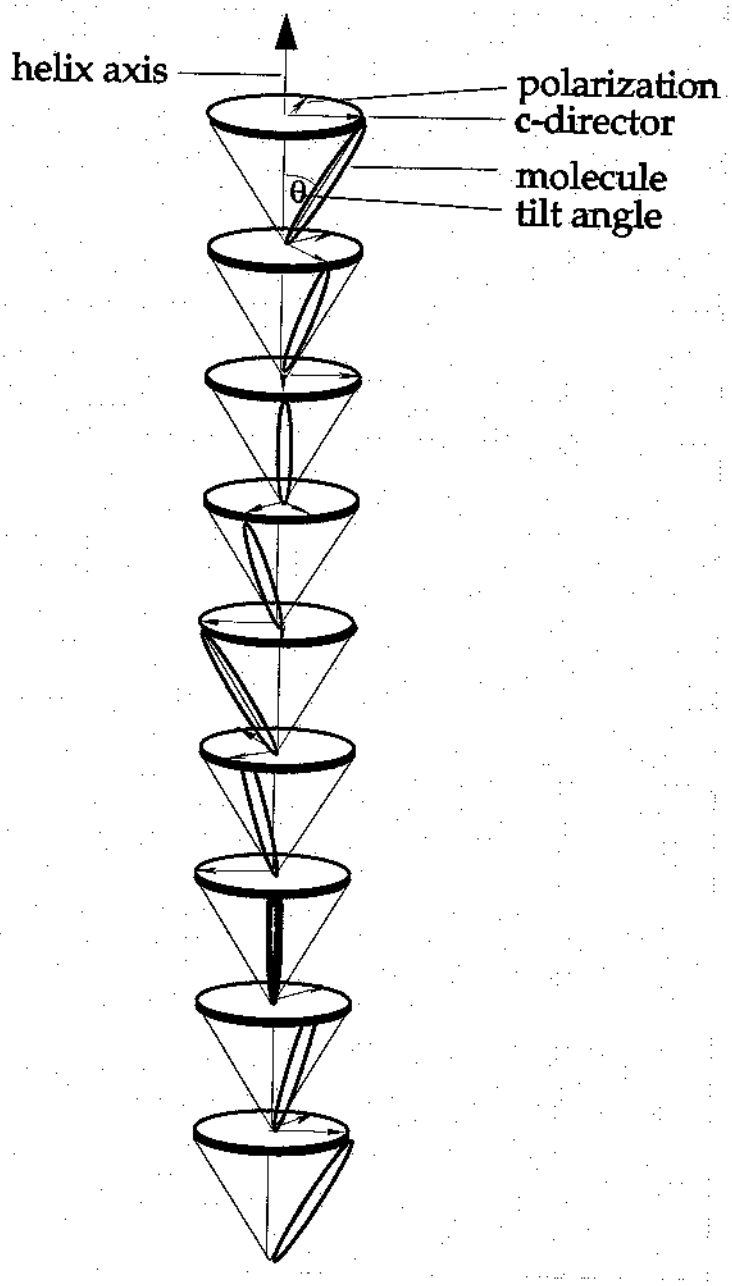

Figure 1.4 Schematic representation of the helical smectic C* phase in which the director (and its projection **c** on the smectic plane) spiral along the helix axis, resulting in cancellation of the polarization P_S and a reduction of the bulk polarization to zero. The figure shows one full turn of P_S and ***c***.

1.4 POLAR LIQUID CRYSTALLINE PHASES

The subject of this thesis is focused on *polar* liquid crystal materials, it is thus of importance to explain, in general, what is meant by polar materials with emphasis on polar liquid crystals.

A molecule that has an electric dipole moment in the absence of an external electric field is called a *polar molecule*. The dipole moment is measured in a unit known as Debye (D). In the SI system, $1\ D = 3.3\text{x}10^{-30}$ Cm. As examples of polar molecules CO, NH_3 and H_2O. All liquid crystalline materials consist of polar molecules. Such molecules tend to orient itself in an electric field. On macroscopic scale, the distribution of these dipoles are governed by a Boltzmann factor $e^{-U/kT}$ where $U = -\mu \cdot \boldsymbol{E}$ is the potential energy of the dipole in an electric field. By comparing the value U and thermal energy kT it is found that $kT >> U$ which means that the thermal fluctuations, over macroscopic scale, strongly counteract the orientational effect of the field. In the absence of an external field, these dipoles averaged out to zero macroscopic polarization. Thus, although we call, for example, water a *polar liquid*, it does *not* mean that it posseses a *macroscopic polarity*.

The vast majority of liquid crystalline molecules are polar. The dipole moment μ, in general, makes an angle with the long molecular axis. Thus, it has parallel μ_l and perpendicular μ_t components (the subscripts l and t stand for longitudinal and transverse, re-

spectively). In the nematic phase, the local order (described by the director $\boldsymbol{n}$) is characterised by axial symmetry. This means that $\boldsymbol{n}$ and $-\boldsymbol{n}$ describe the same state , thus all physical properties are invariant under the sign reversal of $\boldsymbol{n}$, i.e. $\boldsymbol{n} \rightarrow -\boldsymbol{n}$, symmetry operation. This invariance is equivalent to the absence of macroscopic polarity. This means that μ_l for two adjacent molecules favours antiparallel order. Thus, the nematic phase, on *macroscopic* scale, is a *non-polar* phase, and thus, it can not possess ferroelectric properties along the director. If there will be any macroscopic polar effects it would be examined in the direction perpendicular to $\boldsymbol{n}$. However, since the nematic phase has a continuous rotational symmetry D_∞ with a mirror plane along $\boldsymbol{n}$ direction it, thus, excludes the possibility of any macroscopic polar ordering in the direction perpendicular to $\boldsymbol{n}$. The same argument holds for the smectic A phase which is characterised by a cylindrical symmetry. However, if the smectic A is build up of *chiral* molecules, the chirality removes the *mirror plane* but the director $\boldsymbol{n}$ still obeys the $\boldsymbol{n} \rightarrow -\boldsymbol{n}$ condition. In this case, smectic A* phase can not possess any macroscopic polar order along $\boldsymbol{n}$. As in the nematic phase, the smectic A (and SmA*) phase has the same point group symmetry D_∞ , however, the translational symmetry is spontaneously broken at the nematic to SmA transition. Therefore, in order to get any macroscopic polar effects, we have to, further, diminish the symmetry of the phase. The smectic C phase has a lower symmetry than the smectic A and nematic phases. We will not discuss the existence of any macroscopic polarity along $\boldsymbol{n}$

direction since $\boldsymbol{n}$ and $-\boldsymbol{n}$ are equivalent. Contrary to the nematic and the SmA (and SmA*) phases, the SmC, due to the tilt, does not possess a cylindrical symmetry. Moreover, the molecular rotation around the long axis is *biased*. This means that μ_t on average favours a certain direction compared with others. Non-chiral SmC possess a mirror symmetry leaving the system with no polar axis. However, if the molecules in the SmC phase are chiral, then the mirror plan is removed and there will be a net macroscopic polar order over one smectic layer. Thus, the SmC* phase is the first anisotropic liquid with macroscopic polar order.

1.5 MOTIVATION FOR STUDYING FERROELECTRIC LIQUID CRYSTALS

Ferroelectric liquid crystals in its SSFLC structure has binary properties and the switching from one state to the other takes place with a speed which is typically 10^3 times more rapid than in twisted nematic *TN* and super twisted nematic liquid crystal displays STN-*LCDs*. It opens a wealth of applications in fast electro-optic switching devices: all kinds of electrically controlled devices working in binary modes, like modulators, spatial light modulators, optical computing elements and displays.

Ferroelectric liquid crystals are a recent development which, as LC, are completely in a class by themselves. With no comparison they have the highest potential among other liquid crystals as electro-optic media, whether intended for switching devices, optical modulators, large area displays, electro-optic memories or non-linear optical devices for second harmonic generation. Ferroelectric liquid crystals have giant second harmonic coefficients, making them the preferred for non-linear optics applications. These properties are just on the verge of being recognized, and a huge development can be foreseen in this important field.

From the stand point of condensed matter physics, the structure change from one state to another is taking place by the excitation of a *Goldstone mode* around the smectic layer normal. In 1988, the Chalmers liquid crystal group [10] went further to exploit the *soft mode* excitation in the chiral smectic A* phase adjacent to the smectic C* phase. The smectic A* phase is in fact a paraelectric phase. The electro-optic effect connected with the soft mode fluctuations is a linear effect with no bistability (memory) but is about 100 times more rapid than the ferroelectric smectic C* phase. It is one of the central points in the present work to study the dielectric properties of *Goldstone mode* and *soft mode* in the smectic C* and smectic A*. This enables us, as will be shown in the present work to extract a very important information about the viscosity properties of these systems. This study plays an important role in the men-

tioned technological applications of the paraelectric and ferroelectric liquid crystals.

CHAPTER 2

DIELECTRIC PROPERTIES OF LIQUID CRYSTALS

2.1 THE STATIC DIELECTRIC PERMITTIVITY

Liquid crystals are dielectrics and for low electric fields the induced polarization per unit volume $\boldsymbol{P}$ is proportional to the applied electric field $\boldsymbol{E}$ [11].

$$P = \varepsilon_0 \chi E \tag{2.1}$$

where χ is the dielectric susceptibility and ε_0 the dielectric permittivity of free space. For an isotropic dielectric, the electric displacement $\boldsymbol{D}$ is:

$$D = \varepsilon_0 D + P = \varepsilon_0 (\chi + 1) E = \varepsilon_0 \varepsilon E \tag{2.2}$$

where the constant ε is the relative dielectric permittivity, or dielectric constant.

There are two types of polarization induced by the applied electric field, both of which contribute to the dielectric permittivity. Firstly, the field induces a polarization (P_∞) through the relative displacement of the electronic and atomic densities, which is represented by the molecular polarizability α. The contribution from these displacements is small and usually ignored. Polar materials, i.e. e. materials in which we have local dipole moments bound to the molecules, also include an orientation polarization (P_D) in the case that the molecules have some degree of rotational freedom. This is due to the tendency of the molecular dipole moments to align with the field. Thus, we may reshape (2.1) into

$$\varepsilon_{st} - 1 = \frac{P}{\varepsilon_0 E} \tag{2.3}$$

or

$$\varepsilon_{st} - 1 = \frac{P_\infty + P_D}{\varepsilon_0 E} \tag{2.4}$$

explicitly expressing the polarizability and dipolar contributions to the permittivity. Here the subscripts ∞ and D represent the electronic and the dipolar part of the total dielectric polarization, respectively, and the subscripted *st* indicates that the frequencies considered is effectively zero (static fields). The infmity sign reflects the fact that electronic reorientation usually occurs at very high, or

optical, frequencies, whereas the dipolar contribution is restricted to relatively low frequencies.

If we consider the medium to be isotropic and without polar order in the field-free case, both constituent parts of the total dielectric polarization $\boldsymbol{P}_\infty$ and $\boldsymbol{P}_D$ can be written in terms of the molecular parameters

$$\begin{aligned} P_\infty &= N\alpha E_i \\ P_D &= N\langle\mu\rangle = N\mu\langle\cos\theta\rangle \end{aligned} \tag{2.5}$$

where N is the number of the particles per unit volume, α is the electronic polarizability, $\langle\mu\rangle$ is the thermal average of the dipole moment and θ is the angle between the individual dipole and the field. $\boldsymbol{E}_i$ is the internal field which is not identical to the external, applied field $\boldsymbol{E}$. The dependence of $\langle\mu\rangle$ on $\boldsymbol{E}_i$ can be calculated from the Boltzmann probability distribution function $e^{-\frac{W}{kT}}$, where

$$W = -\vec{\mu}\,\vec{E}_i = -\mu E_i \cos\theta \tag{2.6}$$

is the energy of the dipole in the internal field. Integrated over the distribution of a sphere, this gives

$$\langle\cos\theta\rangle = \frac{\mu E_i}{3kT} \tag{2.7}$$

and hence

$$P_D = \frac{N\mu^2}{3kT} E_i \tag{2.8}$$

Combining equations (2.5) and (2.8)and inserting in (2.4) yields

$$(\varepsilon_{st} - 1)E = \frac{N}{\varepsilon_0}\left(\alpha + \frac{\mu^2}{3kT}\right) E_i \tag{2.9}$$

We note that if E_i were identical to E, then this would give (the incorrect)

$$\varepsilon_{st} - 1 = \frac{N}{\varepsilon_0}\left(\alpha + \frac{\mu^2}{3kT}\right) \tag{2.10))}$$

The correct relation requires knowledge of the relation of E_i to E. This relation, which was first derived by Lorentz [12] at the same time as he introduced the concept of internal field, is

$$\mathrm{E_i} = \frac{\varepsilon_{st} + 2}{3}\mathrm{E} \tag{2.11}$$

With this expression, the relation (2.9) instead takes the form

$$\frac{\varepsilon_{st} - 1}{\varepsilon_{st} + 2} = \frac{N}{3\varepsilon_0}\left(\alpha + \frac{\mu^2}{3kT}\right) \tag{2.12}$$

Which is the well-known Debye equation. Without the dipole part on the right side a similar equation

$$\frac{\varepsilon_{st}-1}{\varepsilon_{st}+2}=\frac{N}{3\varepsilon_0}\alpha \tag{2.13}$$

had been derived much earlier first by Mossotti in 1847 [12] and independently by Clausius [13] in 1879, but in a very different way and without any explicit notion of internal field.

The theory relating molecular properties and macroscopic permittivity for an isotropic liquid was revised in 1936 by Onsager [14] He was first to make a further distinction between the internal field E_i as an average field acting locally to result in a displacement, and field E_d, called directing field, exerting a torque on the dipoles, showing that these fields are not necessarily identical. Equation (2.9) than has to be replaced by

$$(\varepsilon_{st}-1)E=\frac{N}{\varepsilon_0}\left(\alpha E_i+\frac{\mu^2}{3kT}E_d\right) \tag{2.14}$$

With the parameters

$$h=\frac{3\varepsilon_{st}}{2\varepsilon_{st}+1}, \tag{2.15}$$

$$g=\frac{2N}{3\varepsilon_0}\left(\frac{\varepsilon_{st}-1}{2\varepsilon_{st}+1}\right) \tag{2.16}$$

and

$$F = \frac{1}{1 - \alpha g} \tag{2.17}$$

Onsager was able to express the relation between the fields as

$$E_i = hF\,E \tag{2.18}$$

and

$$E_d = hF^2\,E \tag{2.19}$$

Inserted in (2.14) this gives the basic expression

$$\varepsilon_{st} - 1 = \frac{N h F}{\varepsilon_0}\left(\alpha + \frac{F\mu^2}{3kT}\right) \tag{2.20}$$

Which is widely used today for isotropic media and which has to be further generalized for liquid crystals being anisotropic media, cf. section 2.3.

2.2 FREUQENCY DEPENDENCE OF THE DIELECTRIC PERMITTIVITY

2.2.1 Debye Relaxation Theory (single relaxation mechanism)

The dielectric permittivity coincide with the static one at sufficiently low frequencies, when the molecular dipoles are at equilibrium. Re-orientation of the dipoles generally takes a finite time in response to changes in the external electric field, and therefore the dielectric response is complicated by a phase lag between polarization and applied field. At high frequencies the polar contribution to the dielectric permittivity is unable to follow the electric field and the permittivity thus solely depends on the molecular polarizability,

$$\varepsilon_{\infty} - 1 = \frac{P_{\infty}}{\varepsilon_0 E}. \qquad (2.21)$$

According to the thermodynamics of irreversible processes we can assume that the polarization approaches the equilibrium value with a speed proportional to the distance from equilibrium. This process is then described by a differential equation of first order [15],

$$\tau \frac{dP(t)}{dt} = P_{st} - P(t) \qquad (2.22)$$

where τ is a characteristic time of the process. Several modes of polarization are normally excited in a dielectric, and one of these is the electronic polarization $\boldsymbol{P}_{\infty}$, which is responsible for the optical refraction. This polarization responds to a changing field with no time lag up to at least radio frequencies, and hence may be considered not to enter equation (2.22). Keeping in mind the equation (2.2) one can rewrite the (2.22) as follows

$$\tau \frac{dP_D(t)}{dt} + P_D(t) = (\varepsilon_{st} - \varepsilon_{\infty})\varepsilon_0 E(t) \qquad (2.23)$$

where the right hand side of the equation is the equilibrium value of $\boldsymbol{P}_D$ corresponding to $\boldsymbol{E}$(t).

The equation (2.23) is analogous to that for the charging of a capacitor in series with a resistor. The general solution is a complex exponential $E^*=E_0\exp(j\omega t)$. where ω is the angular frequency ($\omega = 2\pi f$). The solution thus may be expressed in the terms of the complex quantity $\boldsymbol{P}_D^*$ for the dipolar polarization

$$P_D^*(t) = \prod e^{-\frac{t}{\tau}} + \frac{\varepsilon_{st} - \varepsilon_{\infty}}{1 + i\omega\tau}\varepsilon_0 E_0 e^{j\omega t} \qquad (2.24)$$

where the constant Π characterizes the initial polarization. The first term of the expression (2.24) decays with time, and for alternating current measurements it can be neglected in comparison with the second term. Then one may define a dielectric constant

$$\varepsilon^*(\omega) - \varepsilon_\infty = \frac{P_D^*(\omega,t)}{\varepsilon_0 E^*(\omega,t)} \tag{2.25}$$

The asterisk denotes complex quantities. Inspection of equation (2.24) shows that for Π=0

$$\varepsilon^*(\omega) - \varepsilon_\infty = \frac{\varepsilon_{st} - \varepsilon_\infty}{1 + i\omega\tau} \tag{2.26}$$

where $\varepsilon^*(\omega)$ may be separated into its real and imaginary parts (see figure 2.1)

$$\varepsilon'(\omega) = \varepsilon_\infty + \frac{\varepsilon_{st} - \varepsilon_\infty}{1 + \omega^2\tau^2} \tag{2.27}$$

$$\varepsilon''(\omega) = \frac{(\varepsilon_{st} - \varepsilon_\infty)\omega\tau}{1 + \omega^2\tau^2}. \tag{2.28}$$

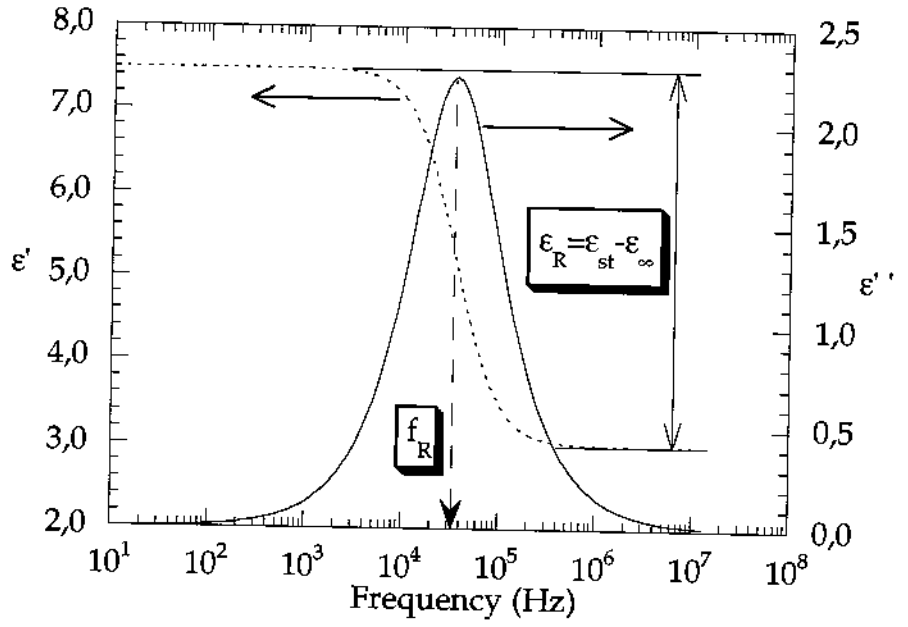

Figure 2.1 The frequency dependence of the real (left axis) ε' and imaginary (right axis) ε'' parts of the complex dielectric permittivity described by Debye relaxation.

The equations (2.27) and (2.28) are known as the Debye equations, since they were first derived by Debye [15] on a molecular basis to describe the orientation polarizability. The Debye theory was the first attempt to relate the relaxation time τ to molecular properties of the media. Note that the relaxation time is related to the relaxation frequency by the relation

$$\tau = \frac{1}{2\pi f_R} \tag{2.29}$$

Later it was extended to the nematic liquid crystals by Maier and Meier [16].

2.2.2 Other Types of Dielectric Relaxations (Cole-Cole relaxation)

Debye relaxation is the simplest type of relaxation and it is observed for the materials having a Boltzmann distribution of the dipoles. The frequency dependence of the real and imaginary parts of the dielectric permittivity is described by the Debye equations (2.27) and (2.28).

Many materials, particularly containing large or long organic molecules, show a broader dispersion curve and a lower maximum dielectric loss than would be expected from the Debye relationships, see figure 2.2. In such cases the ε''- ε' curve falls inside the Debye semicircle (see figure 2.3). One of the possible generalizations of the Debye formulas to account for such a behaviour was given by K. S. Cole and R. H. Cole in 1941.

$$\varepsilon^*(\omega) = \varepsilon_\infty + (\varepsilon_{st} - \varepsilon_\infty)\frac{1}{1+(i\omega\tau)^{1-\alpha}} \qquad (2.30)$$

Separation of the real and imaginary parts leads to expressions for $\varepsilon'(\omega)$ and $\varepsilon''(\omega)$ which are somewhat more complicated than the corresponding equations for a Debye relaxation (equations (2.27) and (2.28)).

$$\varepsilon'(\omega) = \varepsilon_\infty + (\varepsilon_{st} - \varepsilon_\infty)\frac{1 + (\omega\tau)^{1-\alpha}\sin\frac{1}{2}\alpha\pi}{1 + 2(\omega\tau)^{1-\alpha}\sin\frac{1}{2}\alpha\pi + (\omega\tau)^{2(1-\alpha)}} \qquad (2.31)$$

$$\varepsilon''(\omega) = (\varepsilon_{st} - \varepsilon_\infty)\frac{(\omega\tau)^{1-\alpha}\cos\frac{1}{2}\alpha\pi}{1 + 2(\omega\tau)^{1-\alpha}\sin\frac{1}{2}\alpha\pi + (\omega\tau)^{2(1-\alpha)}} \qquad (2.32)$$

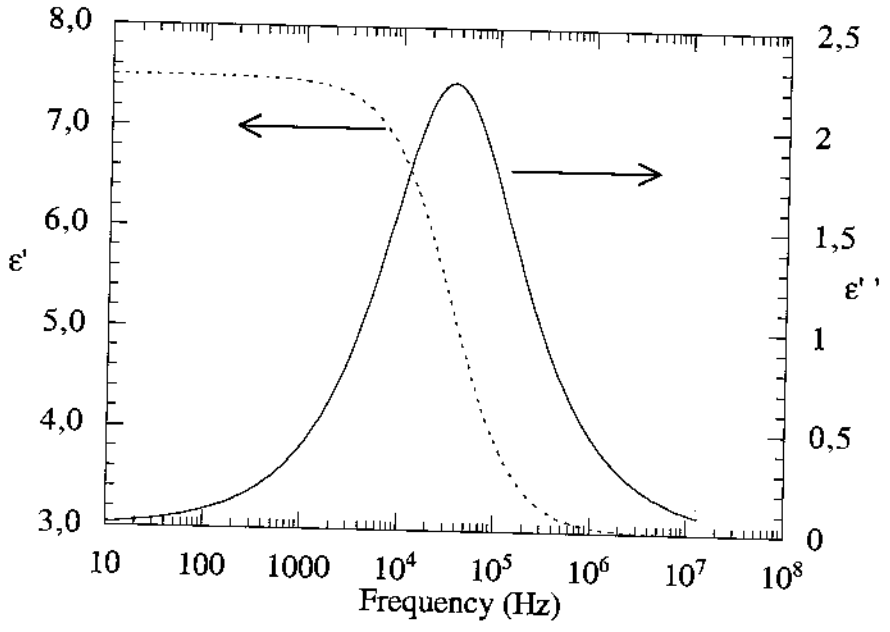

Figure 2.2 Frequency dependence of the real and imaginary parts of the permittivity corresponding to the Cole-Cole equation with a distribution parameter α=0.33.

The Cole-Cole relaxation can be visualized as a distribution of the Debye relaxations over a certain frequency domain. The distribution is *symmetric* around the angular frequency $\omega=1/\tau$. The distribution parameter α is a measure of the breadth of the distribution domain as contrasted with a single relaxation. The smaller the value of the parameter α, the smaller is the difference between the Cole-Cole relaxation and a pure Debye relaxation.

The broader peak of the Cole-Cole relaxation is represented as an arc with the larger part of the semicircle lying under the abscissa axis. The distance between the centre of the semicircle and the abscissa axis is determined by the distribution parameter α.

There are different models which describe other forms of relaxation processes for which the absorption is not symmetric. However, in the present work, it is found that all observed relaxation processes could be successfully described by either Debye or Cole-Cole equations.

2.3 DIELECTRIC PERMITTIVITY OF LIQUID CRYSTALS

In an anisotropic medium the scalar permittivity ε must be replaced by a tensor of rank two $\hat{\varepsilon}$, and $\boldsymbol{D}$ is usually not parallel to the direction of the electric field $\boldsymbol{E}$.

$$D = \varepsilon_0 \hat{\varepsilon} E \tag{2.33}$$

The dielectric permittivity of the undisturbed nematic liquid crystal as well as for undisturbed non-tilted smectic liquid crystal has two independent principal components.

$$\hat{\varepsilon} = \begin{pmatrix} \varepsilon_\perp & 0 & 0 \\ 0 & \varepsilon_\perp & 0 \\ 0 & 0 & \varepsilon_\parallel \end{pmatrix} \tag{2.34}$$

A component of the tensor parallel to the director $\boldsymbol{n}$ is denoted the by $\varepsilon_{\|}$ and component in a plane perpendicular to the director is denoted by $\varepsilon_{\perp}$ as depicted in figure 2.3.

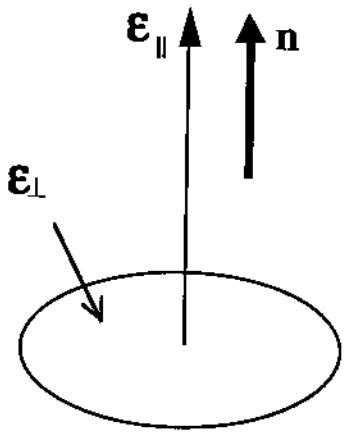

Figure 2.3. The definitions of the molecular axes and components of dielectric tensor in the uniaxial phases like nematic and smectic A phases.

Phases having that type of symmetry are called uniaxial. The dielectric anisotropy $\Delta\varepsilon$ for the uniaxial phase is defined as

$$\Delta\varepsilon = \varepsilon_{\|} - \varepsilon_{\perp} \tag{2.35}$$

Phases having a biaxial symmetry (biaxial phases) has three independent components of the dielectric permittivity tensor which will not be discussed in this work.

Usually, the average dielectric permittivity for a uniaxial phase is defined as

$$\bar{\varepsilon} = \frac{\varepsilon_{\parallel} + 2\varepsilon_{\perp}}{3} \tag{2.36}$$

The theoretical treatment describing the dielectric properties of the uniaxial nematic liquid crystal was first given by Maier and Meier [17] who reformulated the Onsager treatment for the isotropic liquid. They introduced the molecular anisotropy together with the nematic order parameter S described by equation (1.1).

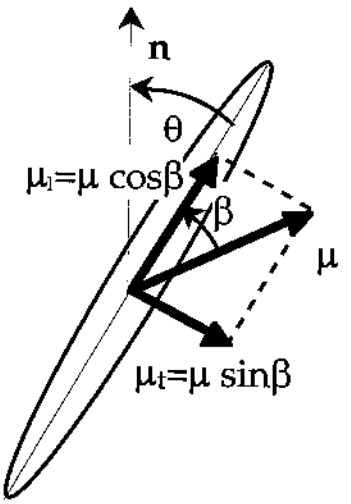

Figure 2.4 The elongated molecule tilted at the angle θ relative to the director, i.e. relative to the average orientation of the local neighbourhood surrounding the molecule. The molecule is assumed to possess a dipole μ attached at an angle β to its long axis.

The molecular dipole μ has two components parallel to the longitudinal and the transverse molecular axes (denoted by the subscripts l and t). Maier and Meier were able to shape the nematic permittivity

components in the following form, which is a straightforward generalization of the Onsager expression (2.20).

$$\varepsilon_{\parallel} - 1 = \frac{NhF}{\varepsilon_0}\left(\overline{\alpha} + \frac{2}{3}\Delta\alpha S + \frac{F}{3kT}\left[\mu_l^2(1+2S) + \mu_t^2(1-S)\right]\right) \qquad (2.37)$$

$$\varepsilon_{\perp} - 1 = \frac{NhF}{\varepsilon_0}\left(\overline{\alpha} - \frac{1}{3}\Delta\alpha S + \frac{F}{3kT}\left[\mu_l^2(1-S) + \mu_t^2\left(1+\tfrac{1}{2}S\right)\right]\right) \qquad (2.38)$$

The main polarizability $\overline{\alpha}$ and the anisotropy of polarizability $\Delta\alpha$ are defined by

$$\begin{aligned} \overline{\alpha} &= \frac{\alpha_l + 2\alpha_t}{3} \\ \Delta\alpha &= \alpha_l - \alpha_t \end{aligned} \qquad (2.39)$$

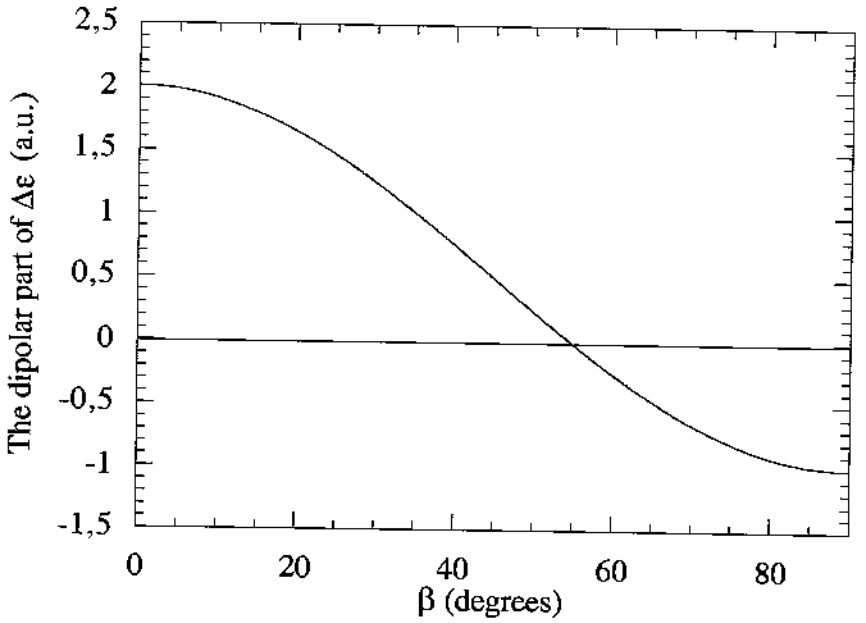

Figure 2.5 Dependence of the dipolar part of dielectric anisotropy on the angle β between the director ***n*** and the direction of the dipole $\boldsymbol{\mu}$.

If we use the fact that $\mu_l = \mu \cos\beta$ and $\mu_t = \mu \sin\beta$ (cf. figure 2.4) from the expressions (2.37) and (2.38) can easily yield the standard expression for the dielectric anisotropy $\Delta\varepsilon$ of a nematic

$$\Delta\varepsilon = \frac{NhF}{\varepsilon_0}\left(\Delta\alpha + \frac{F}{2kT}\mu^2\left(1-3\cos^2\beta\right)\right)S \qquad (2.40)$$

where β is the angle between the dipole moment μ and the director $\boldsymbol{n}$. The angle β between the dipole μ and the long molecular axis is seen to be of importance. If the dipole is oriented 54.7° to the director, then $\Delta\varepsilon$ is determined solely by the anisotropy of polarizability $\Delta\alpha$, which usually is positive. If the dipole is along the molecular axis (β=0) we get a positive contribution proportional to $2\mu^2$, whereas if a dipole of the same size is perpendicular to the axis we get a negative contribution proportional to μ^2, i.e. to half the amount. The local rotational symmetry around the director is the reason why the perpendicular component is less efficient and hence why it is easier to synthesize molecules with a high positive dielectric anisotropy than such with a high negative anisotropy.

2.4 COLLECTIVE AND NON-COLLECTIVE PROCESSES IN CHIRAL AND NON-CHIRAL LIQUID CRYSTALS

The dielectric spectra of chiral and non-chiral liquid crystalline phases contain different absorption that could be assigned to four main molecular origins and could be summarised in the following points.

2.4.1 Non-Collective Processes

In the homeotropic orientation of orthogonal and tilted phases (like nematics and smectics) the dielectric spectrum exhibits one absorption which is connected with the molecular reorientation around the short axis of molecule. This process is characterised by s single relaxation time and usually observed in the kHz and MHz regions of the spectrum.

In the planar orientation, a broad absorption peak usually resolved in the spectrum which is attributed to the molecular reorientation around the long axis of molecules. The absorption peak of this processes is located in the high MHz regime of the spectrum. These two mechanisms are observed in chiral and non-chiral liquid crystalline phases.

2.4.2 Collective Processes

The dielectric spectrum of chiral smectic (like SmA* and SmC*) is characterised by two main absorption peaks. In the SmA* phase, the observed absorption varies in its location and amplitude strongly with temperature. The relaxation frequency of this process decreases when approaching the SmA* to SmC* transition and its absorption maximum varies in an opposite fashion. This is related to the collective tilt fluctuation of the director and knows as the soft mode. The name soft mode originates from the fact that the elastic constant controlling the tilt fluctuations gets soften at the vicinity of SmA* to SmC* transition.

In the smectic C* phase, beside the soft mode, the dielectric spectrum is characterised by an absorption of a very large amplitude and a low relation frequency. This peak usually varies weakly with temperature and attributed to the *collective tilt fluctuations* of the director. This is knows as the Goldstone mode. The Goldstone mode is usually observed when we cross a phase transition from a high symmetry to a low symmetry phase. The Goldstone mode type excitation are of hydrodynamic nature, i.e. it frequency goes to zero as its wavelength diverges to infinity.

2.5 LANDAU THEORY OF THE SMECTIC C* PHASE

The Landau Free energy expansion is a basis for the phenomenological of the thermodynamical properties of the smectic C* phase. The simplest version of the theory was given by Meyer [18]. In the majority of cases, the smectic C* phase appears when cooling the smectic A* phase, and then the transition can be of second order type. In its simplest form, the order parameter which is characterizing the appearance of molecular tilt at the transition temperature T_C can be taken as the tilt angle θ. We may thus write the smectic C* free energy density F in terms of a Landau expansion in powers of θ. Because of the symmetry along the smectic layer, the free energy must be independent of the sign of the tilt ($\pm\theta$). Hence, we may write, keeping the only first terms of θ,

$$F = F_0 + \tfrac{1}{2}a\theta^2 + \tfrac{1}{4}b\theta^4 + ... \qquad (2.41)$$

Here, for the second order smectic A-C transition, the general case, b is greater than zero and only weakly dependent on temperature, whereas a has to change sign in order to allow the transition, at $T = T_C$. Thus, with $a = \alpha(T - T_C)$ as the simplest choice,

$$F = F_0 + \tfrac{1}{2}\alpha(T - T_C)\theta^2 + \tfrac{1}{4}b\theta^4 + ... \qquad (2.42)$$

By minimizing F, i.e. $dF/d\theta = 0$ we get

$$\theta = \left(\frac{a}{b}\right)^{\frac{1}{2}} (T_C - T)^{\frac{1}{2}} \qquad (2.43)$$

This simple parabolic function of T - T_C is shown in Figure 2.6 and indeed qualitatively describe the temperature behaviour of the tilt for a material having smectic A to C transition. For small tilt angle, the spontaneous polarization $\boldsymbol{P}$ is linearly related to θ, or $P \sim \theta$.

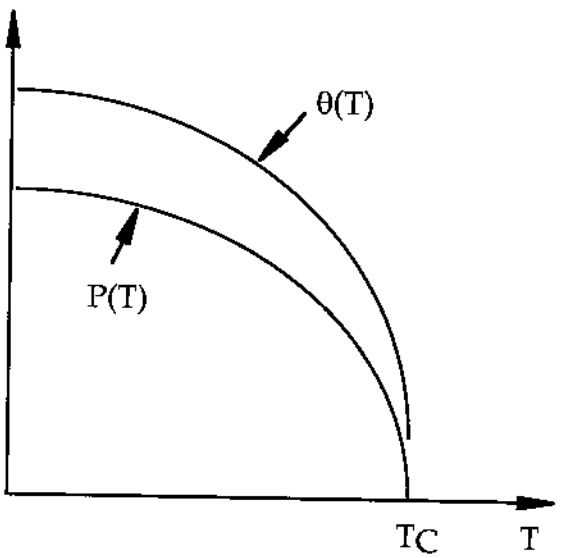

Fig. 2.6 Schematic temperature dependence of the tilt angle θ and polarization P at second order smectic A* to smectic C* transition.

This means that the functional dependence of θ is going to be closely reflected in the dependence of $\boldsymbol{P}$ as depicted in figure 2.6.

On entering the smectic C phase (the same for smectic C*) the molecules must tilt, and in figure 2.7 the tilt has been chosen in

the plane of the paper. By symmetry, infinitely of such planes can be chosen in the same way. The tilt direction is given by the azimuthal angle φ. The complete order parameter thus has to have two component, reflecting both the magnitude of the tilt and its direction in space and can be written as

$$\xi = \theta e^{j\varphi} \tag{2.44}$$

The full order parameter ξ is shown schematically in figure 2.7 illustrating the conical degeneracy of the smectic C phase. The fluctuations in φ around the smectic C cone is characterized by long wavelengths on a molecular scale. This is an elementary excitation sometimes called spin mode (it is very similar to the spin wave motion in ferromagnetism).

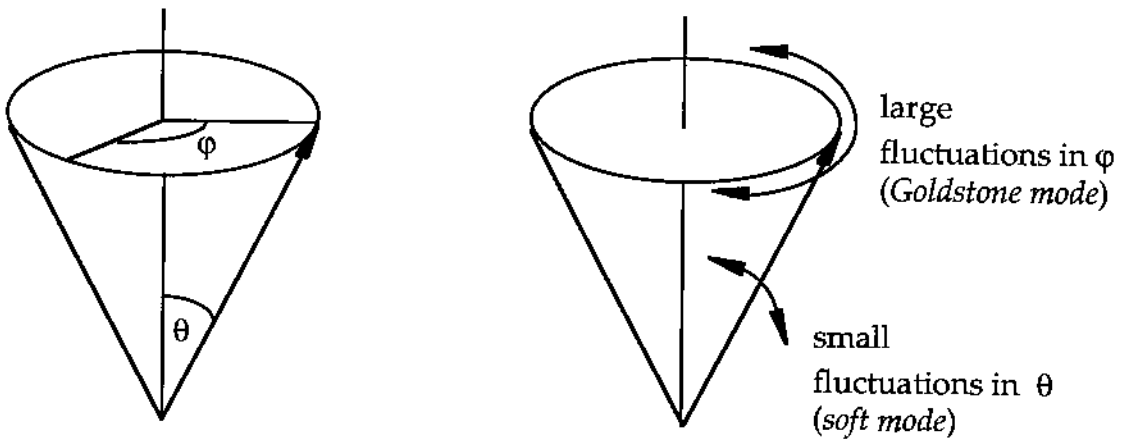

Fig. 2.7 Illustrating the two-component order parameter (θ and φ), and describing the director fluctuations in φ (Goldstone mode) and θ (soft mode).

In condense matter physics this mode is the *Goldstone mode*. The other component of the order parameter which is θ has its own characteristic fluctuations (tilt mode) that exist in both the smectic A and C phases. This mode is called the *soft mode*. One of the central points in the proposed project is to study the contribution of the Goldstone mode and soft mode to the complex dielectric permittivity by means of dielectric relaxation spectroscopy in the frequency region 10 Hz to 10 MHz.

Chiral smectics are complicated systems. The Landau free energy expansion describing the smectic A* to smectic C* transition can be written as [19]

$$\begin{aligned} F = F_0 + \tfrac{1}{2}a(\xi_1^2 + \xi_2^2) + \tfrac{1}{4}b(\xi_1^2 + \xi_2^2)^2 - \Lambda\left(\xi_1 \tfrac{d\xi_2}{dz} - \xi_2 \tfrac{d\xi_1}{dz}\right) \\ + \tfrac{1}{2}K_{33}\left[\left(\tfrac{d\xi_1}{dz}\right)^2 + \left(\tfrac{d\xi_2}{dz}\right)^2\right] + \tfrac{1}{2\varepsilon_0\varepsilon_\infty}\left(P_x^2 + P_y^2\right) \\ - \mu\left(P_x \tfrac{d\xi_1}{dz} + P_y \tfrac{d\xi_2}{dz}\right) + C\left(P_x\xi_2 + P_y\xi_1\right) \end{aligned} \qquad (2.45)$$

in this expression, additional terms; ξ_1 and ξ_2 describe the molecular tilt of the molecule, P_x and P_y are the components of the polarization in the smectic plane, K_{33} is the elastic constant, Λ is the coefficient of the Lifshitz term responsible for the helicoidal structure and ε_∞ is the high frequency dielectric permittivity. The coefficients C and μ are the flexo-electric and piezo-electric coupling between director gradient and polarization, and between tilt and polarization, respectively. Full theoretical treatment of this problem is given in [19].

In this thesis, we are interested in studying the dielectric response and relaxation frequency of different molecular processes. In general, the dielectric permittivity is a complex function $\varepsilon^*(f,T)$ which depends on the frequency of the applied field and temperature, and it can be written as

$$\varepsilon^*(f,T) = \varepsilon'(f,T) - j\varepsilon''(f,T) = \sum_i \frac{\Delta\varepsilon_i(T)}{1 + j\left(\frac{f}{f_R(T)}\right)^{1-\alpha}} + \varepsilon_\infty \quad (2.46)$$

where ε' and ε'' are the real and imaginary parts of ε^*. $\Delta\varepsilon_i$ is the dielectric strength of the i^{th} process, defined as the difference between the dielectric permittivity measured at low ε_0 and high ε_∞ frequencies. f_R and α are the relaxation frequency and distribution parameter of a certain molecular process, respectively.

In the presence of an external weak electric field E applied perpendicular to the helical axis, an additional term must be added to the free energy expansion of Eq. (2.45)

$$F_E = -P_x E_x \quad (2.47)$$

In this case, by minimizing the free energy density with respect to the polarization which can be substituted into Eq. (2.45) from which we can get the following expressions for the dielectric contribution of the soft mode ($\Delta\varepsilon_S$) and Goldstone mode ($\Delta\varepsilon_G$);

$$\varepsilon_0 \Delta\varepsilon_S = \frac{\varepsilon_0 \varepsilon_\infty}{\alpha(T - T_C) + Kq_0^2}, \qquad T > T_C \tag{2.48}$$

$$\varepsilon_0 \Delta\varepsilon = \varepsilon_0 (\Delta\varepsilon_S + \Delta\varepsilon_G) = \tfrac{1}{2} \varepsilon_0^2 \varepsilon_\infty^2 C^2 \left(\frac{1}{2\alpha(T - T_C) + Kq_0^2} + \frac{1}{Kq_0^2} \right) \tag{2.49}$$

where q_0 is the helical wave vector related to the helical pitch p by $q_0 = 2\pi/p$, note that the subscript $_0$ in q_0 refers to the wave vector value at the A* to C* transition. The Goldstone mode dielectric contribution can also be written in terms of material parameters (tilt angle, helical pitch and spontaneous polarization) as

$$\varepsilon_0 \Delta\varepsilon_G = \frac{1}{2K_\varphi} \left(\frac{P}{q\theta} \right)^2 \tag{2.50}$$

where K_φ is the elastic constant of the cone motion that will be determined also in the present work.

The relaxation frequency of the order parameter fluctuations is obtained by means of the Landau-Khalatniov equations of motion

$$\frac{d\xi_1}{dt} = -\Gamma_1 \frac{\partial F}{\partial \xi_1} \tag{2.51}$$

$$\frac{d\xi 2}{dt} = -\Gamma_2 \frac{\partial F}{\partial \xi_2} \tag{2.52}$$

where Γ_1 and Γ_2 are the kinetic coefficients for the director reorientation and assumed to degenerate at the SmA*-SmC* transition. These two coefficients are the inverse of the viscosity coefficients that will be determined in the present study. From the equations of motion Eq. (2.51, 2.52), we can get the relaxation frequencies of the soft mode f_S and Goldstone mode f_G are given by

$$f_S = \frac{1}{2\pi\gamma_S}\left[\alpha(T - T_C) + Kq_0^2\right] \tag{2.53}$$

$$f_G = \frac{K_\varphi q^2}{2\pi\gamma_G} \tag{2.54}$$

CHAPTER 3

EXPERIMENTAL

3.1 THE MEASUREMENT CELL

Most of the measurements presented in this work were made using cells of a kind illustrated in figure 3.1. The cells were designed to fit easily into a special cell holder.

Each cell was constructed from two pieces of flat glass plates partially coated with conducting layer. Whenever possible the conducting layer was chosen to be transparent for visible light. The transparent layer was made from Indium Tin Oxide (ITO) ensuring high transparency, but with electrode resistivity of about 20 Ω/square. The active area was formed by the overlap of the electrodes on either plate (see figure 3.1). The active area was 30 mm^2.

The conducting layer was covered by an evaporated silicon oxide (SiO_2) layer. Silicon oxide is an insulator, so it electrically separates the electrodes from the liquid crystal. Liquid crystal mixtures are not absolutely free from impurities, hence, when an electric field is applied, there is a certain movement of electric charges, which is partially blocked by the SiO_2 layer. The ions cause the appearance of induced

opposite charges in the silicon oxide. A double layer is created and may cause problems, because it acts as a large series capacitance with losses. The largest contribution of this double layer is naturally seen at low frequencies. However, the cell equipped with a blocking layer is superior to a cell without silicon oxide layers which is even more dominated by ions at low frequencies.

A properly evaporated silicon oxide layer has an additional positive effect - it aligns the liquid crystal molecules in the plane of the surface. We were using an SiO_2 layer evaporated perpendicular to the surface, which usually gives a good planar orientation.

Homeotropic and quasi-homeotropic orientations were achieved by coating with tensile-like substances like lecithin or chrome complex deposited on the electrodes. It was experimentally observed, that tensiles adhered better to a clean metal than to silicon oxide. Thus, a blocking silicon oxide layer was not used for this type of cells.

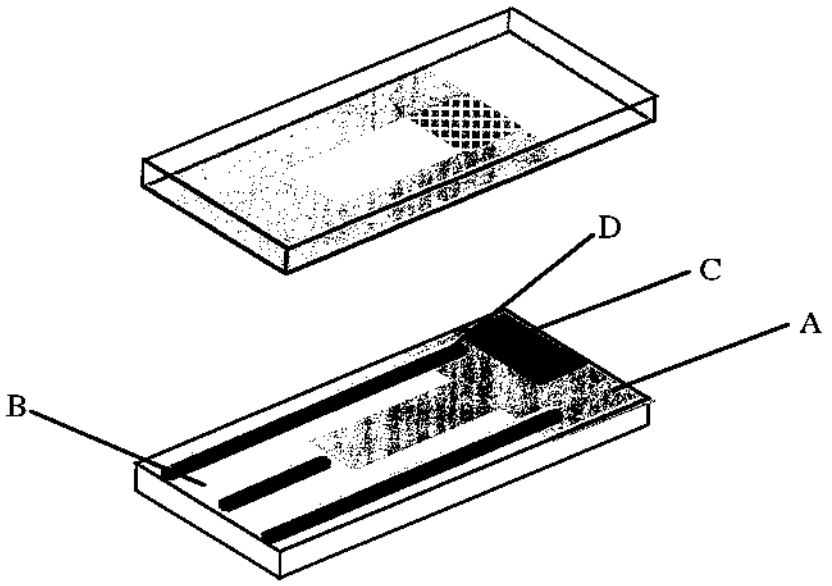

Figure 3.1 The measurement cell. **A** is the T-shaped conductive layer (middle gray) covered by insulating SiO_2 (light gray), **B**, except on a smaller part (darker gray) left uncovered for the contacting purpose, **C**. The long spacer rails of 2μm thick SiO_2 are also shown as **D**. The hatched part of the electrode shown on the top plate illustrates the overlap electrode area, which is the active capacitor surface..

The two glass plates were separated by mylar spacers of appropriate thickness whenever the liquid crystal layer was in the range 5-100 μm. For 2 μm cells like the one shown in the figure 3.2 the spacers were evaporated directly onto the glass plates, on top of the silicon oxide layer.

The cell was assembled and placed into a sample holder equipped by a shearing mechanism. The holder shown in figure 3.2 was designed to fit easily into a built in-house temperature hot stage controlled by Julabo LC4F temperature controller permitting a temperature control better than 0.1 °C. The temperature was measured by means of platinum resistance sensor. As the sample holder should have an appropriate

thermal mass, it was made from brass. The cell was placed on a piece of silicon rubber **D** on the bottom of the sample holder **F**. It was held in place by a piece of mylar **B** and by the lid **A**. The rod **G** is able to exert a shearing force to the edge of the upper glass plate on turning the knob to the right. The spring **E** is creating a return force, so that the upper glass plate can move back and forth and transfer the shearing action to the liquid crystal. Approximately 10 cm long grounded cables **H** were soldered to the conductive layer using ultrasonic soldering equipment. The grounded cables were connected to the measuring equipment.

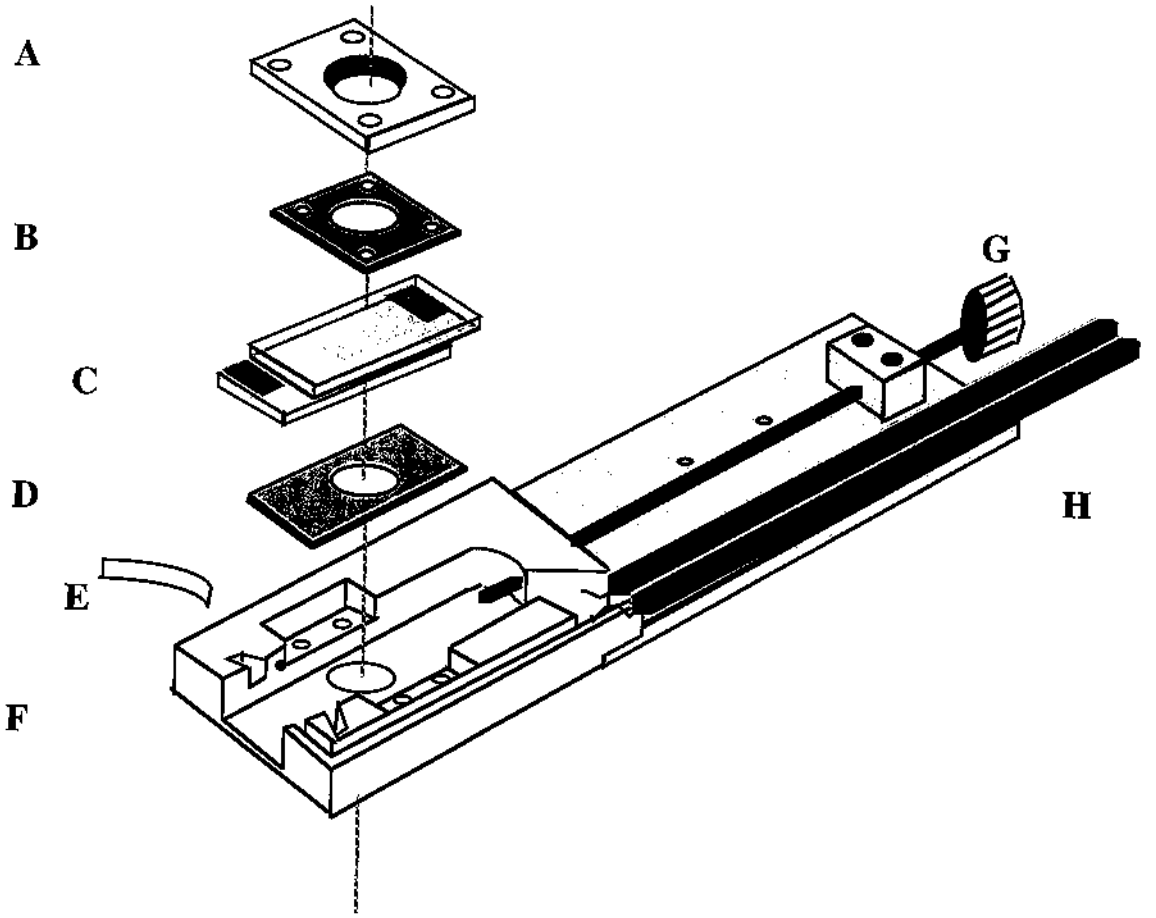

Figure 3.2 The shearing equipment consists of a massive brass holder **F** equipped with a lid **A**. A piece of a silicon rubber **D** and a piece of mylar **B** are reducing the friction and thereby ensuring the smoothness of the shearing movement. The shearing force is applied to the upper glass plate of the cell **C** by the shearing rod **G**. The spring **E** is creating the return force.

A small quantity of the liquid crystalline material was deposited to the edge of the cell which was heated to high temperature for filling in a special chamber.

3.2 MEASUREMENT GEOMETRIES

As mentioned above the liquid crystal is brought to either planar or homeotropic orientation. However, for smectics, and in particular for chiral smectics, alignment is a more involved feature than for the nematics. It is convenient to call the case, when the molecules of the liquid crystal are aligned parallel to a certain direction along the substrate *parallel alignment* (see figure 3.1).

There are two basic forms of alignment (measurement geometries) of liquid crystal molecules used in optical microscopy known as planar and homeotropic orientations as shown in figure 3.3. In the planar orientation (figure 3.3a), the molecules of a liquid crystal phase are oriented in a direction parallel to the supporting substrates. In case of smectic phases, the planar orientation is called a bookshelf geometry because the smectic layers are stacked as books on shelves. Planar samples of smectic phases exhibit birefringence and a coloured textures are observed when viewed between cross polarizers (see Plates 1 to 3). In the homeotropic orientation (Figure 3.3b) the molecules that

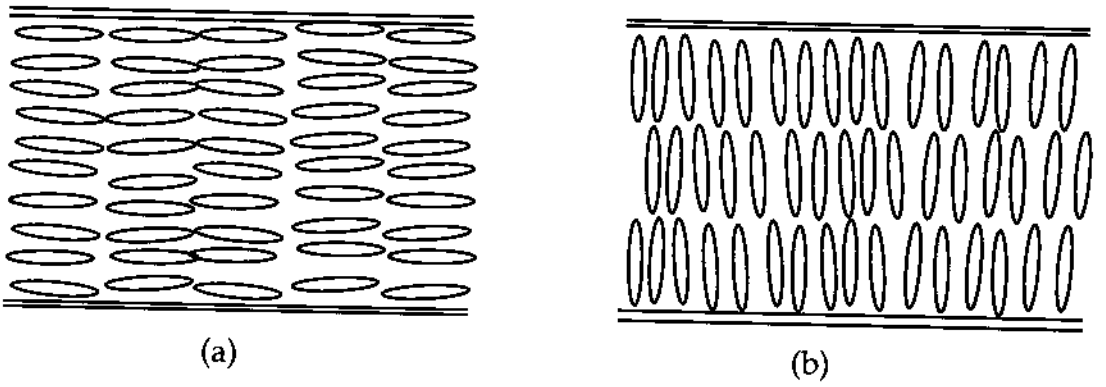

Figure 3.3 Different types of measurement geometries; (a) planar orientation, (b) homeotropic orientation.

constitute the phase are oriented such that their long axes (or their optic axis) are normal to the substrates. When a linearly polarized light passes through a homeotropically aligned sample, it is unaffected by the material so the light cannot go further through the analyzer. Thus, an observer looking through the polarizing microscope will see complete blackness. A situation which is valid for nematics and orthogonal smectics.

For measurements in the parallel alignment the glass plates were coated with silicon monoxide, the sample was filled in vacuum in the isotropic phase and very slowly cooled down to the smectic A* phase in presence of an electric field. In most cases the orientation was good enough for dielectric measurements to be carried out. If too many defects appeared under cooling or the sign of dielectric anisotropy was not proper for the application of the field, then the sample was gently sheared. Such efforts usually gave satisfactory results.

For measurements in the *homeotropic* alignment (see Figure 3.3) the glass plates has been treated with tenside-like substances widely known as surfactants, and strongly (not weakly) sheared. In most of measurement cells a chloroform solution of lecithin was used for coating. A few drops of lecithin solution was placed on the glass surfaces and the chloroform was left to evaporate for a half minute. The cell was then filled with the liquid crystal in the isotropic phase and cooled down to the smectic phases. For some substances the homeotropic or quasi-homeotropic orientation was obtained without any additional effort, but there were substances which spontaneously took the parallel orientation. In such cases the cells were strongly sheared in the smectic A* phase.

The homeotropic orientation may be inspected in the microscope as a uniform non-birefringent area and its quality may be checked by the optical conoscopy. Because the smectic A* phase has no helix and its local director is parallel to the smectic layer normal, the conoscopy is the most powerful tool to detect small deviations from a good homeotropic alignment.

3.3 IMPEDANCE MEASUREMENTS

The impedance measurement were made at low signal voltages over the frequency range 5Hz to 13MHz using the HP4192A impedance analyzer. This apparatus generates a variable sinusoidal test signal, and measures

the impedance and the phase angle across its four terminals. Then, according to preset network mode the analyzer interpreted the results and calculated the capacity and resistivity. Throughout the present work, a parallel resistor-capacitor network was assumed.

The analyzer has the capacity of applying a bias voltage during the impedance measurement. It superposes low signal voltage with the high bias voltage and measures the response to the applied signal.

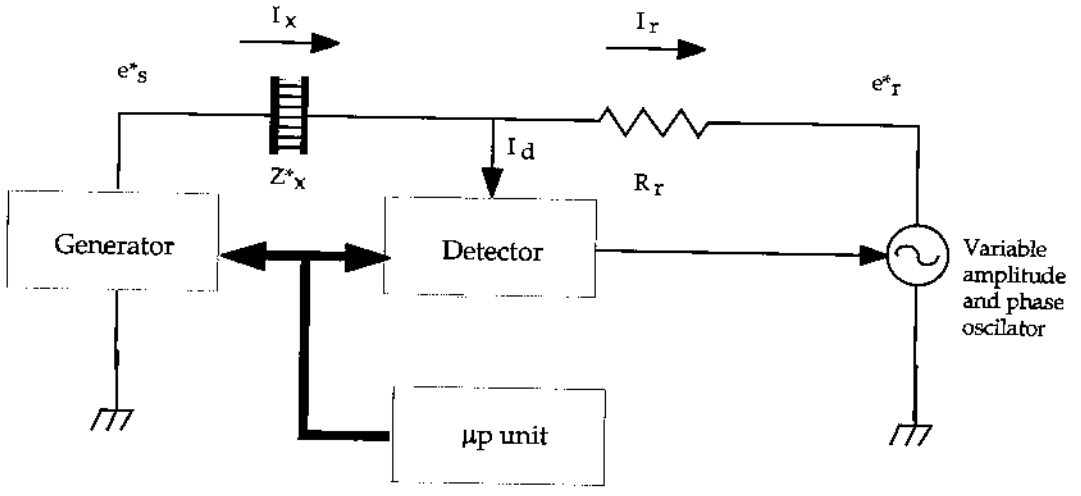

Figure 3.4 The schematic picture of the HP4192A impedance analyzer.

The essential blocks of the measuring part of the HP4192A is shown in the figure 3.4. The general principle is to balance the left and right shoulders of the bridge consisting from the sample with the unknown impedance Z_X^* (the asterisk denotes a complex quantity) and the range resistor with the resistance R_r. Balancing of the bridge means

zeroing of the current I_d flowing through the input of the detector by adjusting the amplitude and the phase of the variable oscillator.

When I_d is zero it implies currents on the left and right shoulders to be equal, or

$$I_x = I_r \tag{3.1}$$

Each current can be expressed as impedance divided by the voltage drop on the corresponding impedance. Thus the unknown complex impedance of the sample Z_X^* is

$$Z_x^* = R_r \frac{e_S^*}{e_r^*} \tag{3.2}$$

where e_S^* and e_r^* is the voltage drop respectively in the left and in the right shoulders of the bridge. Thus, the bridge can measure the complex impedance Z_X^*. It can be expressed in the terms of the real and imaginary parts, Z'_X and Z''_X:

$$Z_x^* = Z'_x + iZ''_x \tag{3.3}$$

The real and imaginary parts are often called resistance and reactance. An ideal resistance between the terminals of the bridge

contributes *only* to the real part and a ideal capacitance between the terminals *only* to the imaginary part. The real capacitance, however, consists at least from the ideal capacitance and the ideal resistor in parallel (or in series). These are the only two types of the networks that can be evaluated by the internal evaluation routine of the HP4192A analyzer from the measured complex impedance Z_X^*

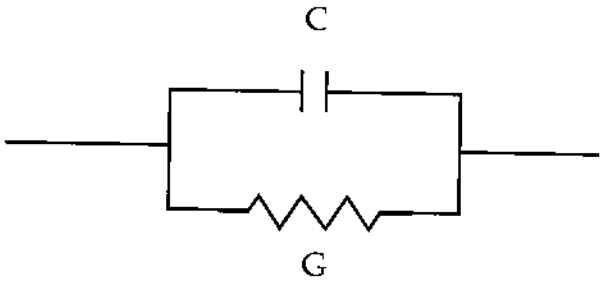

Figure 3.5. The equivalent network as seen by the internal evaluation routine of the impedance analyzer.

For network depicted in figure 3.5 the imaginary part and the real part of the total impedance Z_x^* is

$$\begin{cases} Z'_x = \dfrac{G}{G^2 + \omega^2 C^2} \\ Z''_x = \dfrac{i\omega C}{G^2 + \omega^2 C^2} \end{cases} \tag{3.4}$$

The real cell filled with liquid crystal is represented by another network than it is assumed by the internal evaluation routine of the impedance analyzer. The network of real cell consists of the dielectric material C_{LC} with the losses G_{LC}, the conducting layer having resistance,

denoted as R_{ITO}, and the wires with the inductance L_W attaching the measuring terminals of the impedance analyzer to the cell as shown in figure 3.6.

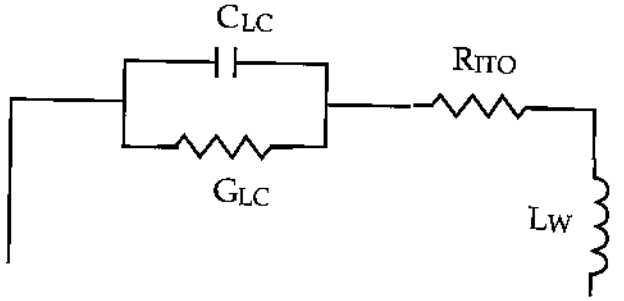

Figure 3.6 The real equivalent network of a liquid crystal cell.

The real and the imaginary parts of the total impedance Z_x* is then

$$\begin{cases} Z'_x = \dfrac{G_{LC}}{G_{LC}^2 + \omega^2 C_{LC}^2} + R_{ITO} \\ Z''_x = \dfrac{i\omega C_{LC}}{G_{LC}^2 + \omega^2 C_{LC}^2} + i\omega L_W \end{cases} \qquad (3.5)$$

By equating expressions (3.4) and (3.5) it is possible to calculate corrections to the measured values appearing due to improper conversion routines. It is worth to point out that problem is more complicated than the "wrong" conversion routine in the impedance analyzer. The analyzer has not enough data in order to be able to estimate four complex components of the network. Thus, the resistance of conductive layer and the inductance of the connecting wires, should be calculated by another

means, for example measuring the frequency spectrum of the empty cell and assuming, that they are frequency independent.

Fortunately, for very high and very low frequencies the corrections are small enough, so that use of the built-in conversion routines is fully possible.

3.4 STRAY CAPACITANCE

Not all the lines of the electric field go from the upper plate of the active capacitor to the bottom plate of the capacitor, passing the sample. Real samples have a finite size, and therefore some lines of the electric field bend out as drawn in Figure 3.4.

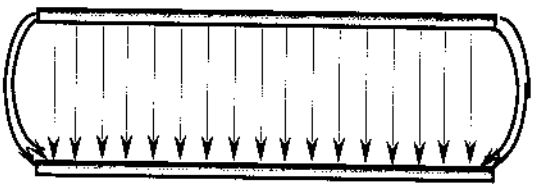

Figure 3.7 The capacitor with stray field at the edges of the plates.

There is therefore a tiny part of the capacitor which is not affected by the introduction of the dielectric material. If we write the empty capacitance as the sum of the ideal empty capacitance and the tiny value which may be called the stray capacitance,

$$C_E = C_0 + C_S \tag{3.6}$$

The measured capacitance of the filled capacitor may be then expressed

$$C_M = \varepsilon C_0 + C_S \tag{3.7}$$

The expressions (3.6) and (3.7) give

$$C_S = \frac{C_M - \varepsilon C_E}{1 - \varepsilon} \tag{3.8}$$

The stray capacitance has to be measured by filling the cell with a material with known dielectric permittivity and using equation (3.8), after which all results can be corrected to their proper value.

3.5 EVALUATION OF THE REAL ε′ AND IMAGINARY ε″ PARTS OF THE COMPLEX DIELECTRIC PERMITTIVITY

The dielectric permittivity $\varepsilon^* = \varepsilon' - j\,\varepsilon''$ is a complex number. From the measured capacitance (C_M) and conductivity (G_M) values evaluated by the impedance analyzer at the spot frequency f. The real part of the complex dielectric permittivity is given

$$\varepsilon' = \frac{C_M - C_S}{C_E - C_S} \tag{3.9}$$

where C_E is the capacitance of the empty cell and C_S is stray capacitance. The imaginary part ε'' of the complex dielectric permittivity ε* is determined using the relation

$$\varepsilon'' = \frac{G_M}{2\pi f(C_E - C_S)}. \qquad (3.10)$$

When we perform a frequency sweep, we see a frequency dependence of both real and imaginary part of the dielectric permittivity. However, because the function representing the imaginary part is peaked (being essentially the derivative of the real part), the frequency dependence of ε'' is used for most purposes when analysing the spectra. A typical example of the measured ε'', the dielectric absorption, is plotted in Figure 3.8.

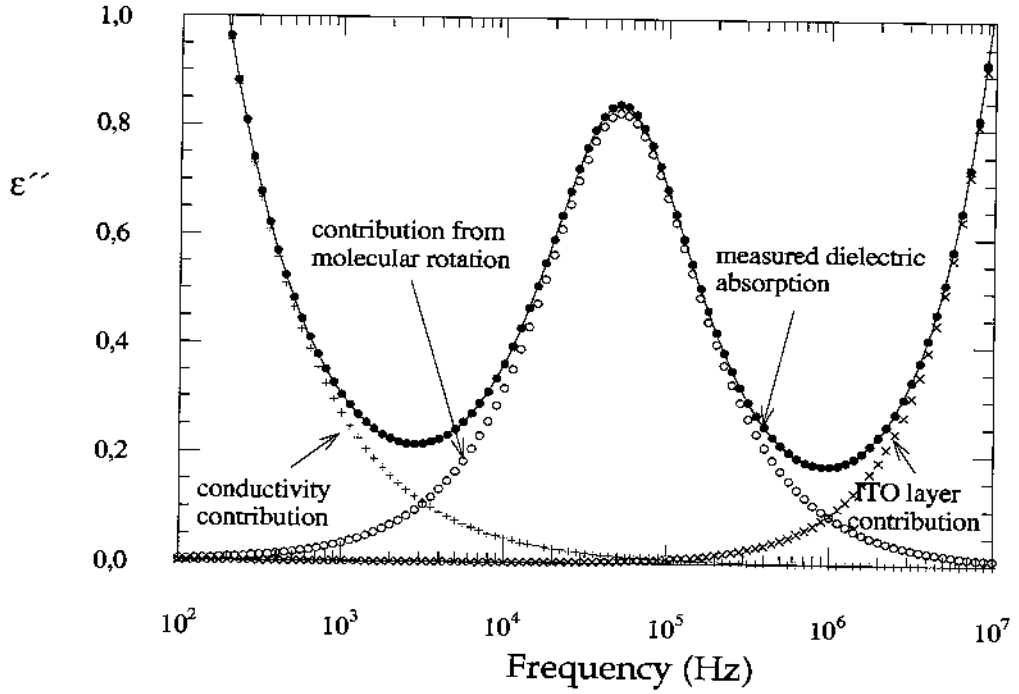

Figure 3.8a Frequency dependence of the dielectric absorption. The solid line represents the fitting of equation 1 to the experimental values of $\varepsilon''(f)$. Beside the contribution from the dipolar rotation (open circles), there is a low frequency background from the freely moving charges (+ symbol). At high frequency the background is due to the ITO conducting layer (x symbol).

A similar plot for another material is shown in Figure 3.8(b). However, in this figure we show a log-log plot of a different measurement of the frequency dependence of dielectric absorption.

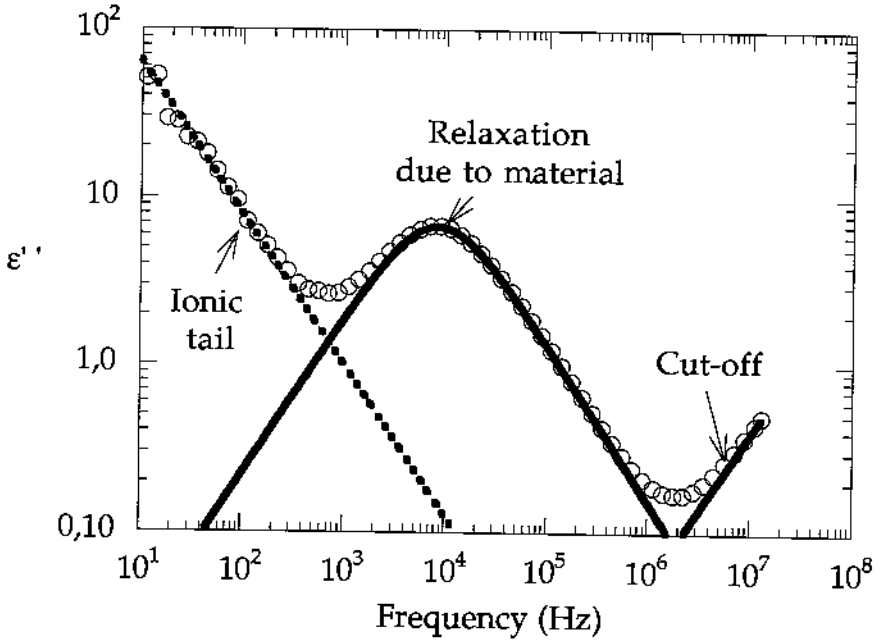

Figure 3.8b A log-log plot of the frequency dependence of the dielectric absorption

.

The middle part of the spectrum can be described by the Cole-Cole relaxation function This is represented by the second term in equation (3.11). The low frequency and high frequency tails seem to lie outside of the model for an ideal dielectric material. The tails belongs to two relaxations: one is appearing at very low and the other at very high frequencies and accounted for by the first and the third terms in equation (3.11), respectively [20]. If we do not have any dielectric absorption, we

will still see these tails in the dielectric spectrum. Hence, they have nothing to do with the liquid crystalline order.

The low frequency relaxation is caused by ions present in the sample. Since liquid crystal materials are not ideal dielectrics, they have a certain concentration of charge carriers which can move on the application of electric field. The dielectric losses introduced by ionic conductivity will appear as a relaxation in the spectrum. The characteristic frequency of this relaxation is very low, and it is always outside of the HP4192A frequency range, and thus only the right wing of this relaxation is visible in the dielectric spectrum.

At high frequencies the electric current is confined to the surfaces of the conductors. The growing resistance of the wires and especially of the ITO layer will introduce losses, which will likewise appear as a relaxation visible in the spectrum [20]. Characteristic for this relaxation is the decrease of the real part ε' of the dielectric permittivity, until it vanishes under the high frequency value of the permittivity $\varepsilon_\infty = n^2$. It is therefore often called the "cut-off" even in the ε'' spectrum. For very thin ITO cells not only the left wing but also the whole "cut-off" is clearly visible. In our cells, depending on thickness and electrode material, the cut-off frequency was somewhere between few MHz and hundreds of MHz.

3.6 DATA ANALYSIS

As already described, the raw data such as frequency, capacity and resistivity were measured by the analyzer and via the GPIB bus transferred to the IBM Personal computer (see the experimental set up in figure 3.9). Then the real and imaginary parts of the dielectric constant were calculated from the these data, and everything was saved in the data file. Such data files were produced for each temperature. Then, the files were read by the plotting program "Kaleidagraph™" on the Apple Macintosh computer. The measured dielectric absorption was then fitted to the following function

$$\varepsilon'' = \frac{\sigma}{2\pi\varepsilon_0}\left(\frac{1}{f^n}\right) + \mathrm{Im}\left(\varepsilon_\infty + \frac{\Delta\varepsilon}{1+\left(j\frac{f}{f_R}\right)^{1-\alpha}}\right) + \frac{\varepsilon_{ITO}\left(\frac{f}{f_{ITO}}\right)}{1+\left(\frac{f}{f_{ITO}}\right)^2} \qquad (3.11)$$

The first term represents the *d. c.* conductivity contribution in which σ is the specific conductivity of the sample ($\Omega^{-1}cm^{-1}$), f is the frequency of the measuring *ac* electric field and. Both σ and n are fitting parameters. The second term is the imaginary part in the Cole-Cole equation where $\Delta\varepsilon$ is the dielectric strength which is the difference between the dielectric permittivity measured at low and high frequencies, f_R is relaxation frequency, and α is a symmetric distribution parameter. The third term

represents the high frequency contribution due to the resistance of the *ITO* conducting layer. The equivalent circuit of this layer is a resistance R_{ITO} and capacitance C_{ITO} connected in parallel and the inverse of the time constant τ_{ITO} is the relaxation frequency f_{ITO} where $f_{ITO} = 1/(2\pi\tau_{ITO})$. If the resistance R_{ITO} is high, say 100 Ω/□, and the capacitance is 5 *pF* this corresponds to $\tau_{ITO} = 500$ *ps*: i.e. $f_{ITO} = 300$ MHz. This means that beside the peak due to dipolar reorientation, there will be another peak cantered around 300 MHz. If the measurement window is limited to 10 MHz then we will see the low frequency part of this absorption. In our dielectric spectrum, this is manifested in an increase in ε'' at frequencies above 1 MHz.

In our measurements, the R_{ITO} value of the used cells is < 20 Ω/□ this means that the f_{ITO} value will further be shifted to higher values. Thus, the ratio f/f_{ITO} is << 1, and thereby the denominator of the third term in Eq. (3.11) $[1+(f/f_{ITO})^2]$ tends to unity, thus it could be rewritten as $\frac{\varepsilon_{ITO}}{f_{ITO}} f$ .For fitting purposes it could be better to write this term in more flexible form by assigning a further free parameter as exponent to f. and the ratio $\frac{\varepsilon_{ITO}}{f_{ITO}}$ could be expressed in a fitting parameter $a_{ITO}(R,C)$ which depends on the values of the resistance and capacitance due to the capacitor at high frequency where the ITO resistive layer has a pronounced effect. For low resistance ITO layers it is thus useful to write equation Eq. (3.110) in the form

$$\varepsilon'' = \frac{\sigma}{2\pi\varepsilon_0}\left(\frac{1}{f^n}\right) + \mathrm{Im}\left(\varepsilon_\infty + \frac{\Delta\varepsilon}{1+\left(j\frac{f}{f_R}\right)^{1-\alpha}}\right) + a_{ITO}(R,C)f^m \quad (3.12)$$

In most cases, the fitting parameter n in most cases tends to be near one. A non-linear regression analysis has been made using two fitting softwares called "proFit™" and "Kaleidagraph™".

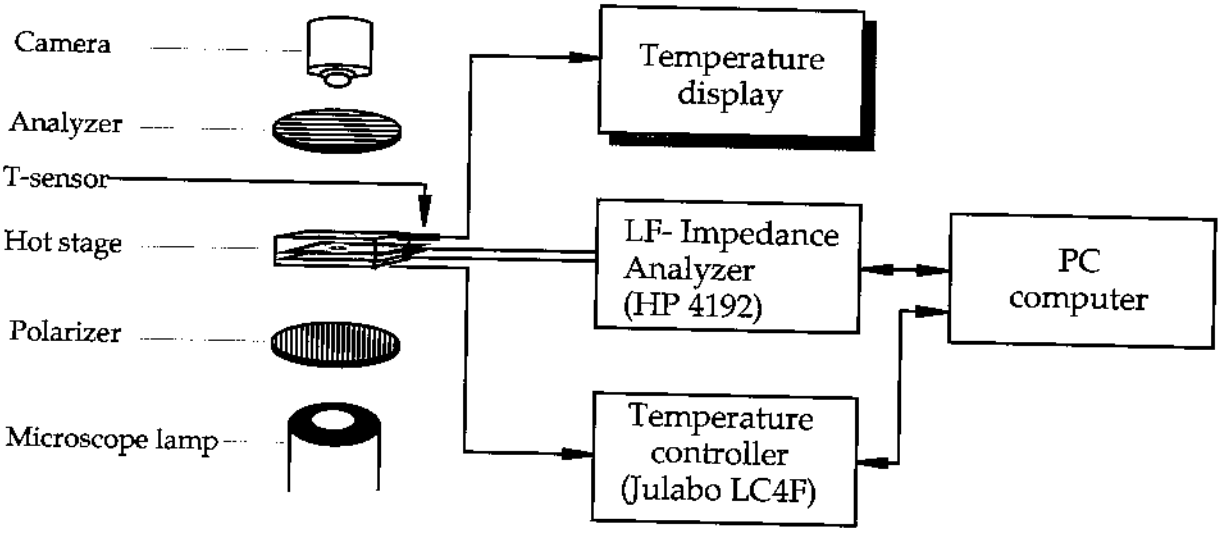

Figure 3.9 The schematic picture of the measurement control system

3.7. THE INVESTIGATED MATERIAL

The investigated material is a recently synthesised single component substance with the chemical formula given below

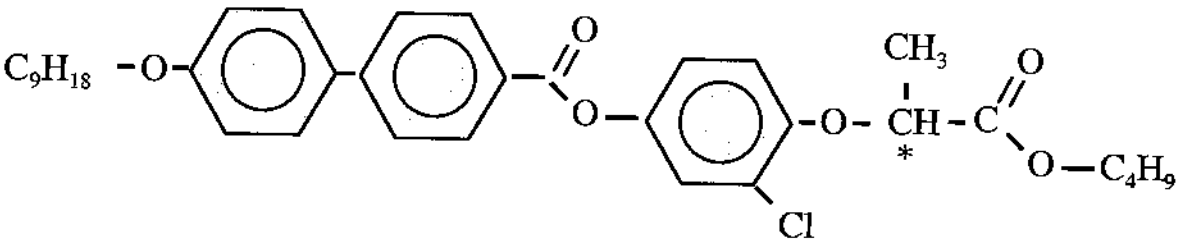

With the transition temperatures

56 °C ← Smectic A* ← 72 °C ← Isotropic

Crystal ← 46 °C (-3 °C Smectic C*) ←

The phase transition temperatures have been determined from polarizing microscope and dielectric spectroscopy measurements. The temperature value (-3 °C) given above means that the SmC* phase can be supercooled to this low temperature.

This compound is a good candidate for this work because the SmA* and SmC* phases exist over a relatively wide temperature interval. Moreover, the isotropic to SmA* transition is not very high, thus, permitting the measurements in the isotropic phase and thereby following the changes in dielectric behaviour from the normal liquid to the liquid crystalline state. Moreover, the investigated compound exhibits a transition to the crystalline phase at a reasonable temperature. One of the important features of this compound is the high value of spontaneous polarization in the SmA* phase beside the remarkable electro-optic response in the SmA* phase, thus, giving a high dielectric response which permitted the study of different molecular processes with adequate accuracy.

CHAPTER 4

STATIC AND DYNAMIC DIELECTRIC PERMITTIVITY

In this work, detailed dielectric spectroscopy measurements have been carried out in different phases of a single component liquid crystalline material. The real and imaginary parts of the complex dielectric permittivity have been determined in two different measurement orientations, namely, the planar and the homeotropic orientations. The complex permittivity has been studied as a function of, frequency, temperature, and bias field. The experimental results have been analysed and fitted by two soft wares: KaleidaGraph and proFit. In this chapter, all these experimental results will be presented and discussed in terms of the Landau theory presented in chapter 2. The results obtained in the planar orientation will be presented first.

4.1 THE TEMPERATURE DEPENDENCE OF THE DIELECTRIC PERMITTIVITY

One of the most common and illustrative ways of presenting the dielectric response through a large temperatures range is to plot ε' as a function of temperature. Figure 4.1 shows the temperature dependence

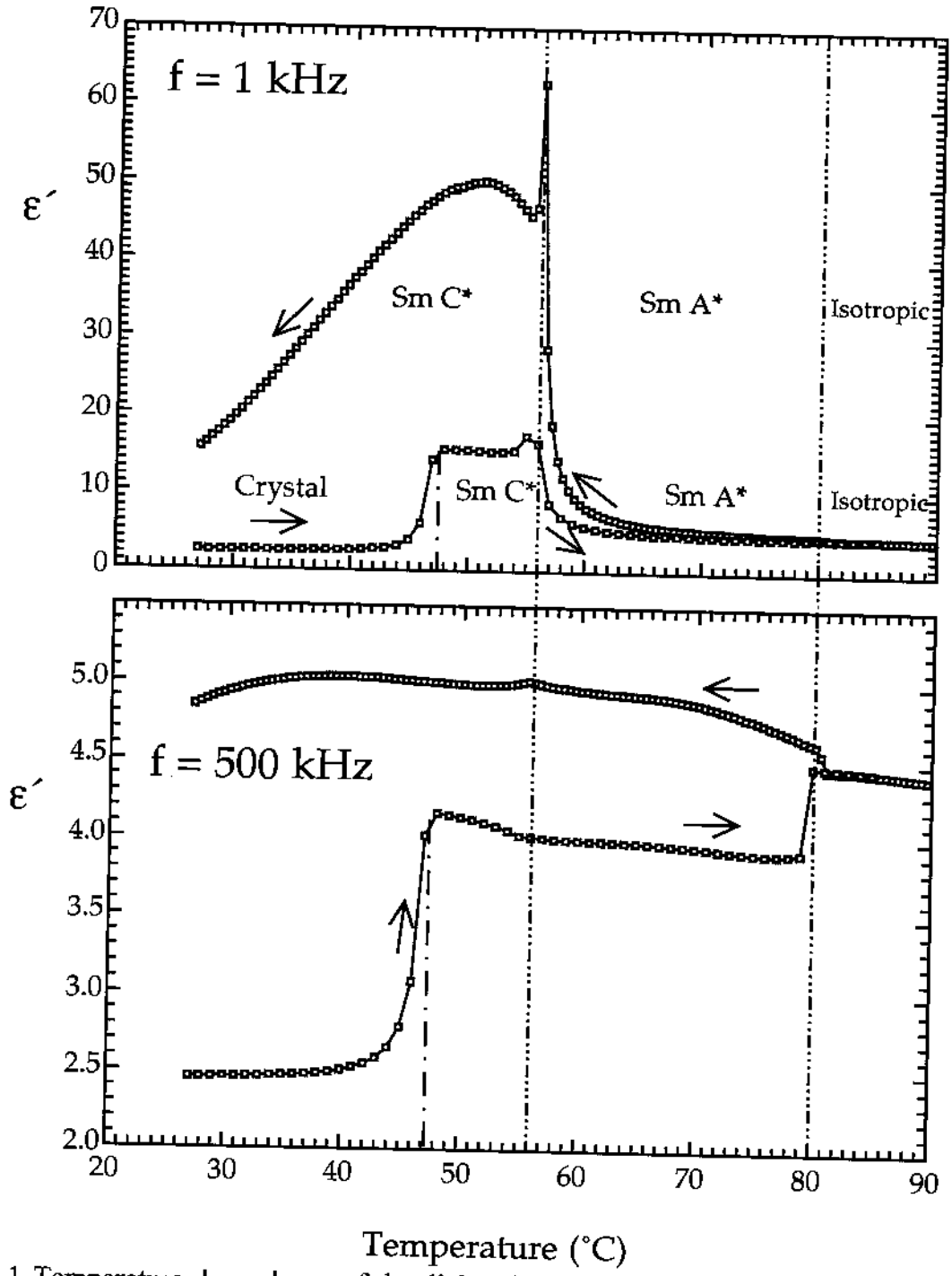

Figure 4.1 Temperature dependence of the dielectric permittivity on cooling and heating at 1 kHz (upper plot) and at 500 kHz (lower plot).

of ε' at different frequencies on both cooling and heating runs. The upper figure is plotted at 1 kHz and the lower at 500 kHz. The results of the cooling and heating sequences were obtained at 0.3 °C/min and 0.5 °C/min, respectively. The sample was first cooled from the isotropic phase to room temperature and left at 27 °C over night where it has been crystallised. The measurements were then carried out from the crystalline phase to the isotropic phase. From microscopic observations by polarising microscope, during the cooling cycle, remarkable texture changes could be observed deep in the SmC* phase which may indicate a slow crystallization process has already started. This may explain the pronounced decrease in the dielectric response from 50 at 57 °C to 15 at room temperature.

Four different phase transitions have been found on both cooling and heating runs. In the isotropic phase, the dielectric permittivity increases slightly with decreasing temperature as normal liquids, and at 80.0 °C, a slight increase in ε' is found indicating the isotropic to SmA* phase transition. This is of first order type. At 500 kHz, ε' increases continuously and crosses the phase transition to the SmC* phase smoothly. However, at 1 kHz, a remarkable increase in ε' is observed with a cusp like behaviour at SmA* to SmC* transition. In the SmC* phase, in the low frequency regime (at 1 kHz) ε' exhibits a broad maximum at 49 °C followed by a monotonic and pronounced decrease. It is obvious that vital information is lost in the high frequency figure. Therefore, a proper frequency must be chosen to trace the contribution of all mechanisms contributing to the dielectric

response. A separate and enlarged plot of the low frequency part of permittivity is depicted in Figure 4.2 plotted in the SmA* and SmC* phases. It is worth noting that the additional increase in ε′ measured in at low frequency results, and disappeared at high frequency, is attributed to the soft mode and Goldstone mode, in the SmA* and SmC* phases, respectively.

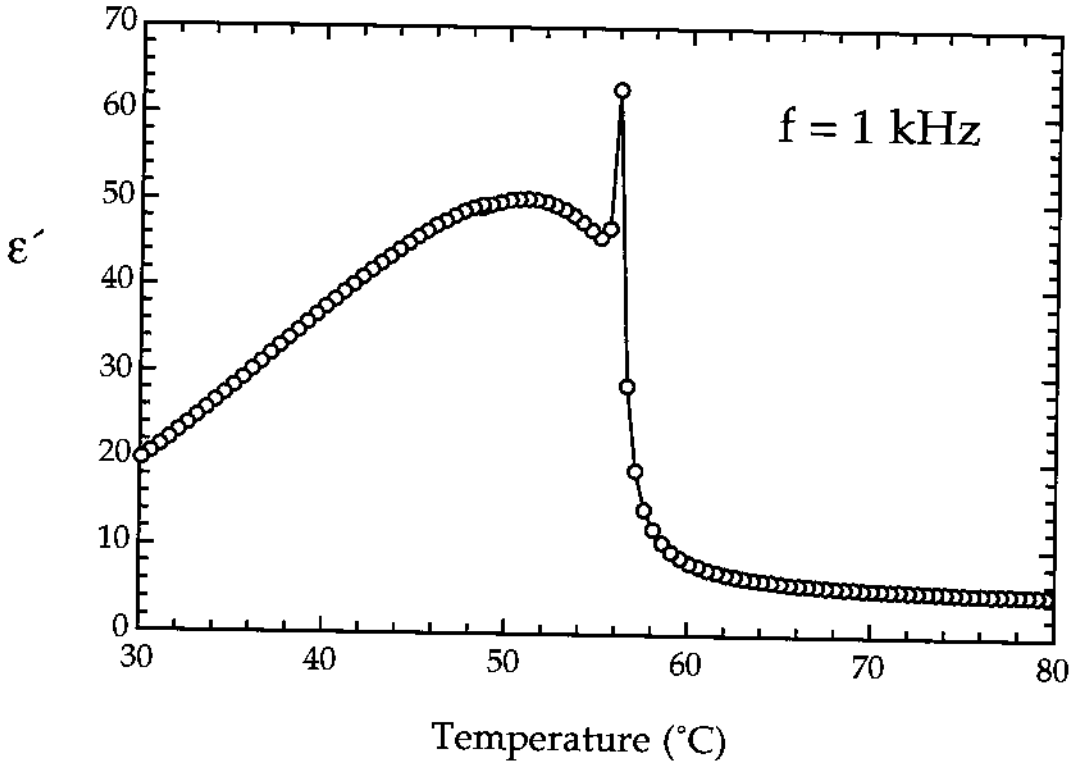

Figure 4.2. Temperature dependence of the dielectric permittivity in the SmC* and SmA* phases measured at 1 kHz. The solid line is just a smooth connecting of the points.

Furthermore, the fact that the soft mode and Goldstone mode disappeared at high frequency clearly indicates that they are characterised by a relatively low frequency process.

In the crystalline phase, see the heating curve, the dielectric permittivity equals to 2.5. This value equals to the n^2 where n is the refractive index which is about 1.6 for most of liquid crystal

materials [6]. Thus, indicating that only the electronic polarizability is mainly contributing to ε′. All other dipolar reorientations of intra-molecular and molecular aspects are frozen out. By further heating from the crystalline phase to the SmC* phase, ε′ increases to 15 at 1 kHz, a value which decreases to 4.2 at 500 kHz. It is obvious that the permittivity value in the SmC* phase when approached from the SmA* side is higher by factor 3 when the SmC* is preceded by the crystalline phase. This could be attributed to the strong first order nature of the crystal to SmC* transition. This implies that on heating, the crystalline phase may coexist in the SmC* phase. Thus, the helicoidal structure of the SmC* phase does not build up in a natural fashion, but is strongly distorted by the existence of the crystalline phase. On further heating, ε′ exhibits a small cusp at the SmC* to SmA* transition. At higher temperatures, ε′ decreases to 4.5 and does not show any remarkable temperature dependence. .

4.2 FREQUENCY DEPENDENCE OF THE DIELECTRIC PERMITTIVITY AND DIELECTRIC ABSORPTION

The frequency dependence of the real and imaginary parts of the complex dielectric permittivity in different phases will be presented. The relevant results will be given in the isotropic, SmA*, SmC* and crystal phases. The molecular origin of each process will be discussed.

4.2.1 The Isotropic Phase

The dielectric spectrum of normal liquids is characterized by an absorption peak located in the microwave regime [21]. This absorption is related to the dipolar rotational diffusion process. In the case of longitudinal organic molecules, it is expected to resolve two absorptions instead [16]. One of these absorptions is related to the rotational motion around the long axis and the other absorption is due to the rotational motion around the short axis. Due to geometrical reasons, the relaxation frequency of the first one is expected to be higher than the second one [16]. In some cases, these two absorptions could be very close to each other and could be split to two distinct peaks, however, a broad absorption is observed and characterized with a large value of distribution parameter [22-29].

Figure 4.3 shows the frequency dependence of dielectric absorption curve in the isotropic phase. In order to characterise the absorption peak that is strongly overlapped with the high frequency background, Eq. (3.6) has been fitted to the experimental data. The fitting results are listed in Table 1.

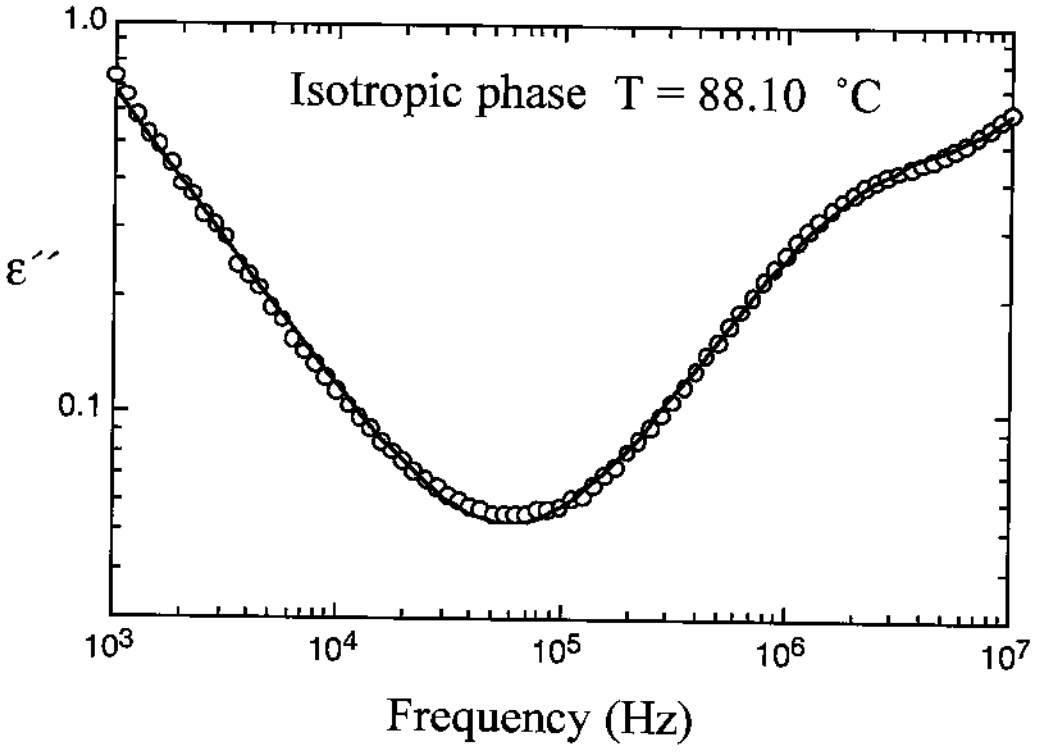

Figure 4.3 Frequency dependence of the dielectric absorption in the isotropic phase. The solid line is the fitting of Eq. (3.6) to the experimental results.

Table I Fitting results of an absorption peak at T = °C in the isotropic phase.

dielectric contribution $\Delta\varepsilon$	0.60
relaxation frequency f_r (Hz)	2.39×10^{6}
distribution parameter α	0.09
conductivity σ (Ω^{-1} cm^{-1})	7.4×10^{-11}
low frequency fitting parameter m	0.77
RC constant of the cell a (sec)	1.4×10^{-10}
high frequency fitting parameter n	0.99

As can be seen from the results in Table 1, the relaxation frequency of the process in the isotropic phase equals to 2.55 MHz and the distribution parameter $\alpha = 0.09$. This value of α does not indicate that there are two *different* overlapped processes, however, it may be attributed to the molecular reorientation around the short axis. The molecular reorientation around the long axis is certainly outside our measurement window and could be observed at several hundred MHz. Moreover, the observed absorption in the isotropic phase has not been assigned to the molecular reorientation around the long axis because this process is characterised by a large value of α (ca 0.2 - 0.4).

In order to characterize the molecular process in the isotopic phase in more details, the measurements have been carried out at a wide temperature interval. The dielectric spectra of the real and imaginary parts are plotted in Figure 4.4 at different temperatures. This set of measurements has been made at temperature step of 0.5 °C. It can be seen that the dispersion and absorption regions are observed above 100 kHz. The fitting results of relaxation frequency, dielectric strength distribution parameters and conductivity are plotted in Figures 4.5.

As illustrated in Figure 4.5a, $\Delta\varepsilon$ decreases with increasing temperature in a linear fashion. This is the expected behaviour as predicated for normal liquid in accordance with the Eq. (2.20). The temperature dependence of the relaxation frequency f_R could be successfully modelled by Arrhenius equation.

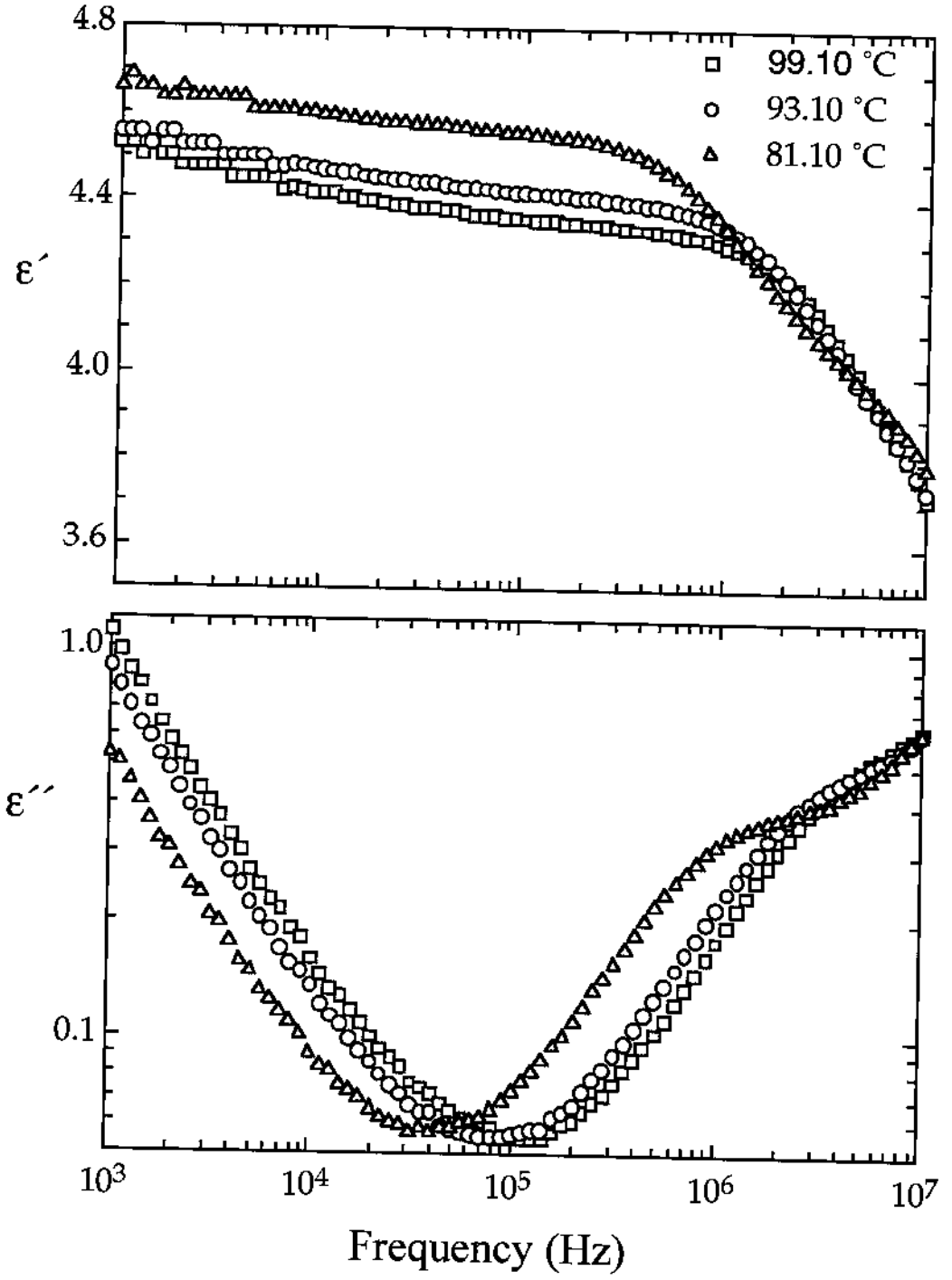

Figure 4.4 Frequency dependence of the real part (upper plot) and imaginary part (lower plot) of the complex dielectric permittivity at different temperatures in the isotropic phase.

$$f_R = f_0 e^{\frac{E_a}{k_B T}} \qquad (4.1)$$

Where f_0 is a constant and E_a is the activation energy. By fitting this equation to the results in Figure 4.5b, it is found that E_a = 0.63 eV. This value of activation energy means that when a molecule flips around the short axis it sees a potential barrier of energy equals to 0.63 eV, a value comparable with that reported in literature [23,27-29]. The values of the distribution parameter at different temperatures are plotted in Figure 4.5c.

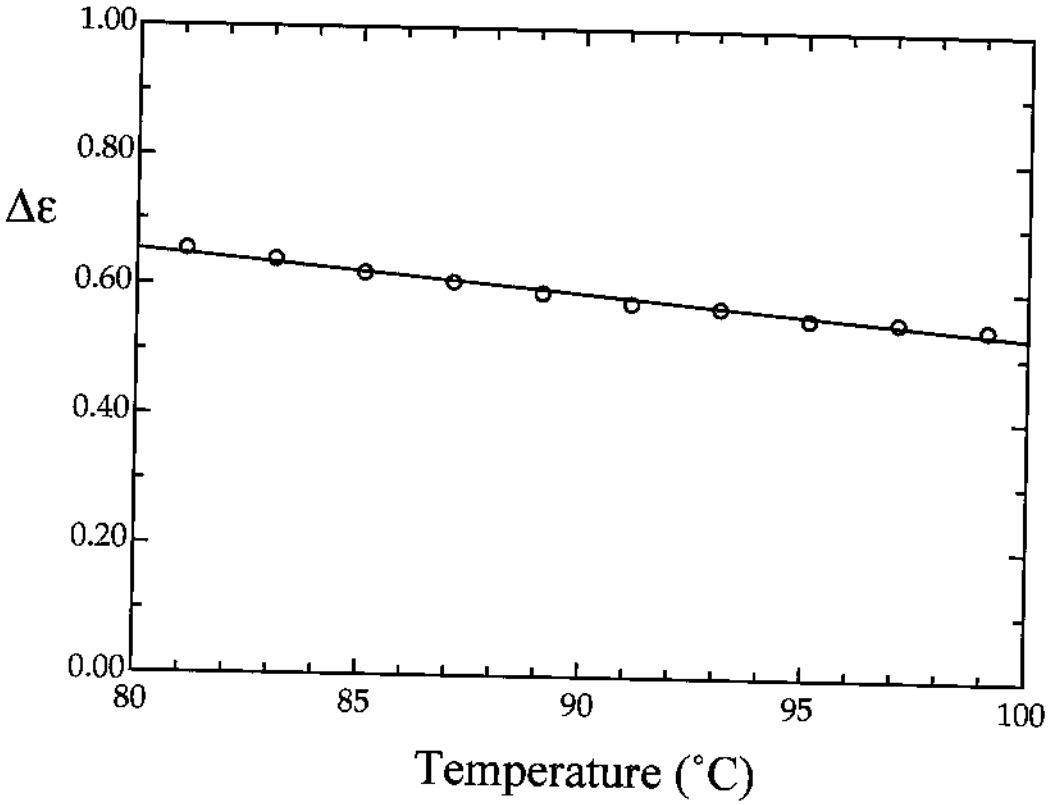

Figure 4.5a Temperature dependence of the dielectric contribution in the isotropic phase.

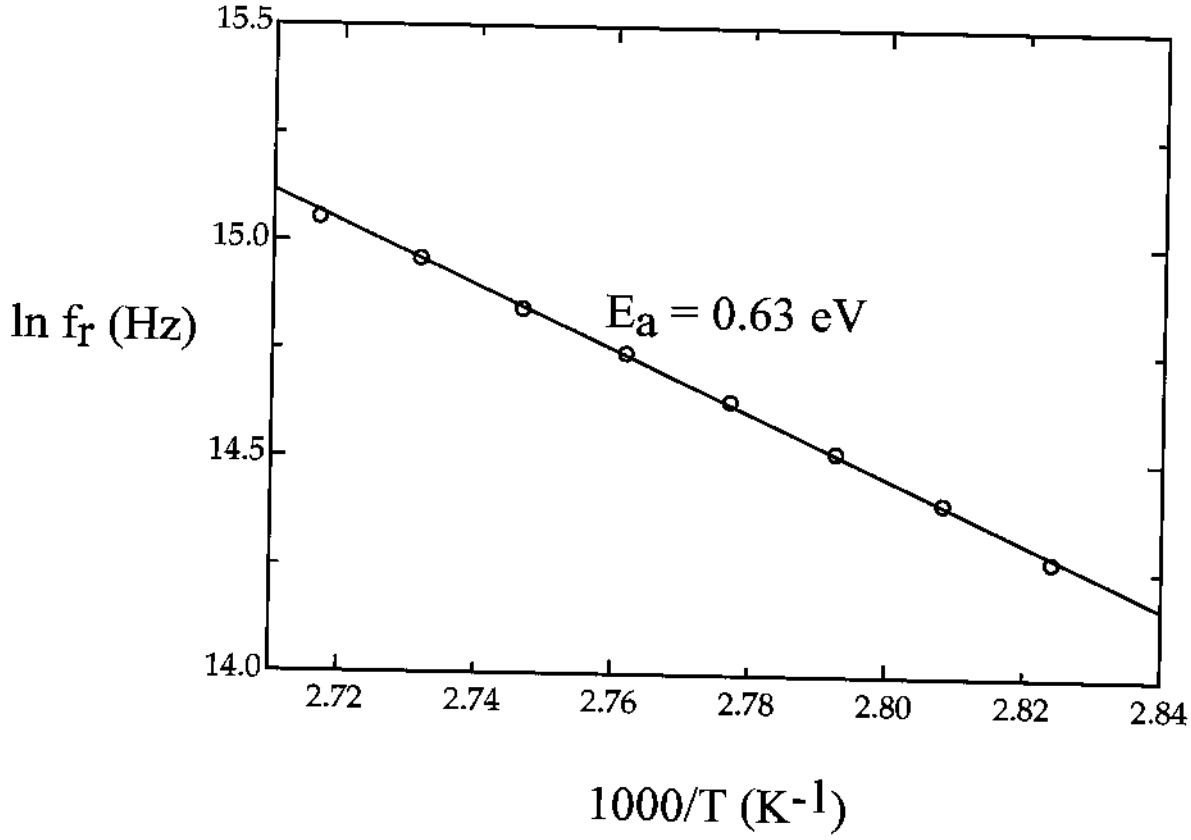

Figure 4.5b Arrhenius plot of the relaxation frequency in the isotropic phase. The value of activation energy is depicted in the figure. The solid line is the best fitting to a linear function.

One would expect that α decreases linearly with increasing temperature as illustrated by the dotted line in the figure. However, this monotonic decrease is found only in a limited temperature interval up to 90 °C, above this temperature a pronounced increase in the values of α is observed. This could be attributed to the overlap of resolved absorption with the high frequency background, thus resulting in a smearing out in the absorption shape which could be manifested in an artefact increase in the distribution parameter. Finally, an important value of the fitting parameters is the conductivity of the sample. As previously explained in chapter 3, this is extracted from the low frequency tail of ε'' versus frequency.

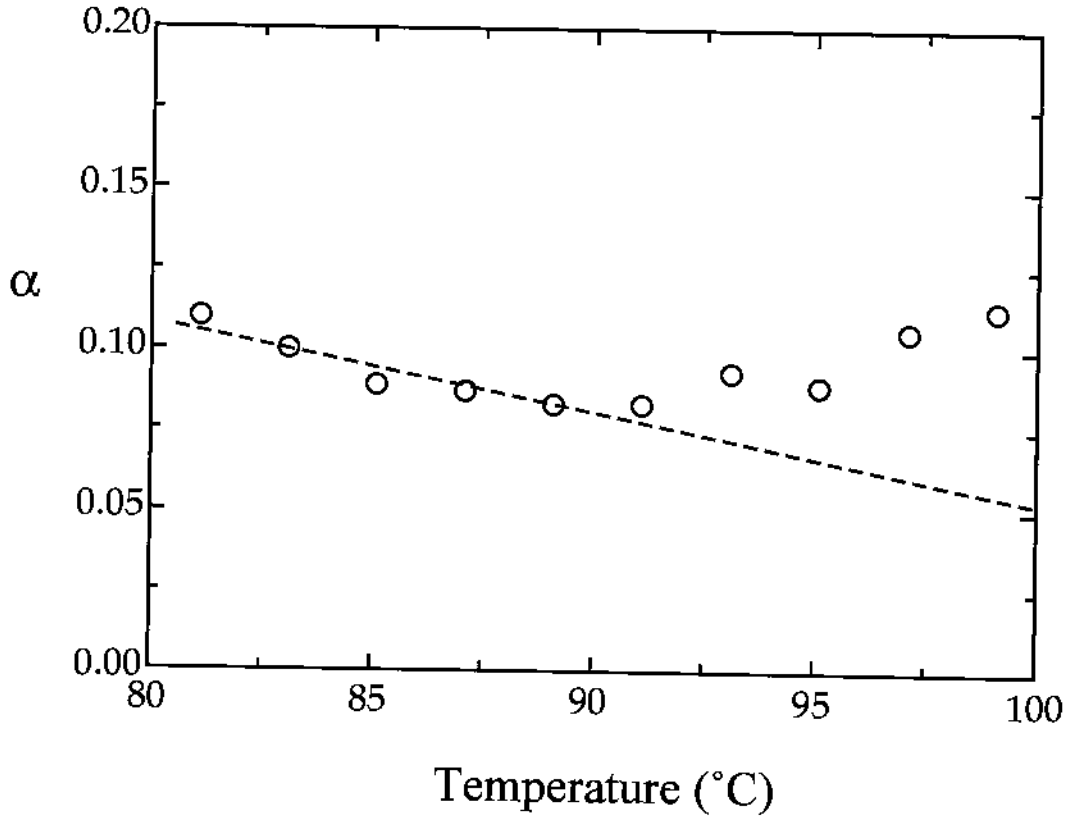

Figure 4.5c Temperature dependence of the distribution parameter in the isotropic phase. The dashed line is plotted for guiding.

The temperature dependence of σ follows an Arrhenius law;

$$\sigma = \sigma_0 e^{\frac{E_a}{k_B T}} \qquad (4.2)$$

The determined activation energy equals to 0.38 eV. It may be noted that the fitting parameter m in Eq. (3.6) deviates slightly from unity and equals to 0.77. The values of conductivity are very close to those reported for standard liquid crystalline materials [30] indicating that the investigated substance is very pure.

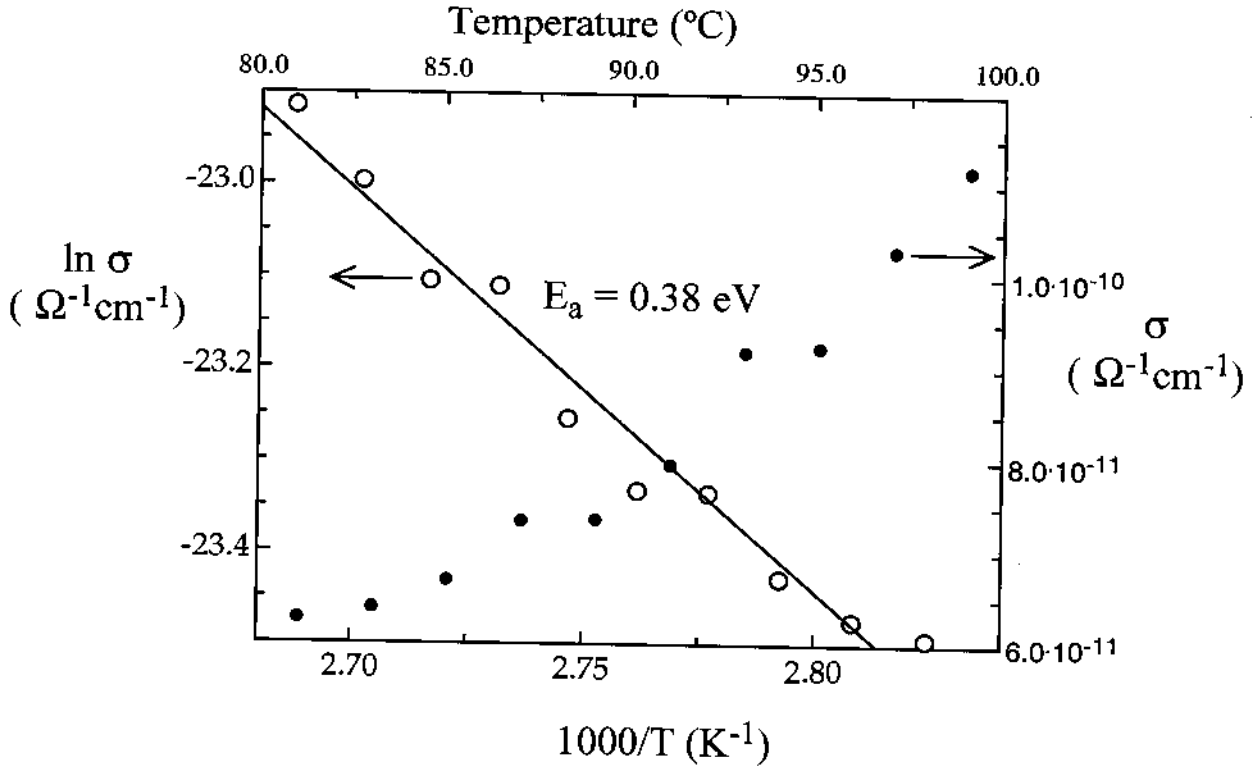

Figure 4.5d. Arrhenius plot of the conductivity in the isotropic phase. The value of activation energy is depicted in the figure.

RESULTS FROM ORIENTED SAMPLES

The dielectric spectroscopy of planar and homeotropic orientations exhibits, in general, completely different absorption peaks. Thus, each measurement geometry has its own "finger print" results. The dielectric spectra of planar sample will be presented in the next section. This will be followed by the respective results in the homeotropic orientation.

4.3 RESULTS FROM PLANAR SAMPLES

4.3.1. The Smectic A Phase (the soft mode dielectric behaviour)*

The frequency dependence of the dielectric dispersion $\varepsilon'(f)$ and dielectric absorption $\varepsilon''(f)$ in the SmA* phase is illustrated in Figure

4.6. The relaxation region is remarkably shifted to lower frequencies when compared with the isotropic phase. In this case, absorption peaks are observed below 1 MHz and its position and amplitude exhibits strong temperature dependence. It can be noted that while the absorption maximum is increasing with decreasing temperature, its relaxation frequency show an appreciable decrease. This is a typical behaviour for dielectric behaviour of the *soft mode (tilt-fluctuations)* [31-38]

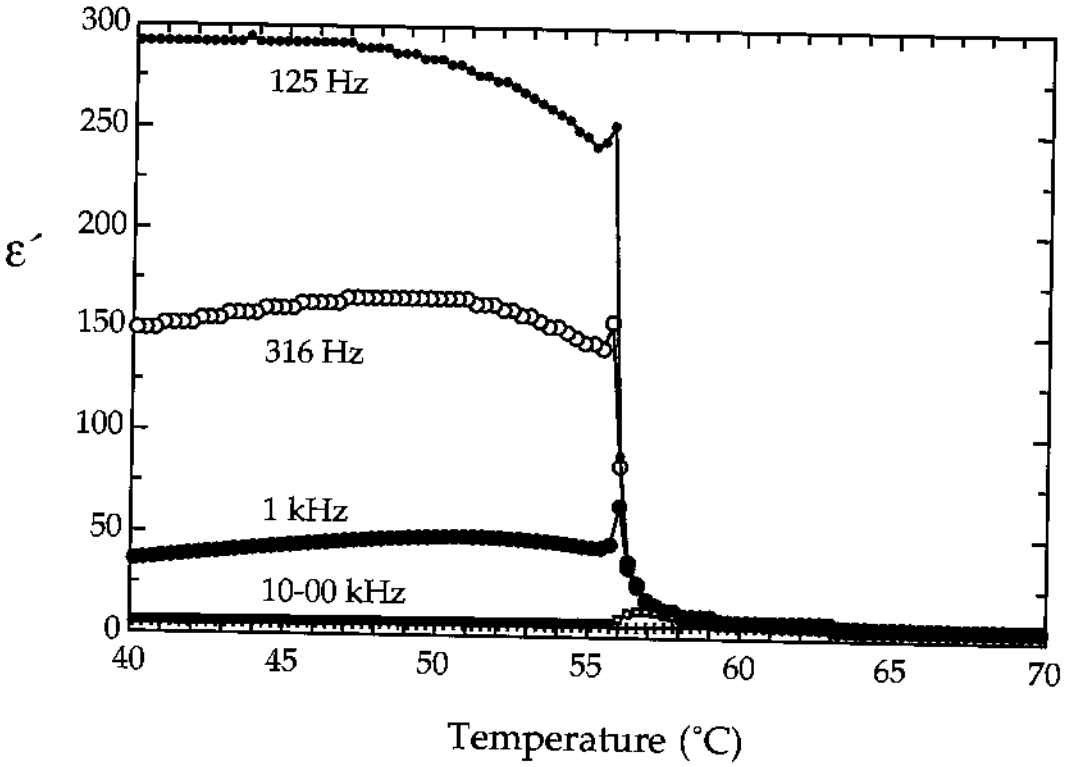

Figure 4.6 Temperature dependence of the dielectric permittivity in the smectic A* and C* phases.

The experimental results have been fitted to the Cole-Cole equation (with one absorption) beside the low and high frequency backgrounds.

The temperature dependence of the dielectric contribution, relaxation frequency and distribution parameter in the SmA* phase is shown in Figure 4.7. It may be noted that the values of $\Delta\varepsilon_S$ increases with decreasing temperature, and diverge with cut-off at the smectic A* to smectic C* transition (T_C). According to Curie-Weiss law, the reciprocal of $\Delta\varepsilon_S$ varies linearly with temperature. In our case, as can bee seen from figure 4.7(b), $1/\Delta\varepsilon_S$ reveals an almost a linear temperature dependence. The values of $\Delta\varepsilon_S$ have been fitted to the relation

$$\Delta\varepsilon_S = \frac{\varepsilon_0\varepsilon_\infty^2 C^2}{\alpha(T-T_C)^\gamma + Kq_0^2} \qquad (4.3)$$

where γ is a critical exponent accounting for the slight deviation from linearity. From fitting γ is found to be 1.21, a value which is slightly different from the Curie-Weiss law with γ=1.

Figure 4.7(d) shows the temperature dependence of the soft mode relaxation frequency in the SmA* phase. It is clearly demonstrated that f_S varies in a non-linear fashion with temperature. The non-linearity in the f_S (T) is much more pronounced compared with $1/\Delta\varepsilon_S$ (T).

Theoretically, the temperature dependence of the soft mode relaxation frequency is given by [19]

$$f_S = \frac{1}{2\pi\gamma_\theta}\left[\alpha(T-T_C)+Kq_0^2\right] \qquad (4.4)$$

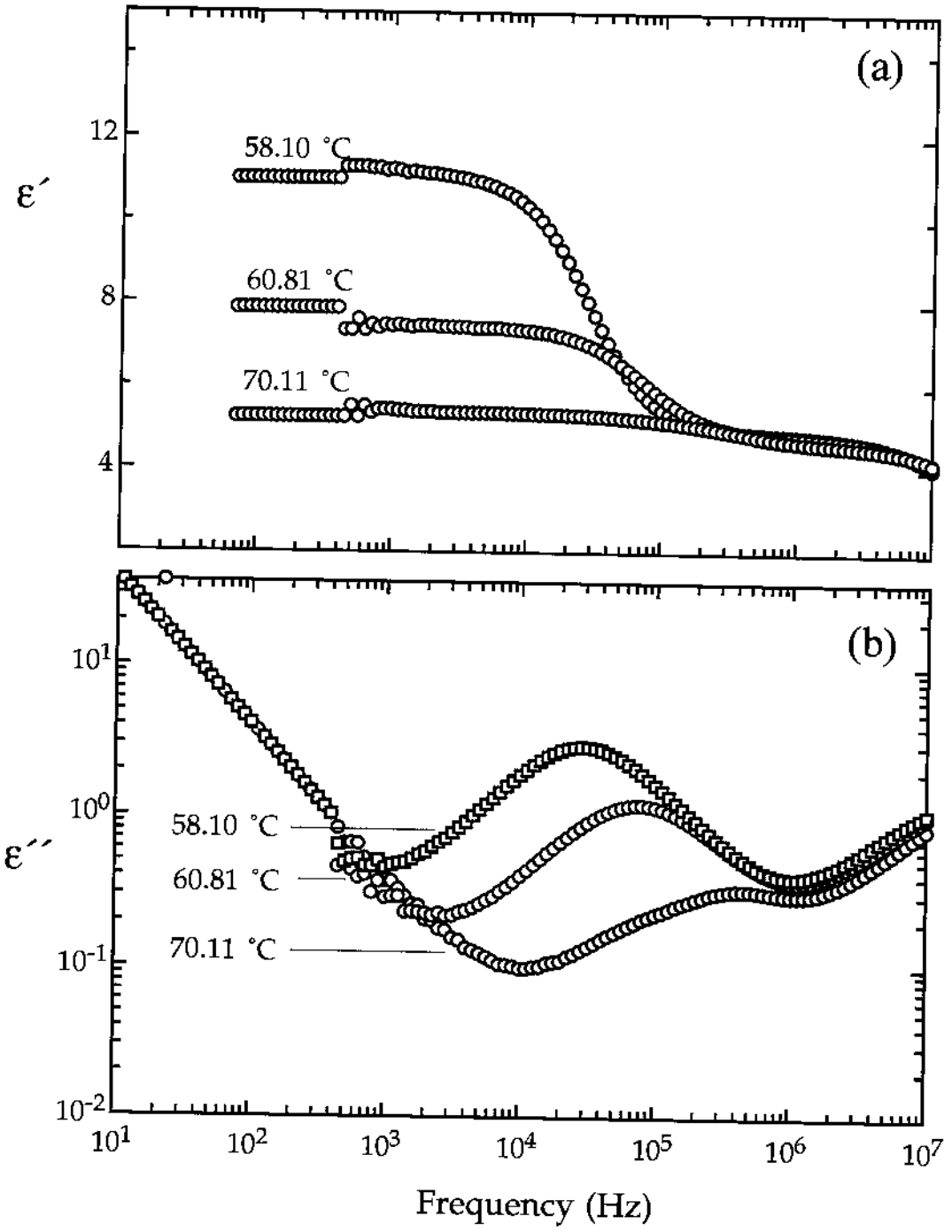

Figure 4.6 Frequency dependence of the real part (a) and imaginary part (b) of the complex dielectric permittivity in the smectic A* phase.

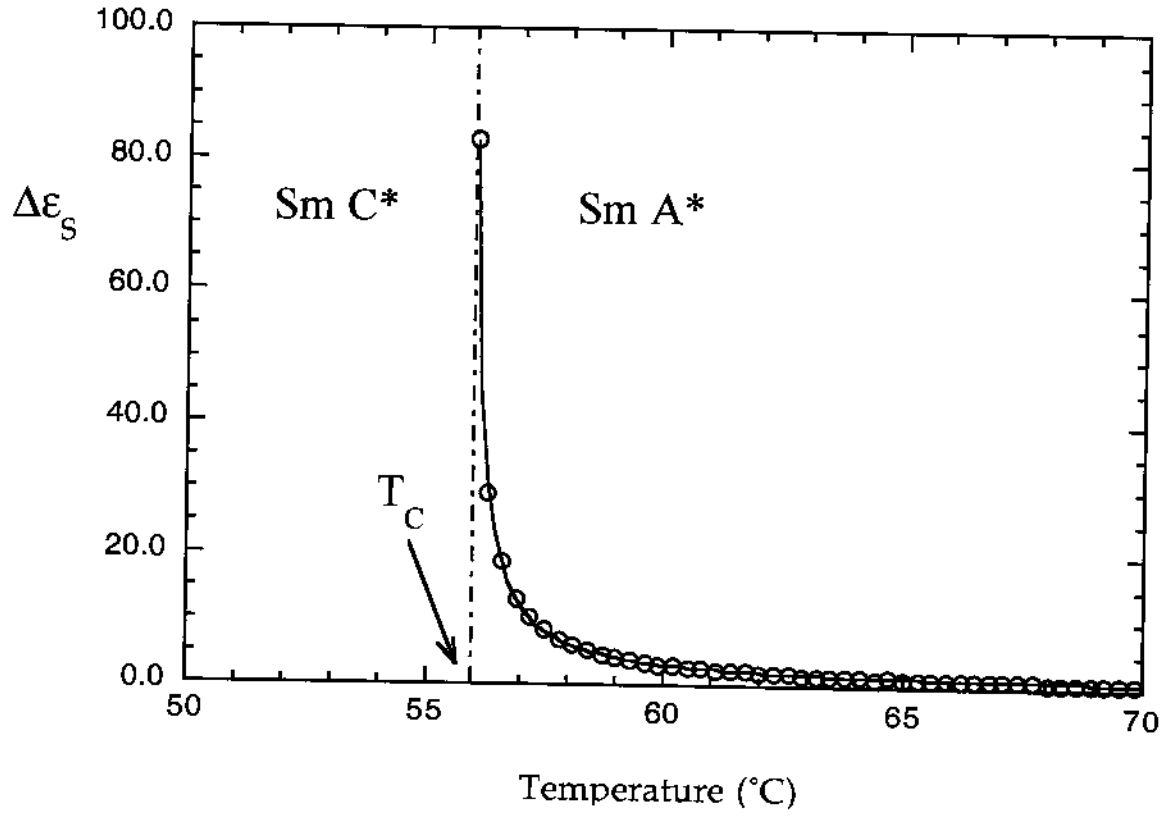

Figure 4.7(a) Temperature dependence of the soft mode dielectric contribution $\Delta\varepsilon_S$ in the smectic A* phase. The solid line is fitted according to Eq. (4.3)

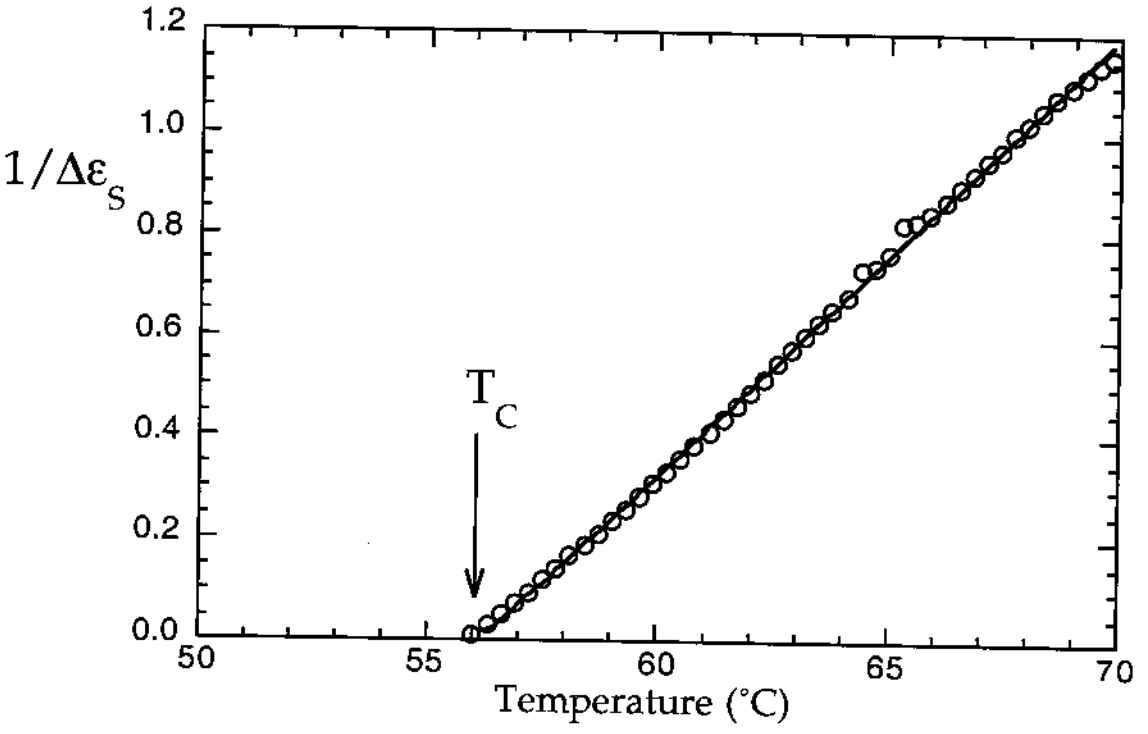

Figure 4.7(b) Temperature dependence of the inverse soft mode dielectric contribution $1/\Delta\varepsilon_S$ in the smectic A* phase. The solid line is fitted according to Eq. (4.3)

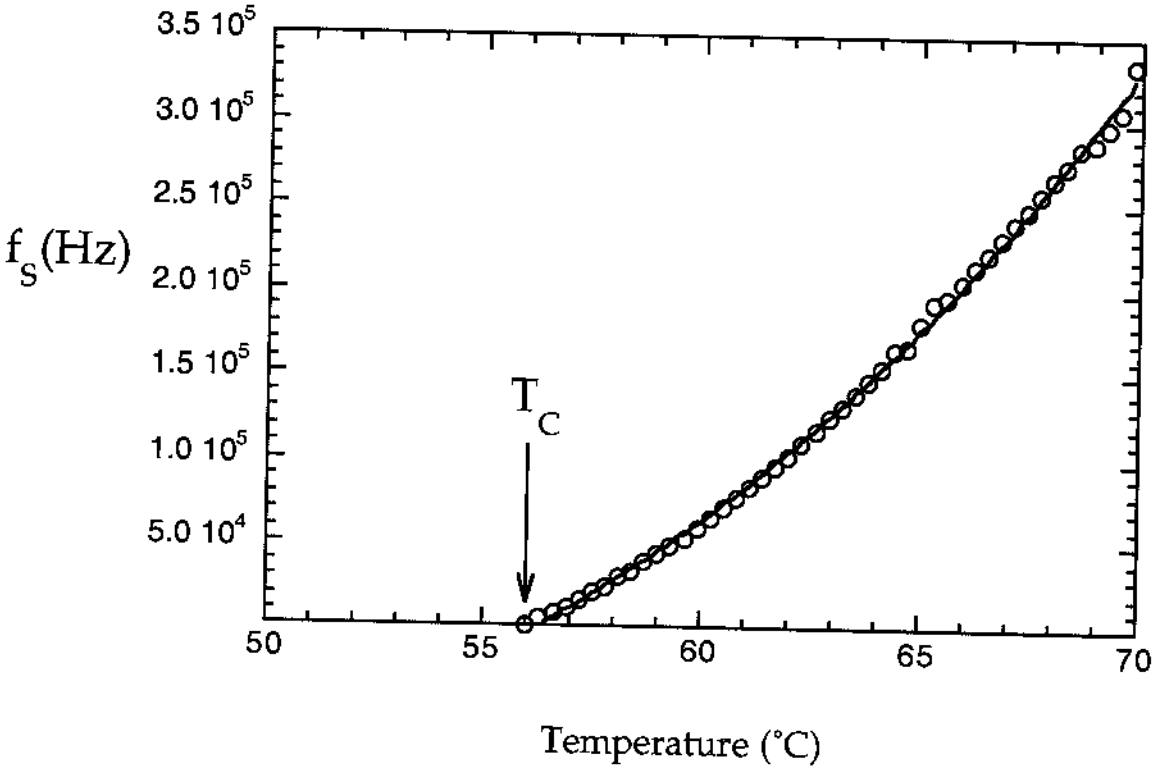

Figure 4.7(c) Temperature dependence of the soft mode relaxation frequency f_S in the smectic A* phase. The solid line is fitted according to Eq. (4.4)

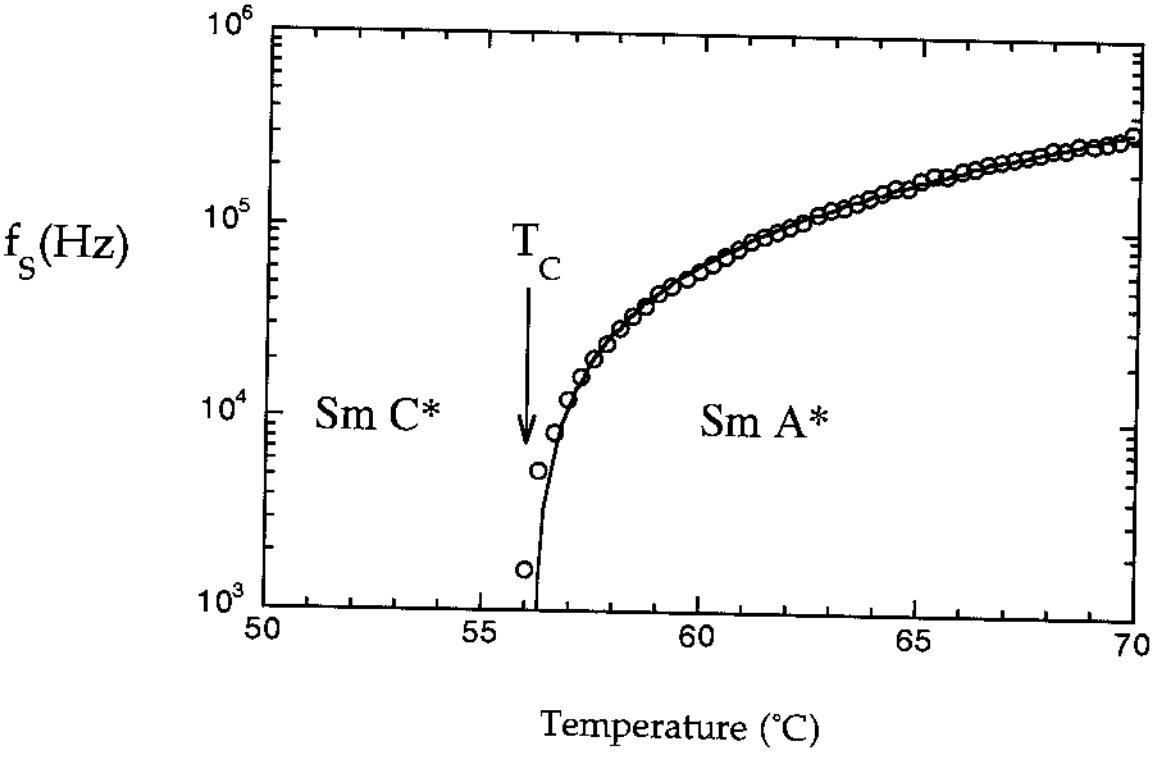

Figure 4.7(d) Temperature dependence of the soft mode relaxation frequency f_S in the smectic A* phase. (Log-linear plot). The solid line is fitted according to Eq. (4.4)

In order to fit Eq. (4.4) to the experimental results shown in figure 4.7(c) the coefficient of rotational viscosity must be given by the well-known Arrhenius equation. Thus, Eq. (4.4) can be rewritten as

$$f_S = \frac{1}{2\pi\gamma^0 e^{\frac{E_a}{k_B T}}}\left[\alpha(T - T_C)^\gamma + Kq_0^2\right] \qquad (4.5)$$

where E_a is the activation energy listed with other fitting parameters in Table II. As can be seen from figure 4.7(c), an excellent fit is obtained. Thus, indicating that the soft mode rotational viscosity can successfully be modelled by Arrhenius equation. As will be shown latter that a modification of Arrhenius equation of γ_θ is needed to describe the exact temperature dependence over a broad temperature interval.

Table II Fitting results of the temperature dependent of the soft mode relaxation frequency in the in the smectic A* phase. Note that the fitting constant α is different from the distribution parameter in the Cole-Cole equation.

$\alpha/(2\pi\gamma_0)$	$9.4\text{x}10^9$
Transition temperature T_C(°C)	56.09
Activation energy (eV)	0.38
kq_0^2/α	0.08

It may be noted that different forms of Eq. (4.5) do not give a good fit even by assigning an exponent to the $(T - T_C)$ term.

4.3.2 *The Smectic C* Phase (the Goldstone dielectric behaviour)*

The dielectric response in the SmC* phase is characterised by a large value which is attributed to the director phase fluctuations (the Goldstone mode) [20,31-41]and director tilt fluctuations (the soft mode). By comparing the dielectric permittivity in the SmC* phase (see figure 4.8) and SmA* phase (figure 4.6) it can be seen that the Goldstone mode contribution in the SmC* phase, in general, is larger than the soft mode contribution by almost two orders of magnitude.

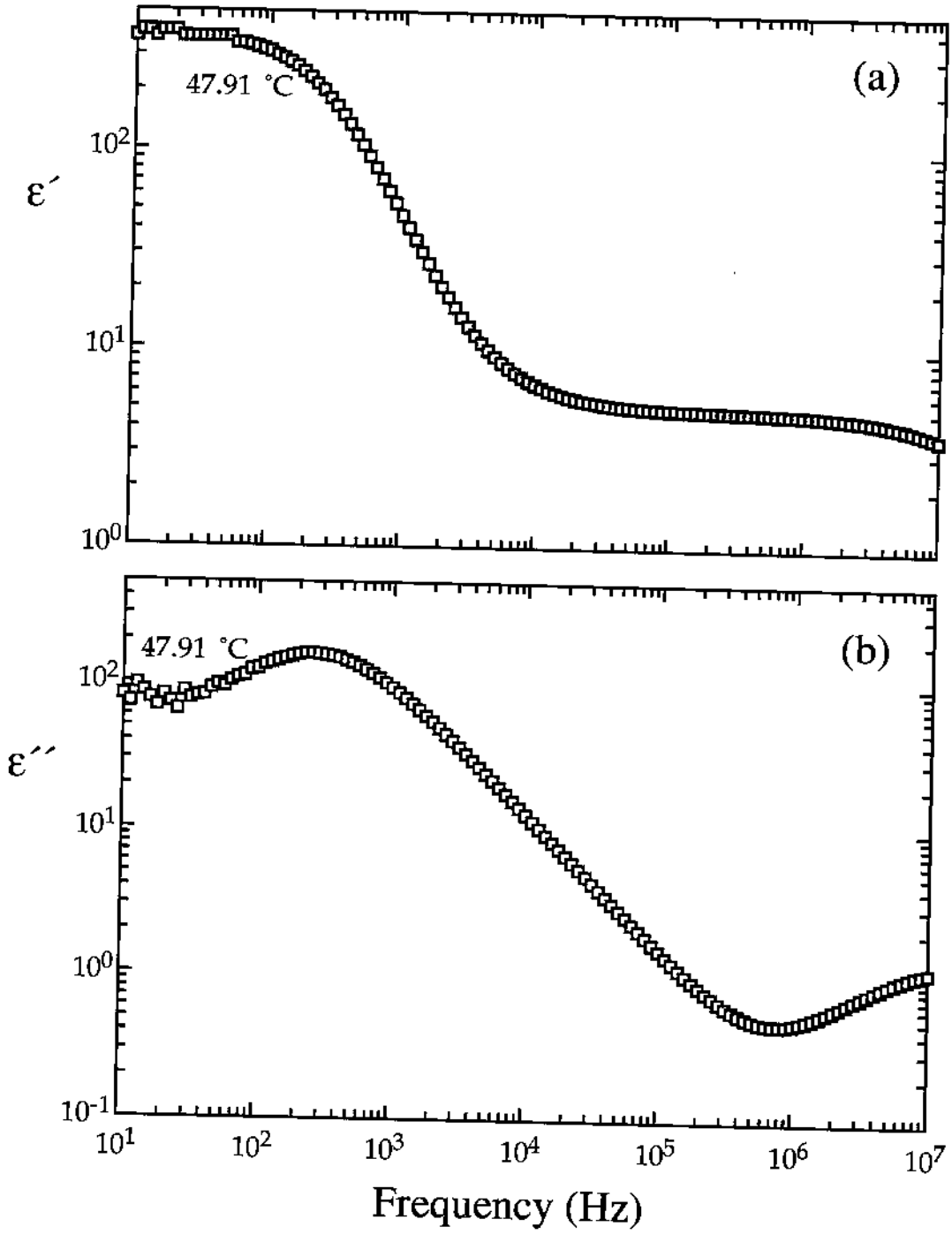

Figure 4.8 Frequency dependence of the real part (a) and imaginary part (b) of the complex dielectric permittivity in the smectic C* phase.

The dielectric dispersion (4.8a) and dielectric absorption (4.8b) of the complex permittivity in the Sm C* phase illustrated in figure 4.8. From the location of the absorption maximum in the spectra, it can be

concluded that the relaxation frequency of the Goldstone is characterised by a low relaxation frequency. The dielectric contribution $\Delta\varepsilon_G$, the relaxation frequency f_G and the distribution parameter α_G have been determined by fitting the Cole-Cole equation with the background terms to the experimental results in figure 4.8(b). The temperature dependence of $\Delta\varepsilon_G, f_G$ and α_G are shown in figure 4.9.

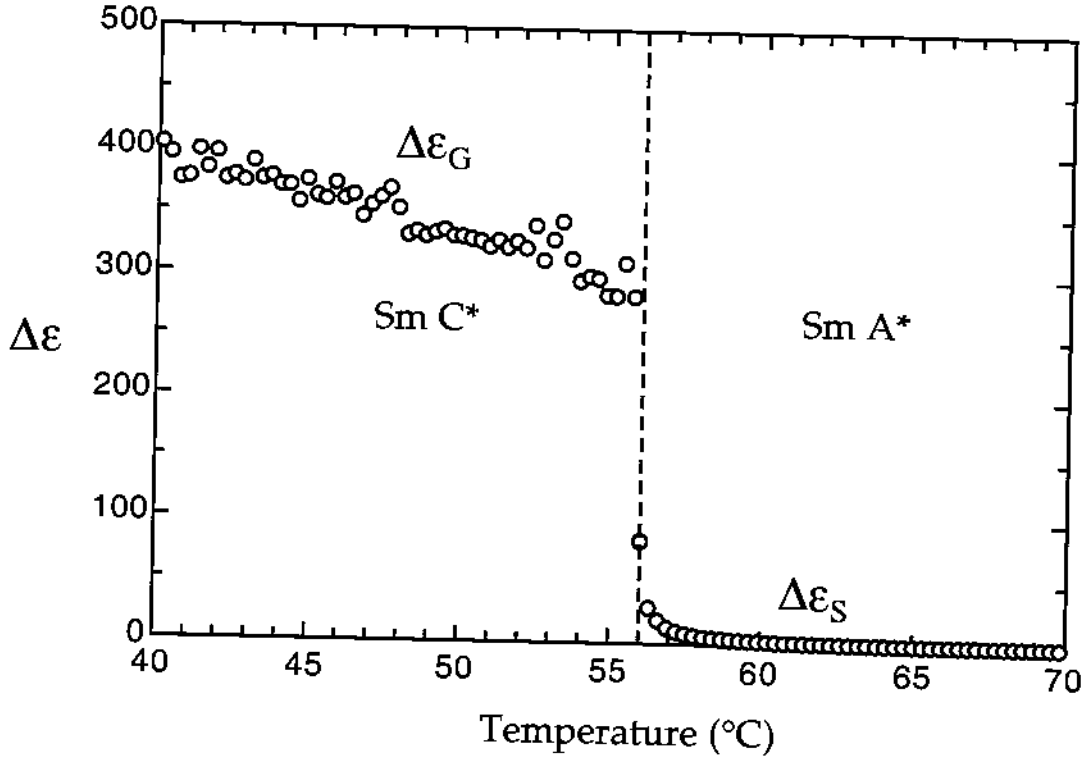

Figure 4.9a Temperature dependence of the Goldstone mode $\Delta\varepsilon_G$ and the soft mode $\Delta\varepsilon_S$ dielectric contribution in the smectic C* and A* phases, respectively.

In order to compare the dielectric contributions of the Goldstone mode and the soft mode, values of $\Delta\varepsilon_S$ are plotted in figure 4.9a.

The relaxation frequency of the Goldstone is plotted in figure 4.9b. The values of soft mode relaxation frequency exhibits a slowing down behaviour with temperature with cut-off at the transition temperature to the Sum C* phase. The relaxation frequency of the Goldstone mode is

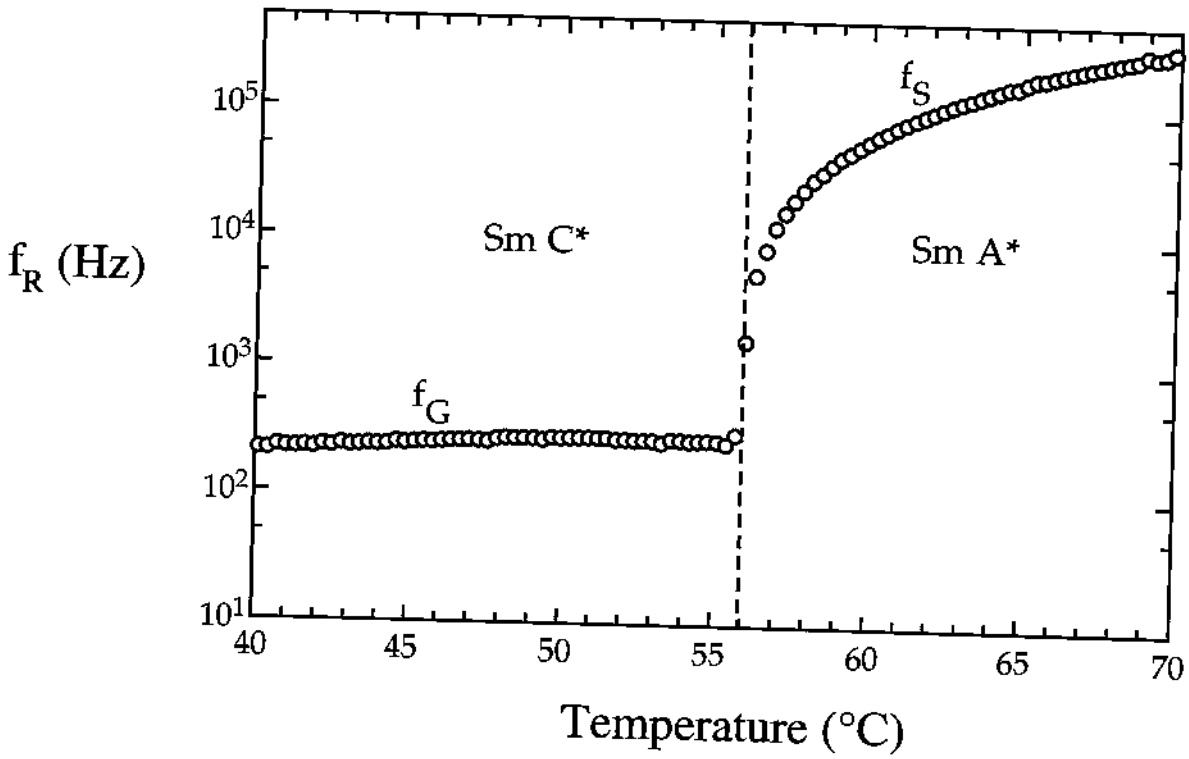

Figure 4.9b Temperature dependence of the Goldstone mode f_G and the soft mode f_S dielectric contribution in the smectic C* and A* phases, respectively.

about 300 Hz and exhibits a weak temperature dependence. It may be noted that f_G and f_S differs at T_C by almost one order of magnitude.

4.3.3 The Molecular Reorientation Around the Long Axis

Due to its rod-like geometry, each molecule is characterised by two main axes; one longitudinal and every axis perpendicular to it, i.e. an infinitely degenerate transversal axis. As pointed earlier in chapter 2, each molecule is rotating around these two axes. These two rotations are manifested in the dielectric spectrum by two absorptions [22-29]. with different frequencies.

The best way to detect the molecular rotation around the long axis of molecule is to prepare a sample with planar orientation, i.e. in the SmA* and SmC* phases the smectic layers are essentially perpendicular to the cell plates. In this case, the measuring electric field "sees" the maximum contribution of the perpendicular component of the permanent dipole moment rotating around the long axis of molecule. Usually this molecular process is characterised by a relaxation frequency in the high MHz region [28] which is above our measurement window. However, since this process is thermally activated, its relaxation frequency decreases at lower temperatures.
Figures 4.10 shows the frequency dependence of the dielectric absorption at different temperatures in the SmC* phase. All the data have been fitted and analysed by the Cole-Cole function and the fitting results are plotted in figure 4.11. It can be seen from the figure 4.10 that the dielectric absorption connected with the rotation around

the long axis is observed at temperatures below 46 degrees. Above this temperature, the low frequency tail of absorption peaks could be measured. It may be noted that at frequencies below 300 kHz the increase in the dielectric absorption is related to the residual absorption (high frequency tail) of the Goldstone mode. In the fitting equation this part was expressed as $1/f^n$ where n is a fitting parameter. Although the high frequency part of the spectra is strongly overlapped with the ITO absorption, nevertheless the fitting at all temperatures was excellent and the fitting parameters of the molecular process ($\Delta\varepsilon$, f_R and α) are physically accepted.

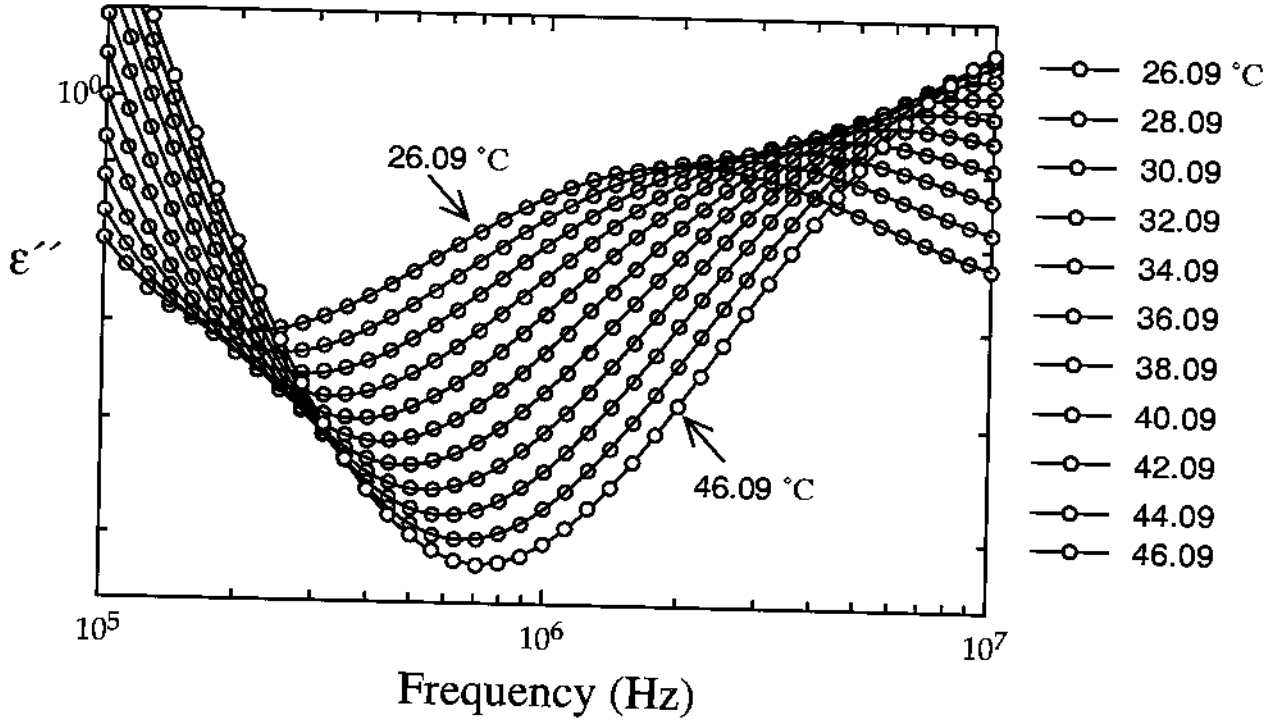

Figure 4.10 High frequency region of the dielectric absorption in the planar orientation at low temperatures in the SmC* phase. The solid line is the fitting of Cole-Cole equation to the experimental values.

Figure 4.11(a) shows the temperature dependence of the relaxation frequency of the molecular reorientation around the long axis. The values increase from 2 MHz to 12 MHz over a temperature interval of 20 degrees. The temperatures dependence of f_R could be successfully modelled by Arrhenius equation as illustrated in figure 4.11(b). By fitting Eq. (1) to the values of f_R at different temperatures, the activation energy is found to be 0.23 eV. This value agrees well the results in literature for similar systems [22-26]. This value of activation energy represents the energy barrier that is "seen" by a molecule when it is reorienting around its long axis. As it will be discussed in the next section, this value of activation energy is less than the activation energy of the molecular reorientation around the short axis.

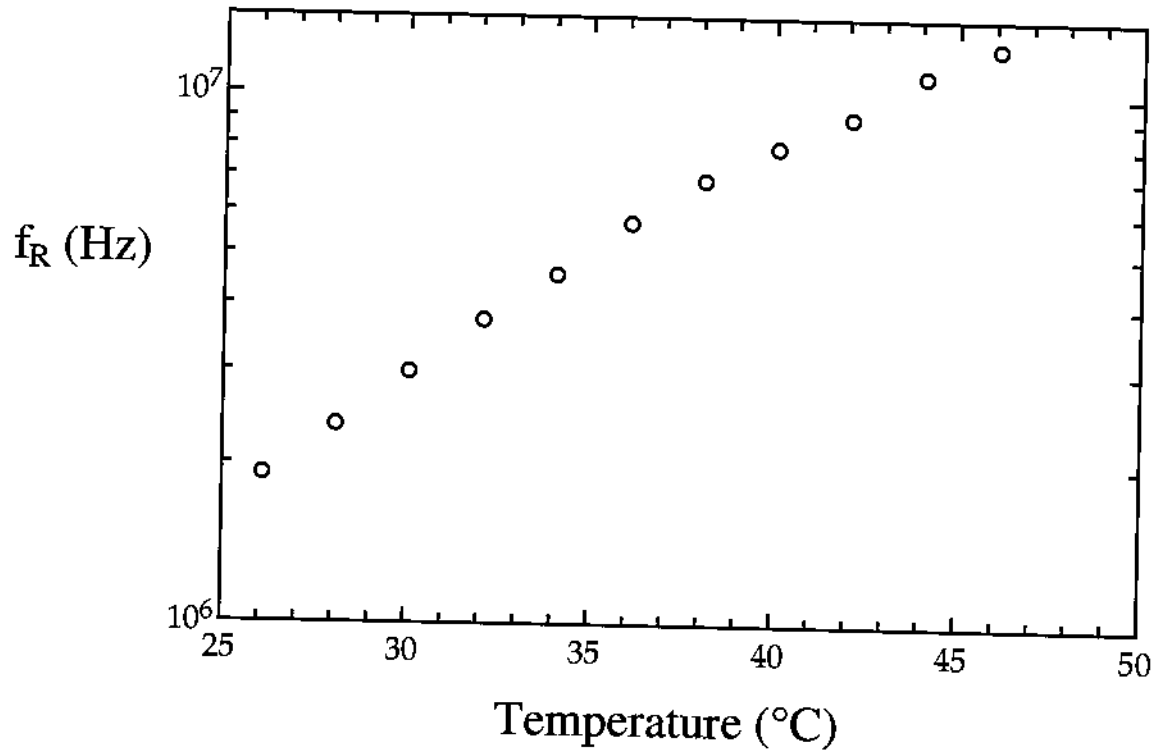

Figure 4.11(a) Temperature dependence of the relaxation frequency of the molecular reorientation around the long axis.

In figure 4.11(c) the values of dielectric strength and distribution parameter are plotted as a function of temperature. By cooling from 46 °C to 34 °C, $\Delta\varepsilon$ exhibits a very weak increase and at lower temperatures it decreases slightly.

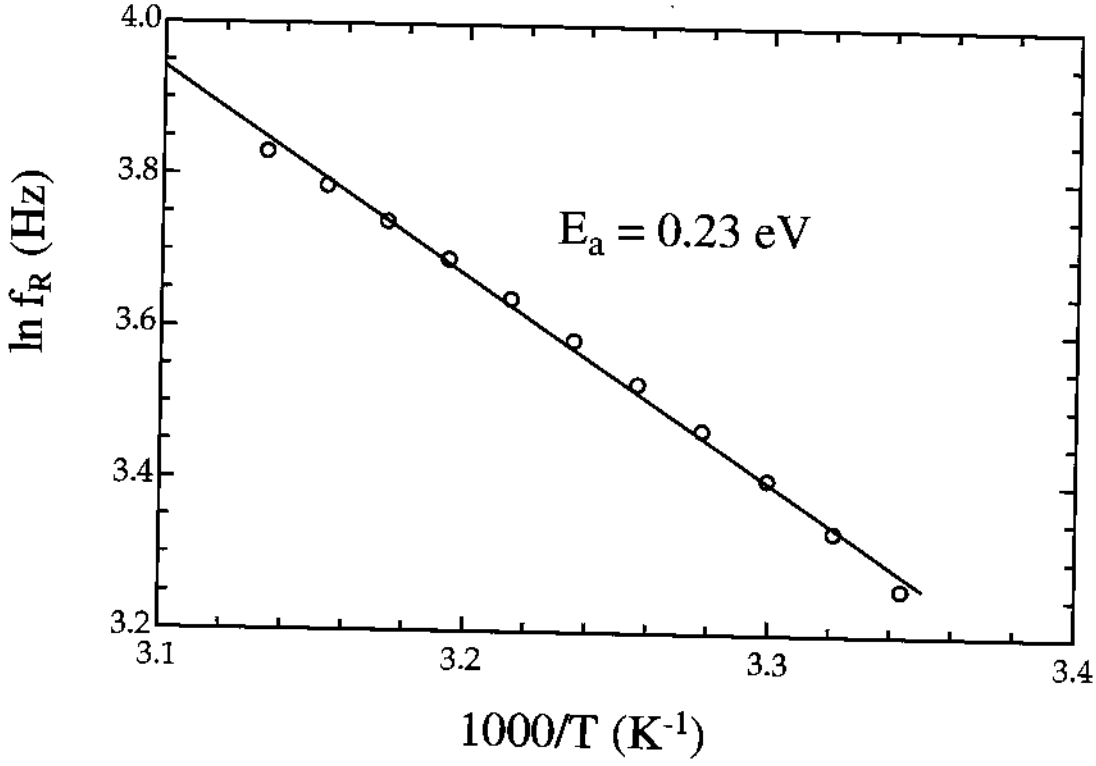

Figure 4.11(b) Arrhenius plot of the relaxation frequency of the molecular rotation around the long axis.

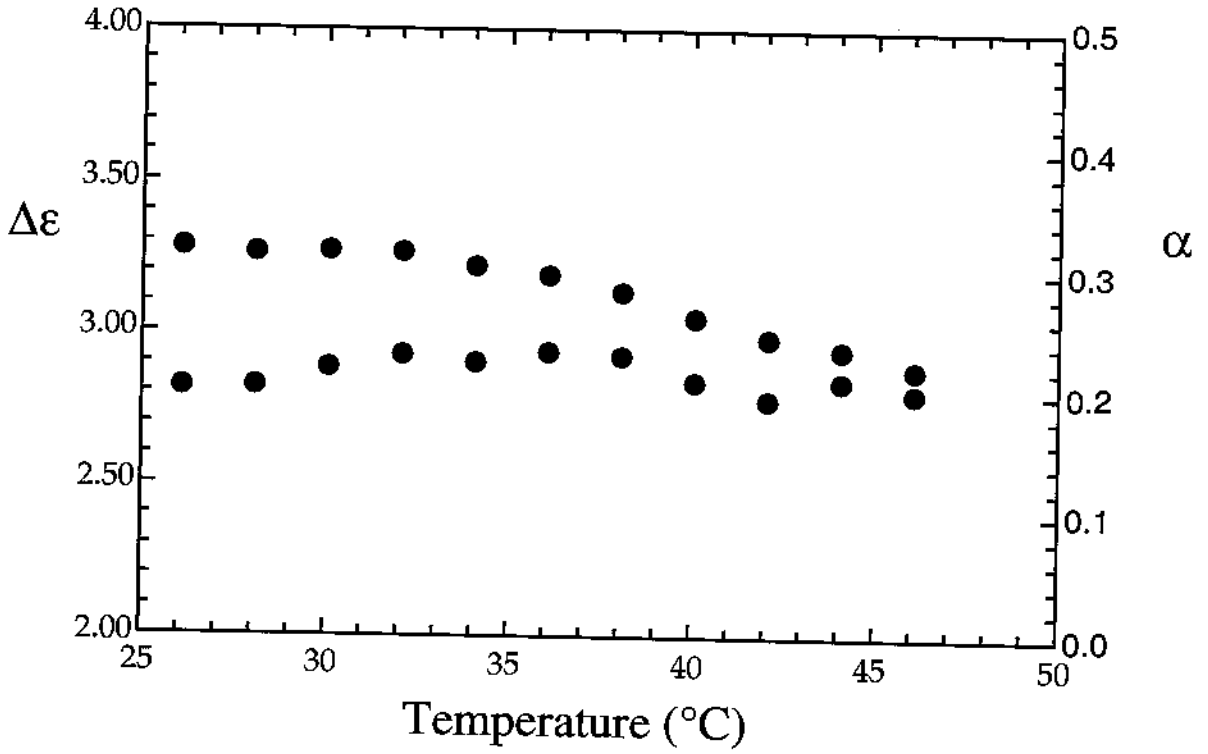

Figure 4.11(c) Temperature dependence of the dielectric contribution (blue points) of the molecular reorientation around the long axis (to the left) and the corresponding distribution parameter (red points, to the right).

At lower temperatures below 34 °C, $\Delta\varepsilon$ decreases slightly, a behaviour which could be attributed to the onset of crystallization in the sample. This argument is confirmed by disappearance of any absorption peak at lower temperature. Moreover, from the texture observations in polarizing microscope has further confirmed this conclusion.

The distribution parameter, as illustrated in figure 4.11(c), increases with decreasing temperature. The values of α are relatively large ca 0.30. In this context, it is important to stress that this large value of α is typical for the molecular reorientation around the long axis, contrary to the molecular reorientation rotation around the short

axis characterised by a single relaxation time, i.e. α equals zero. The large value of distribution parameter could be attributed to the following mechanisms:

- The overall rotation of molecule around its long axis.
- The intra-molecular reorientation of the alkyl group around the single bond attached with neighbouring benzene ring.
- Small angle reorientation of the permanent dipole moment around the director.

Thus, the rotation around long axis is complicated and indicates that the molecule is considered to be very *flexible*. The increase in distribution parameter on cooling could be attributed to the increase in sample density. This means that the collision rate between molecules will increase, thus resulting gin a broadening of absorption.

4.3.4 *Three Dimensional Representation of the ε′(f,T) and ε″(f,T) in Different Phases*

In figure 4.12, a 3D representation of the dielectric permittivity (4.12(a)) and dielectric absorption (4.12(b)) is shown. In both plots the smectic A* to C* transition is clearly observed. If we focus our attention to the absorption curves in figure 4.12(b), we can see the following processes:

In the smectic A* phase, the absorption maximum increase on cooling and their positions are shifted to lower frequencies (see figure

4.12(c)). This is a connected with the collective tilt-angle fluctuations of the director (the soft mode).

In the smectic C* phase, the location and amplitude of the absorption curves exhibit a weak temperature dependence. Moreover, the relaxation frequency is low and the absorption maximum is high. These absorptions are attributed to the collective phase fluctuations of the director (the Goldstone mode).

A new absorption is observed at the high frequency side of the spectrum and shifted slightly to lower frequencies and its amplitude increases at low temperatures. This absorption could be attributed to the molecular reorientation around the long axis of molecule.

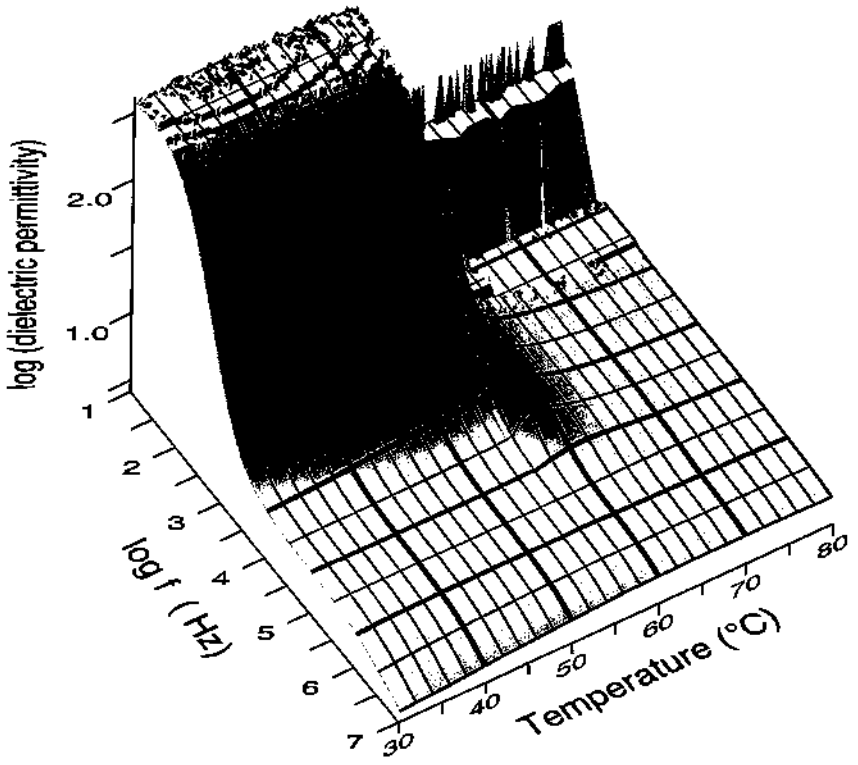

Figure 4.12(a) Temperature and frequency dependence of the dielectric dispersion in the smectic A* and C* phases.

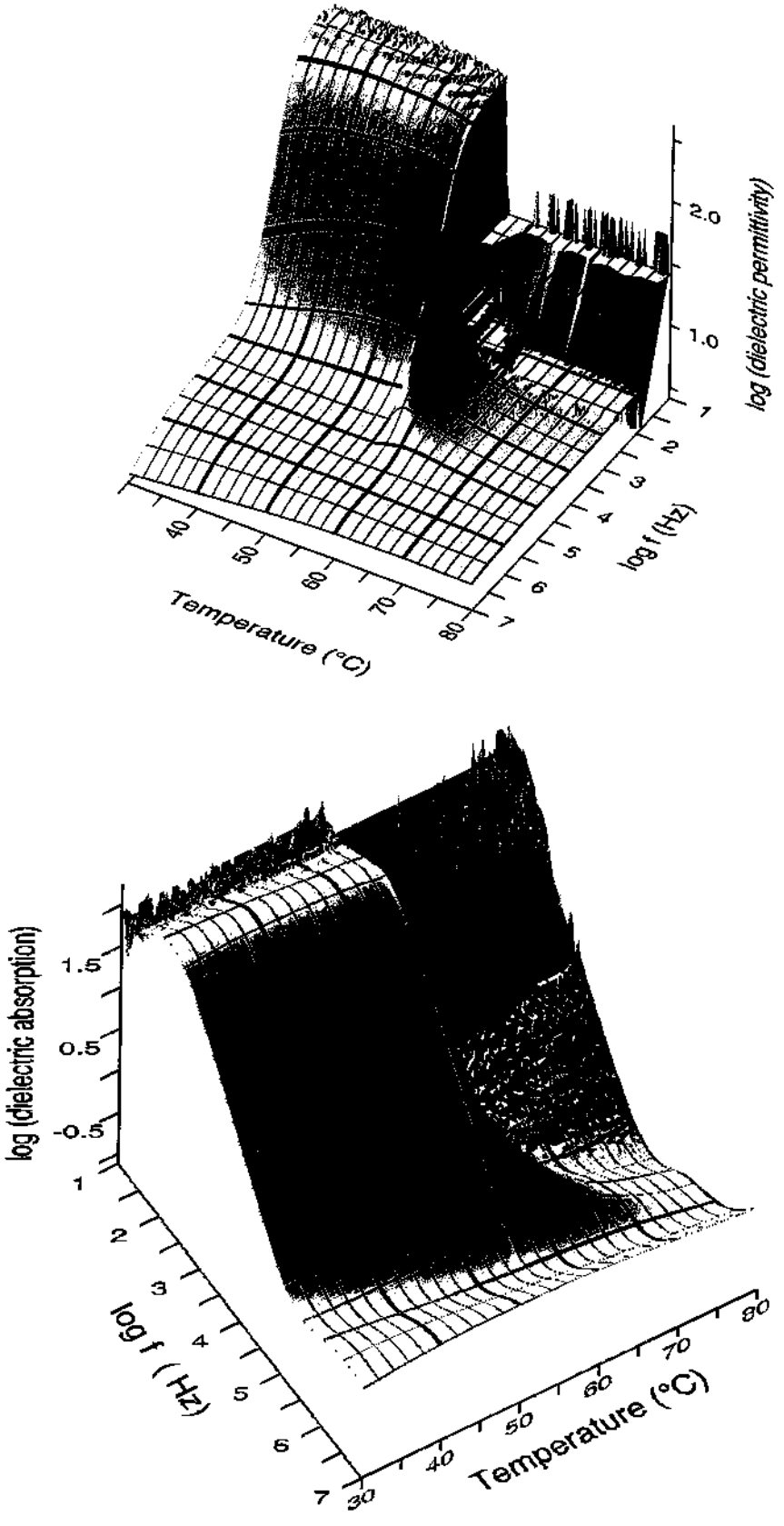

Figure 4.12(b) Temperature and frequency dependence of the dielectric absorption in the smectic A* and C* phases.

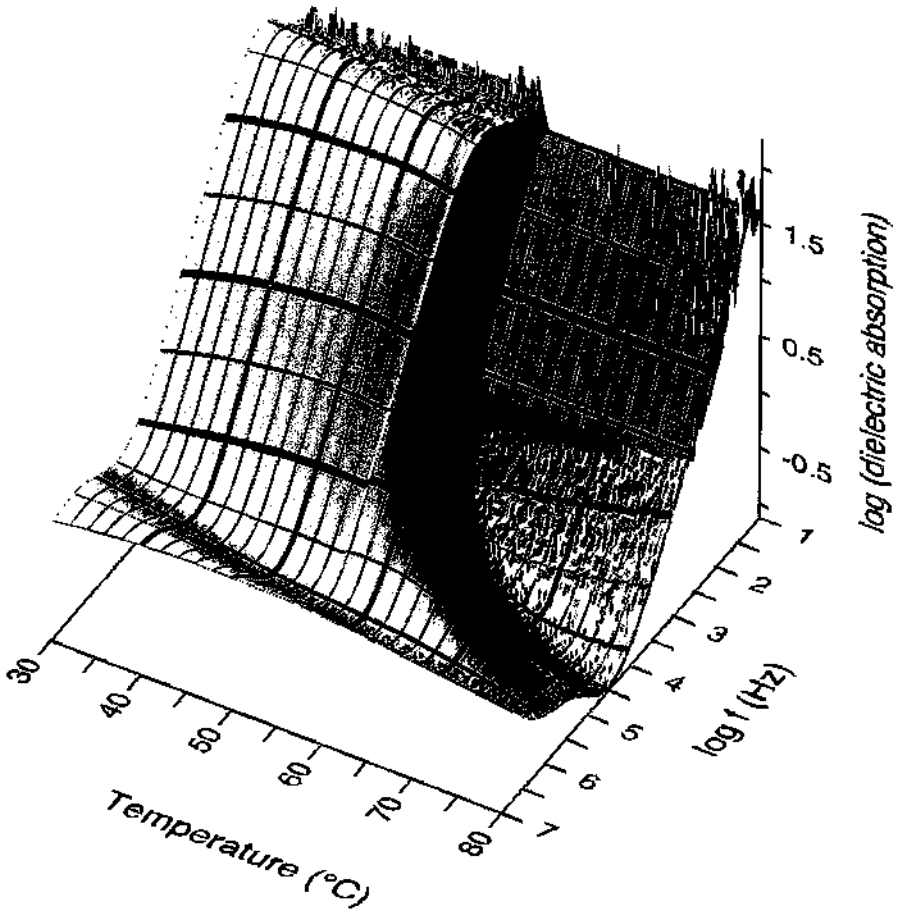

Figure 4.12(c) Temperature and frequency dependence of the dielectric absorption in the smectic A* and C* phases. The spectra is plotted from the smectic A* phase side.

The molecular aspect of the three processes described previously is summarised and depicted in figure 4.12(d).

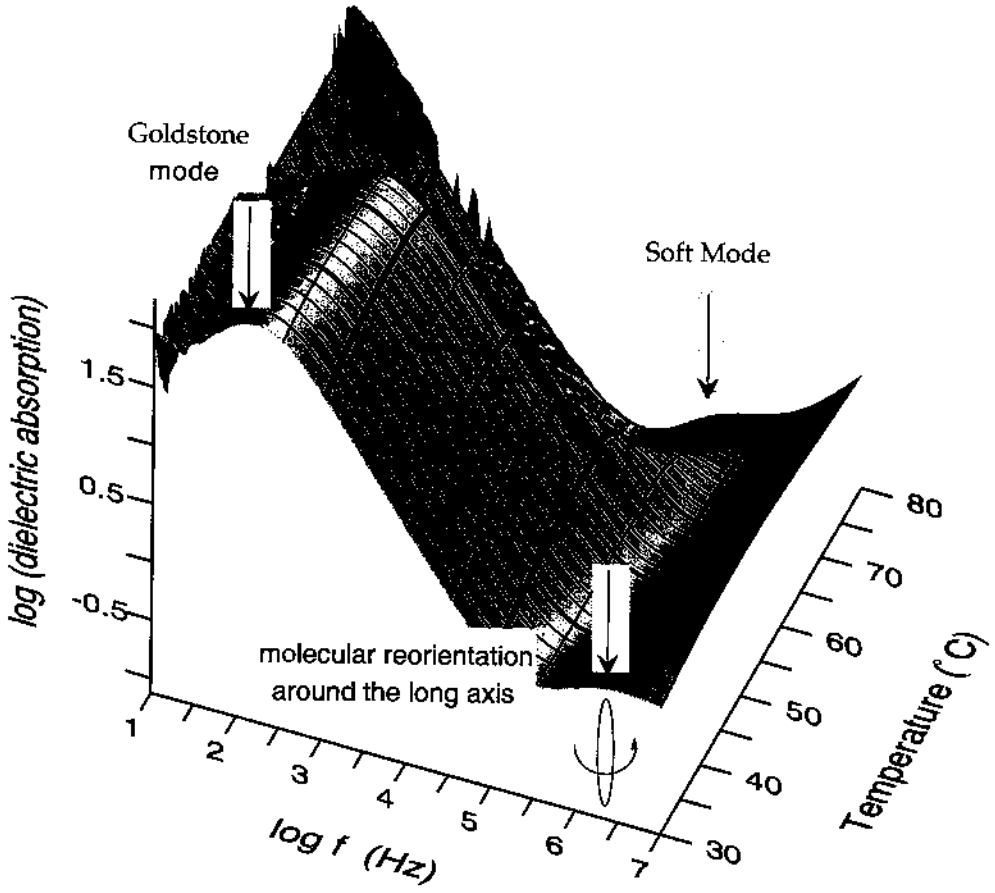

Figure 4.12(d) Molecular assignment of the three absorption curves in the smectic A* and C* phases.

4.3.5 Rotational Viscosities in the Smectic A* and C* Phases

Using dielectric relaxation spectroscopy, it is possible to determine the values of rotational viscosity tensor corresponding to the three Euler angles in the SmA* and SmC* phases. The viscosity coefficients (γ_θ, γ_φ, γ_l) are active in the tilt fluctuations (the soft mode) the phase fluctuations (the Goldstone mode, and the molecular reorientation around the long axis of the molecules, respectively). In the present work, the rotational viscosity coefficients γ_θ and γ_φ have only been determined. The switching time in all electrooptic devices based on the SmA* and SmC* materials are strongly dependent on the viscosity coefficients γ_θ and γ_φ. Therefore different methods [44-50] have been used to determine these viscosity coefficients.

4.3.5.1 The soft Mode Rotational Viscosity in the Smectic A* Phase

As discussed previously, the soft mode dielectric contribution and relaxation frequency are related by the relation

$$\gamma_\theta = \frac{\varepsilon_0 \varepsilon_\infty^2 C^2}{2\pi} \frac{1}{\Delta\varepsilon_S f_S} \qquad (4.6)$$

All quantities in this equation have been defined earlier. In order to calculate γ_θ, a measure of the coefficient C is needed. It can be

calculated from the linear induced tilt angle θ_{ind} dependence on the applied field given by [42]

$$\theta_{ind} = \frac{\varepsilon_0 \varepsilon_\infty C}{\alpha(T - T_C)} E \qquad (4.7)$$

By fitting Eq. (7) to the experimental results shown in figure 4.13 of the field dependence of the induced tilt angle in the SmA* phase, the coupling constant C is found to be 1.08×10^7 V/(m rad). By substituting this value into equation (6) γ_θ has been calculated at different temperatures as shown in figure 4.14(a). The values of γ_θ increases from 4.6 Ns/m^2 at 70 °C to 9 at the SmA* to SmC* transition. In general the rotational viscosity is described by the Arrhenius equation:

$$\gamma = \gamma^0 e^{\frac{E_a}{k_B T}} \qquad (4.8)$$

where γ^0 is constant, E_a is the activation energy and T is the temperature in Kelvin and k_B is the Boltzmann constant. As illustrated in figure 4.14(b), it is possible to fit Eq. (8) over a relatively broad temperature range. However, when approaching T_C, a strong deviation between the

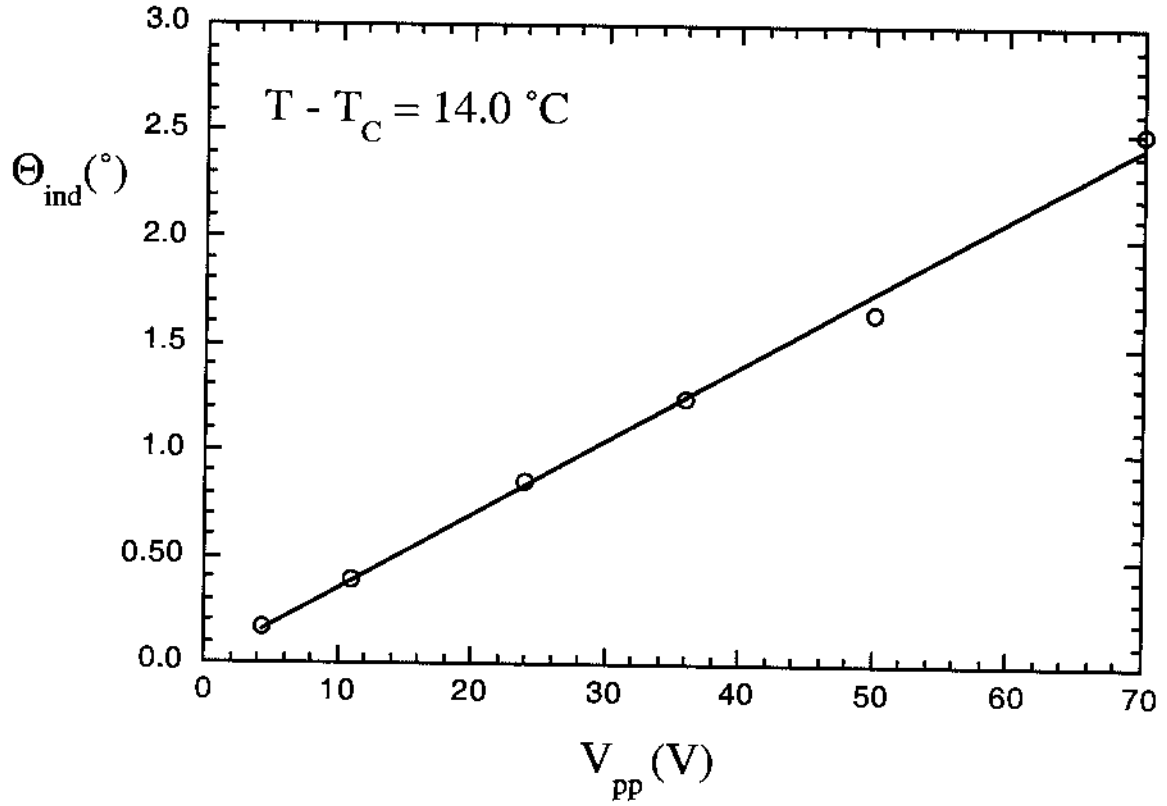

Figure 4.13 Electric Field dependence of the induced tilt angle in the smectic A* phase.

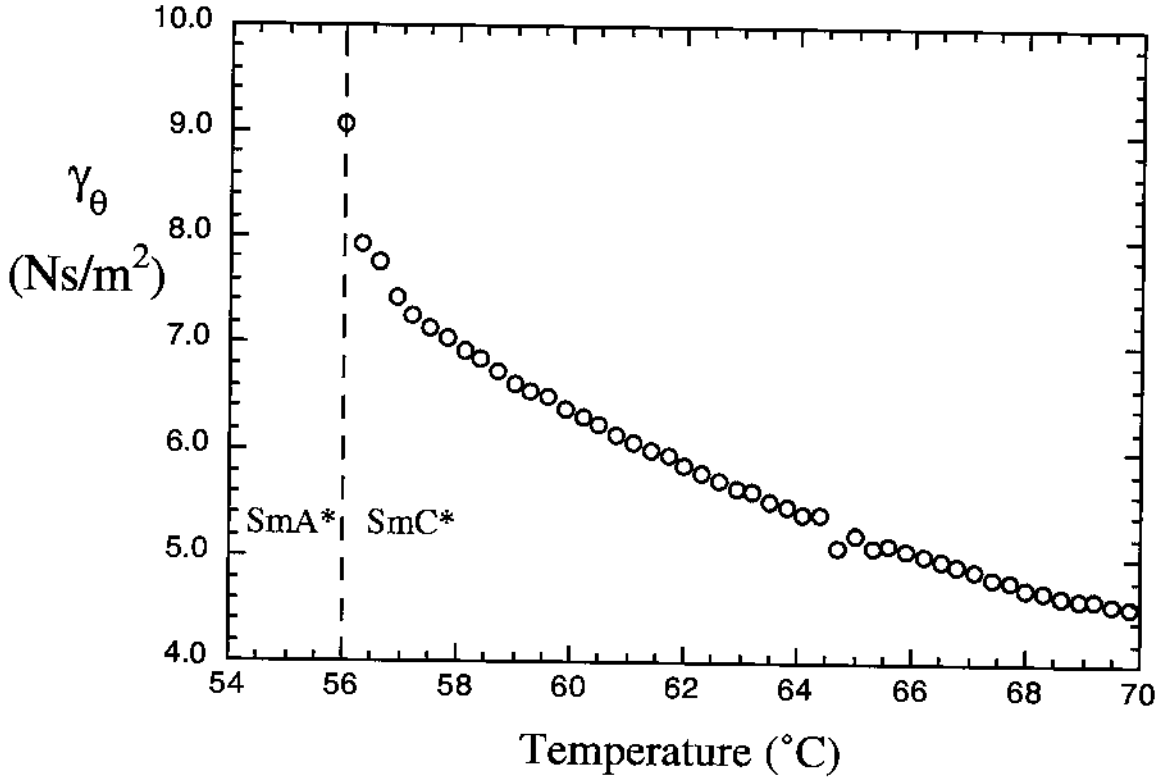

Figure 4.14(a) Temperature dependence of the soft mode rotational viscosity in the smectic A* phase.

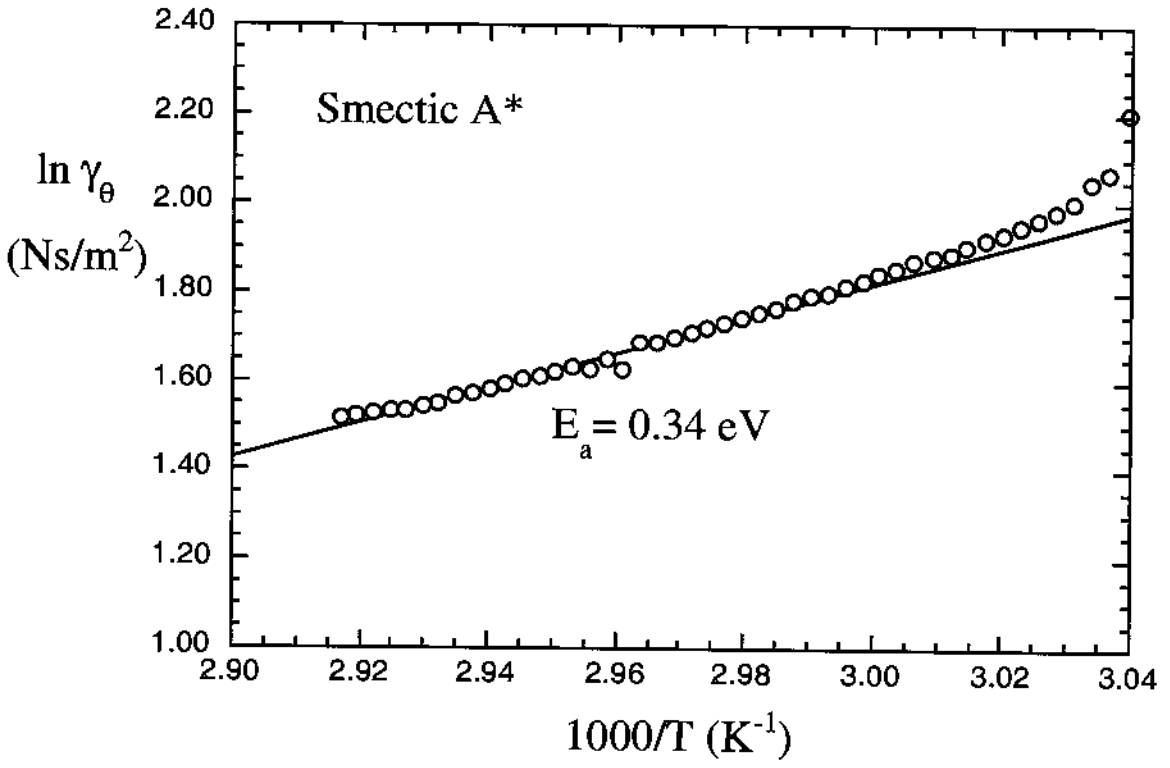

Figure 4.14(b) Arrhenius plot of the soft mode rotational viscosity. The solid line represents the fitting of the linear part. The values of 1000/T above 3.00 have been excluded from the fitting.

experimental results and the fitted line. In order to describe the temperature dependence of the soft mode rotational viscosity, a modification of Arrhenius equation of the form

$$\gamma = \gamma^0 e^{\frac{E_a}{k_B T}} + \gamma_\theta^0 (T - T_C)^{\nu_\theta} \qquad (4.9)$$

successfully models the experimental results. The second term in Eq. (4.9) has a power law form with exponent ν_θ. As depicted in figure 4.14(b), an excellent fit is obtained and the fitting parameters are listed in Table III.

Table III Fitting parameters of the soft mode rotational viscosity given by Eq. ( )

γ^0 (Ns/m^2)	E_a (eV)	γ_θ^0 (Ns/m^{2}K)	T_C (°C)	v_0
1.14x10^{-6}	56.01	2.25	56.01	0.14

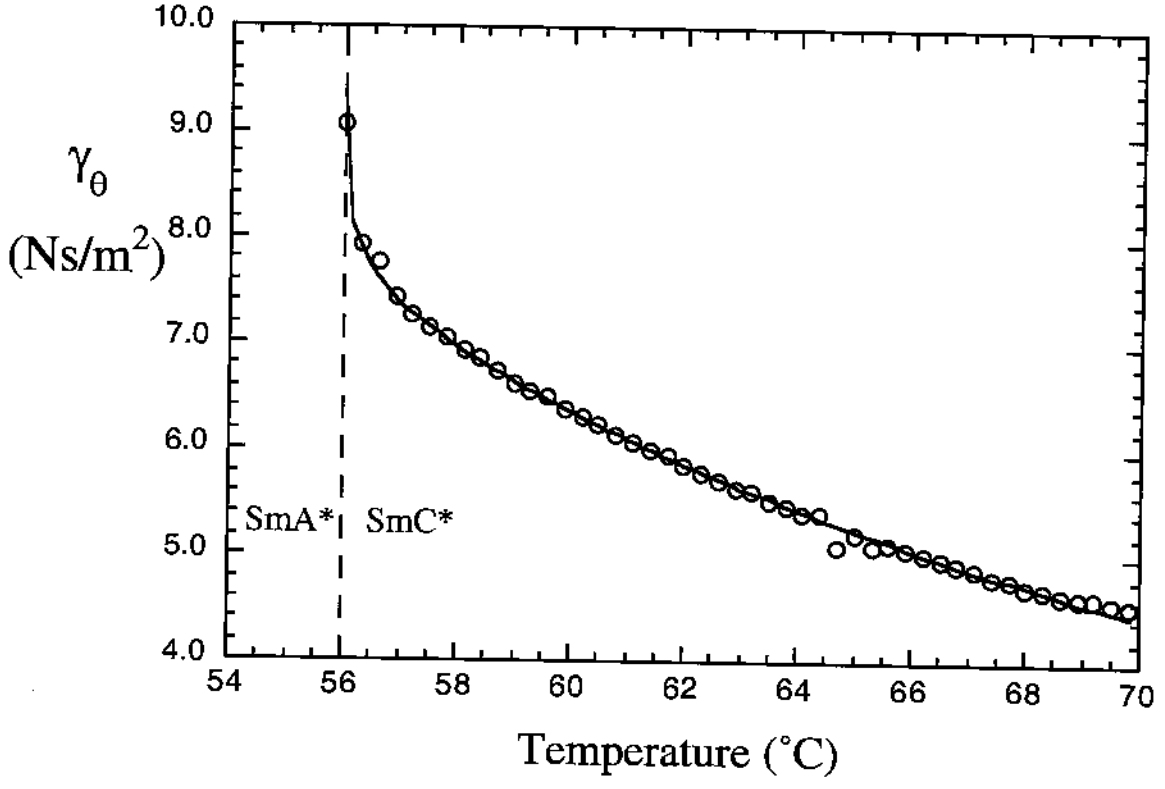

Figure 4.14(c) Temperature dependence of the soft mode rotational viscosity in the smectic A* phase. The solid red line is the fitting of equation (0 to the experimental results.

4.3.5.2 The Goldstone Mode Rotational Viscosity in the Smectic C* Phase

The Goldstone mode rotational viscosity can be calculated in terms of the product $\Delta\varepsilon_G f_G$ using the formula

$$\gamma_\varphi = \frac{1}{4\pi\varepsilon_0}\frac{1}{\Delta\varepsilon_G f_G}\left(\frac{P_S}{\theta}\right)^2 \qquad (4.10)$$

where P_S is the spontaneous polarization, θ is he tilt angle in the SmC* phase. It is obvious that additional two material properties (P_S and θ) are needed to determine the γ_φ. Both P_S and θ have be measured by the bridge technique and the switching between two polarization states $+P_S$ and $-P_S$ corresponding to tilt angles $+\theta$ and $-\theta$ by applying an external a.c. field strong enough to reach the saturated polarization [43]. The spontaneous polarization and the tilt angle are temperature dependent and fall off with a power law (with exponent β) when approaching the SmC* to SmA* transition. The solid line in figure 4.15 represents the fitting to a power law

$$P_S = P_0(T_C - T)^\beta \qquad (4.11)$$

for the tilt angle

$$\theta = \theta_0(T_C - T)^\beta \qquad (4.12)$$

it may be noted that the exponent β for the P_S (in general) is larger than for the tilt angle.

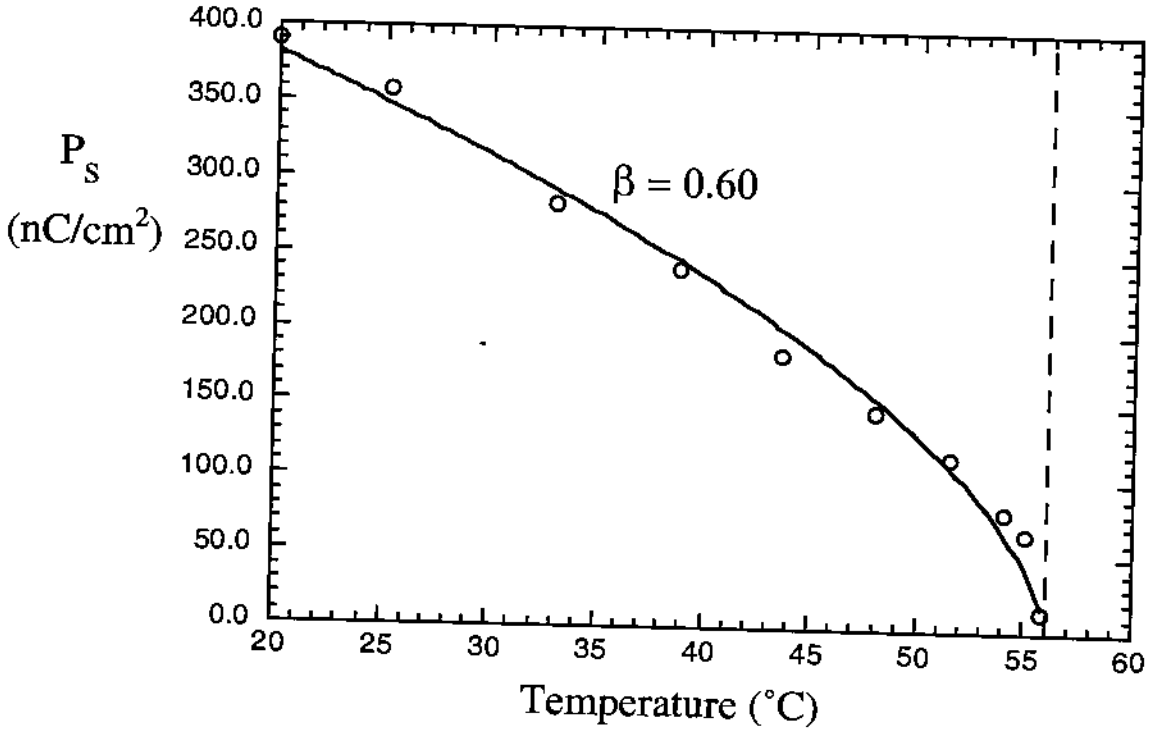

Figure 4.15(a) Temperature dependence of the spontaneous polarization in the smectic C* phase.

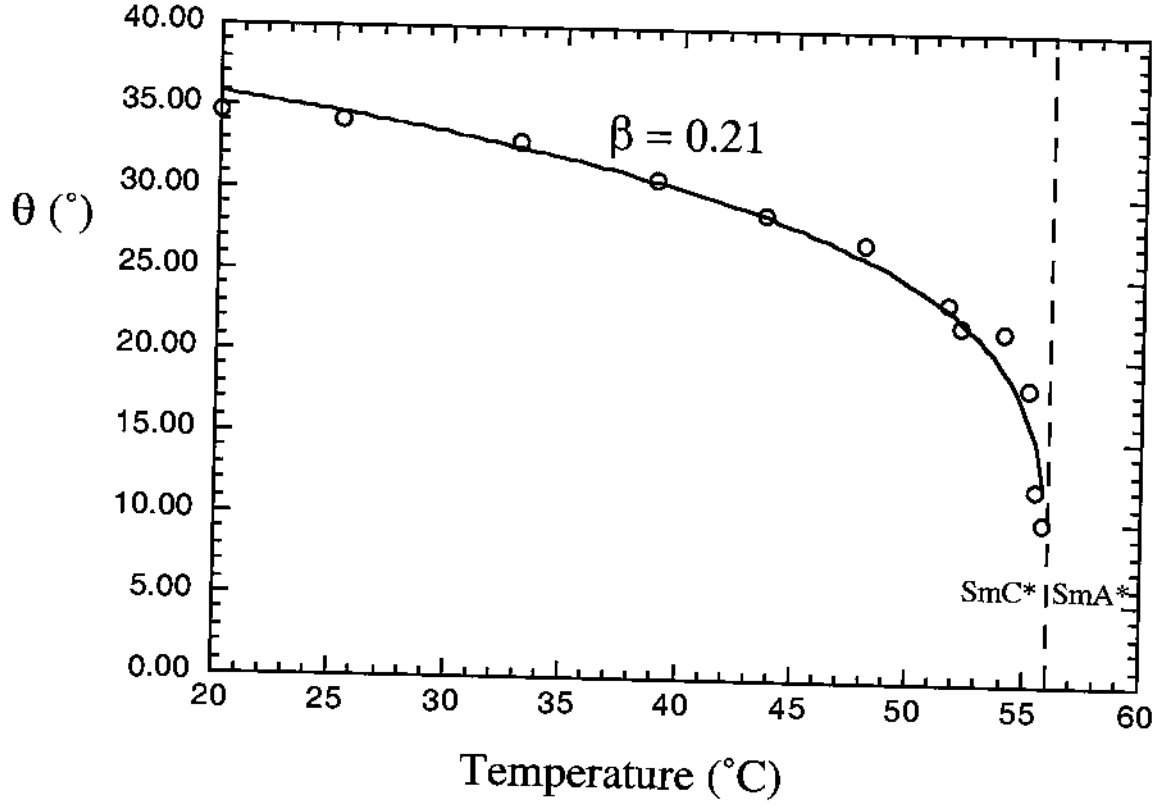

Figure 4.15(b) Temperature dependence of the tilt angle in the smectic C* phase.

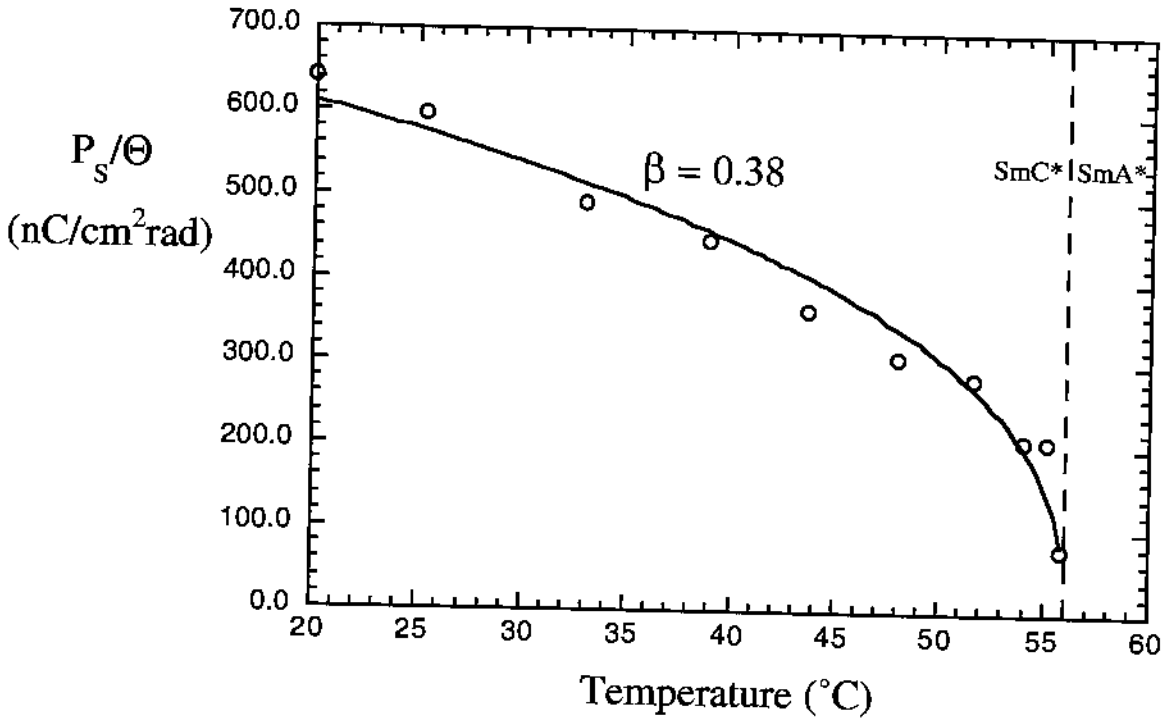

Figure 4.14(c) Temperature dependence of the P_S/Θ in the smectic C* phase.

By substituting the values of dielectric strength and relaxation frequency of the Goldstone mode into Eq.(4.10), γ_φ has been determined as at different temperatures in the SmC* phase as illustrated in figure 4.15. The temperature dependence of γ_φ is successfully modelled by a power

$$\gamma_\varphi = \gamma_\varphi^0 (T_C - T)^{\nu_\varphi} \qquad (13)$$

the exponent $\nu_\varphi = 0.63$.

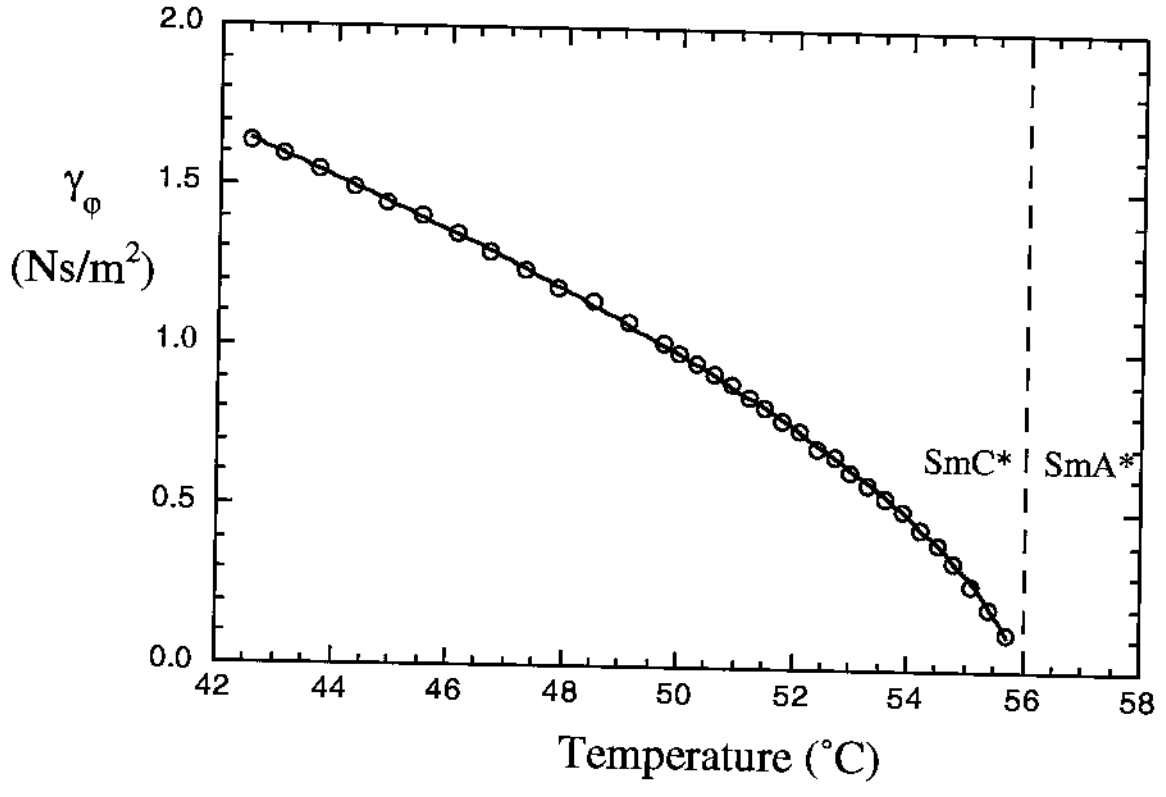

Figure 4.16 Temperature dependence of the Goldstone mode rotational viscosity in the smectic C* phase. The solid red line is the fitting of equation a power law given by equation (4.11).

4.3.5 Comparison of the soft Mode and the Goldstone Mode Rotational Viscosities in the Smectic A* and C* Phases

By comparing the values of γ_θ and γ_φ it is found, as shown in figure 4.17, that is larger than by almost one order of magnitude. The maximum difference is found at T_C. This result contradict the theoretical prediction of the extended Landau model [19] where both viscosity coefficients are degenerate at the transition temperature. Thus the dynamic part of the Landau description ought to be revised. In order to understand, in simple words, the large difference between the values of γ_θ and γ_φ let us take the limit when $\theta \rightarrow 0^\circ$. In this case, γ_φ corresponds to the molecular rotation around the long axis where the friction counteracting the rotation is expected to be small. However, by increasing the tilt γ_φ increases and reach its maximum value in the limit $\theta \rightarrow 90^\circ$ in which $\gamma_\varphi \rightarrow \gamma_\theta$ Note that in this work, the soft mode rotational viscosity has not be determined in the SmC* phase. Along with other viscosity coefficients, such detailed study is convenient for a separate project. Our intension of giving the values of γ_θ and γ_φ is to show that the dielectric relaxation spectroscopy could be extended to calculate a very interesting material property which plays an important role in device applications of ferroelectric liquid crystal materials.

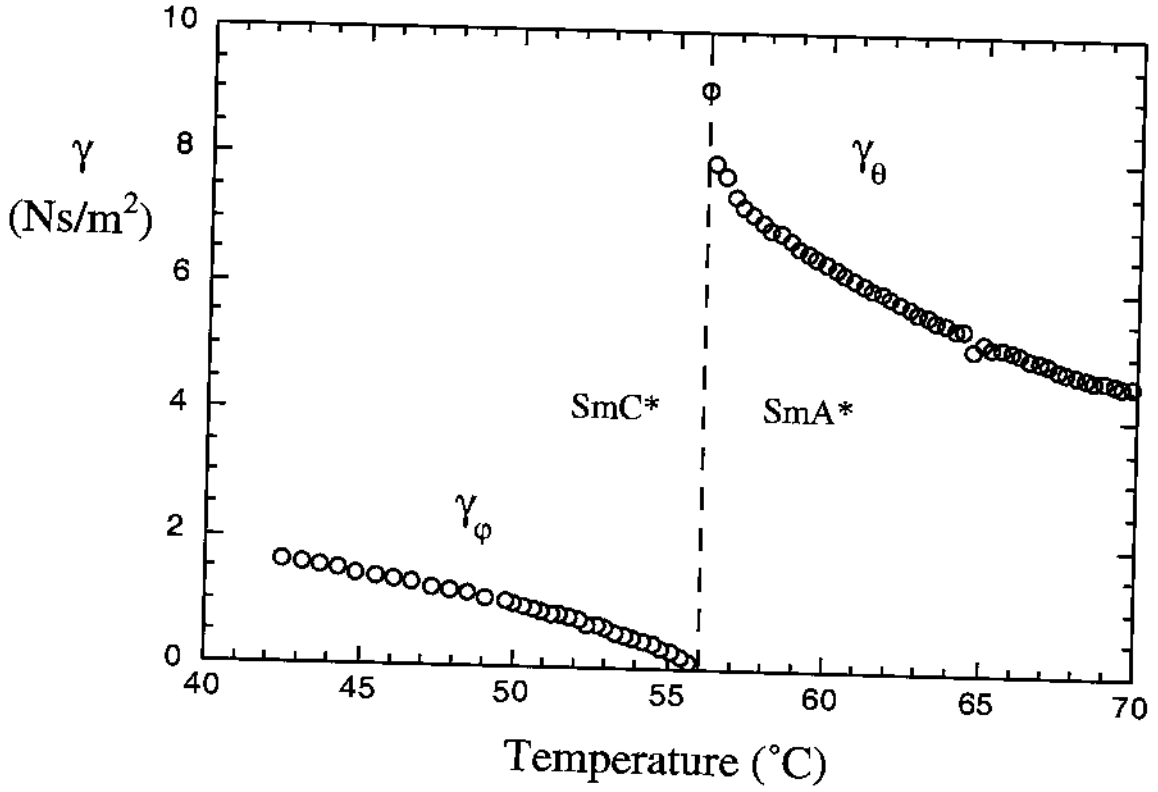

Figure 4.17 Temperature dependence of the soft mode and Goldstone mode rotational viscosities in the smectic A* and C* phases.

4.4 RESULTS FROM HOMEOTROPIC SAMPLES

Samples of homeotropic orientation enable us to investigate the molecular reorientation around the short axis. In this measurement geometry (with the smectic layers parallel to the glass plates), the parallel component of the permanent dipole moment has its maximum contribution in the direction of measuring electric field [27-29].

In tilted smectic, the director makes an angle θ (tilt angle) with the measuring field. In this case, the measurement geometry is called *quasi-homeotropic* orientation. Both homeotropic and quasi-homeotropic orientations allows us to probe the flipping motion around the short axis. At this point it important to stress that in *tilted* smectics (like the SmC* phase) in the quasi homeotropic orientation, the *parallel* and the *perpendicular* components of the electric dipole moment have contributions in the field direction. Thus, permitting the observation of the molecular reorientation around the *short* and *long* axes.

Figure 4.18 shows a 3D plot of the frequency dependence of the dielectric absorption at different temperatures in the homeotropic orientation. In the high temperature interval over the whole SmA* phase, the spectrum is characterised by one absorption peak. On cooling to the SmC* phase a smooth shift in the location of the peak to the low frequency regime is observed. However, at certain temperature interval an additional absorption appears in the spectra.

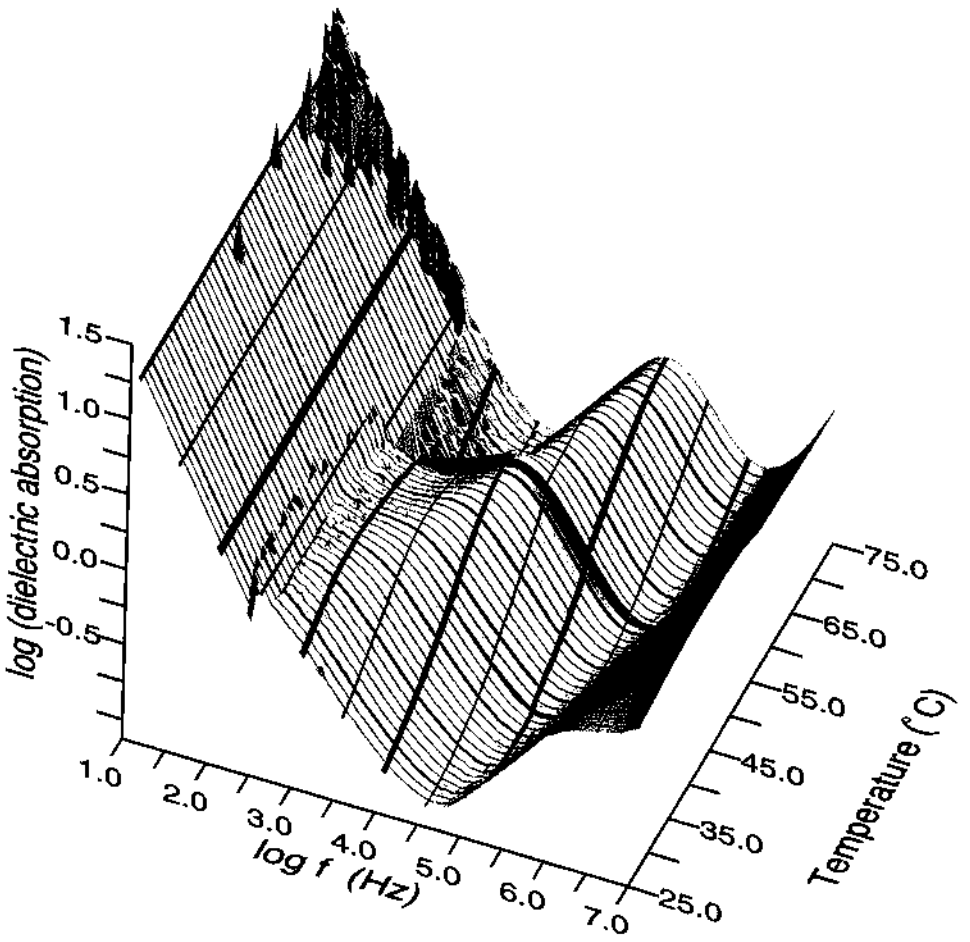

Figure 4.18. Dielectric spectra of the smectic A* and C* phases in the *homeotropic orientation.*

A 2D representation of the spectra is illustrated in figure 4.19. In the SmA* phase at T = 74.9 °C (about 19 degrees above T_C) the dielectric spectra contains only one absorption peak cantered around 100 kHz. This peak is connected with the molecular reorientation around the short axis. The relaxation frequency of this molecular process is temperature dependent and follows Arrhenius behaviour. In the SmC* phase (see figure 4.18) at T = 55.59 (0.4 °C below T_C) the absorption peak is shifted to 10 kHz. At lower temperatures in the SmC* phase, a

new absorption peak is observed and indicated by the blue arrow and is characterised by a relaxation frequency about 2 MHz. In the temperature interval covering the SmA* phase and in the SmC* phase down to 49 °C the

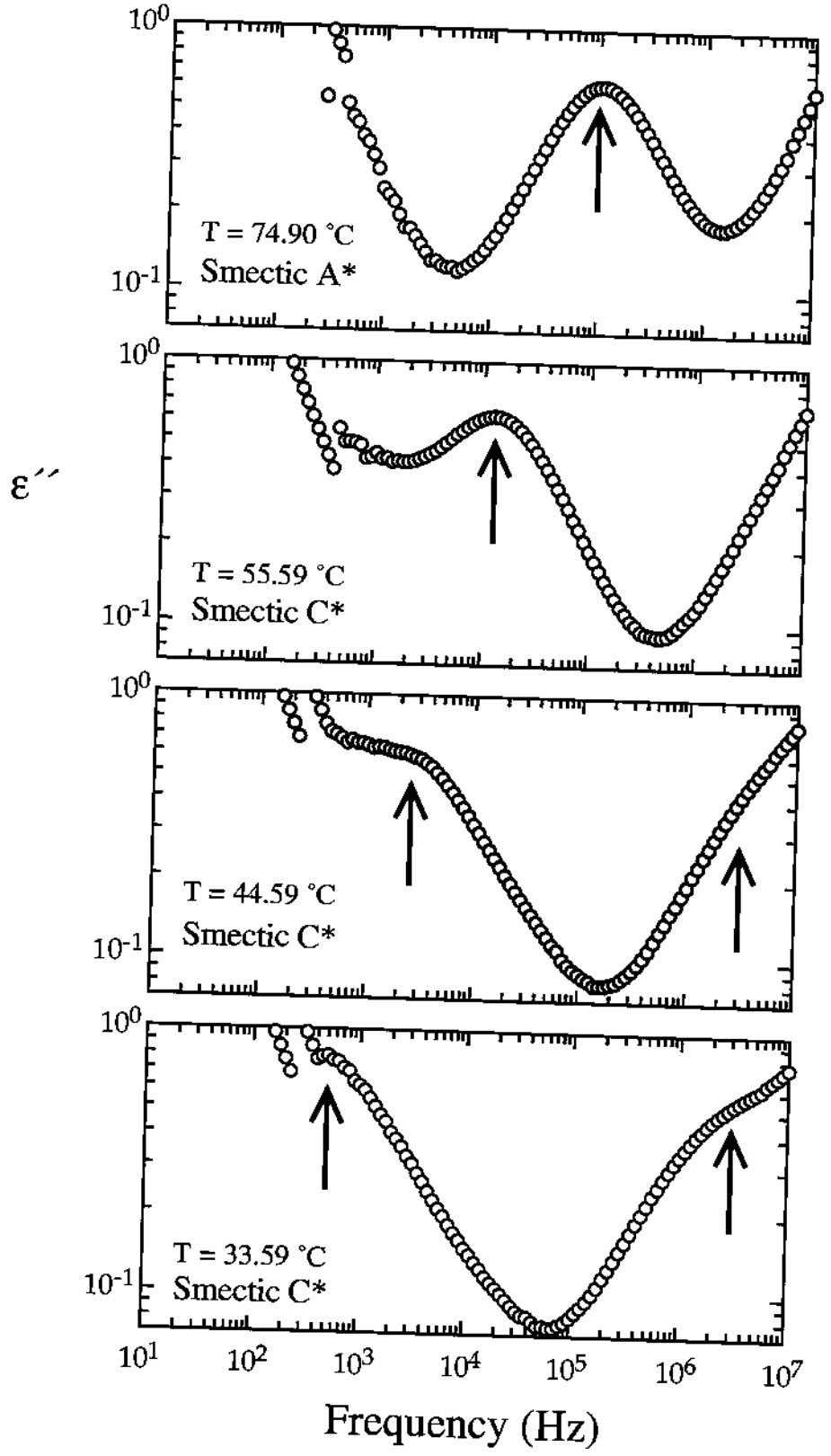

Figure 4.19 Frequency dependence of the dielectric absorption in the *homeotropic orientation* at different temperatures in the smectic A* and C* phases.

dielectric spectra has been analysed by *one* Cole-Cole function. However, below 49.0 °C where the high frequency peak appears, the spectrum has been analysed by *two* Cole-Cole function. This explains the scattering in the fitted values of relaxation frequency around 49 °C in figure 4.20(a). The figure shows the temperature dependence of relaxation frequency in the SmA* and SmC* phases.

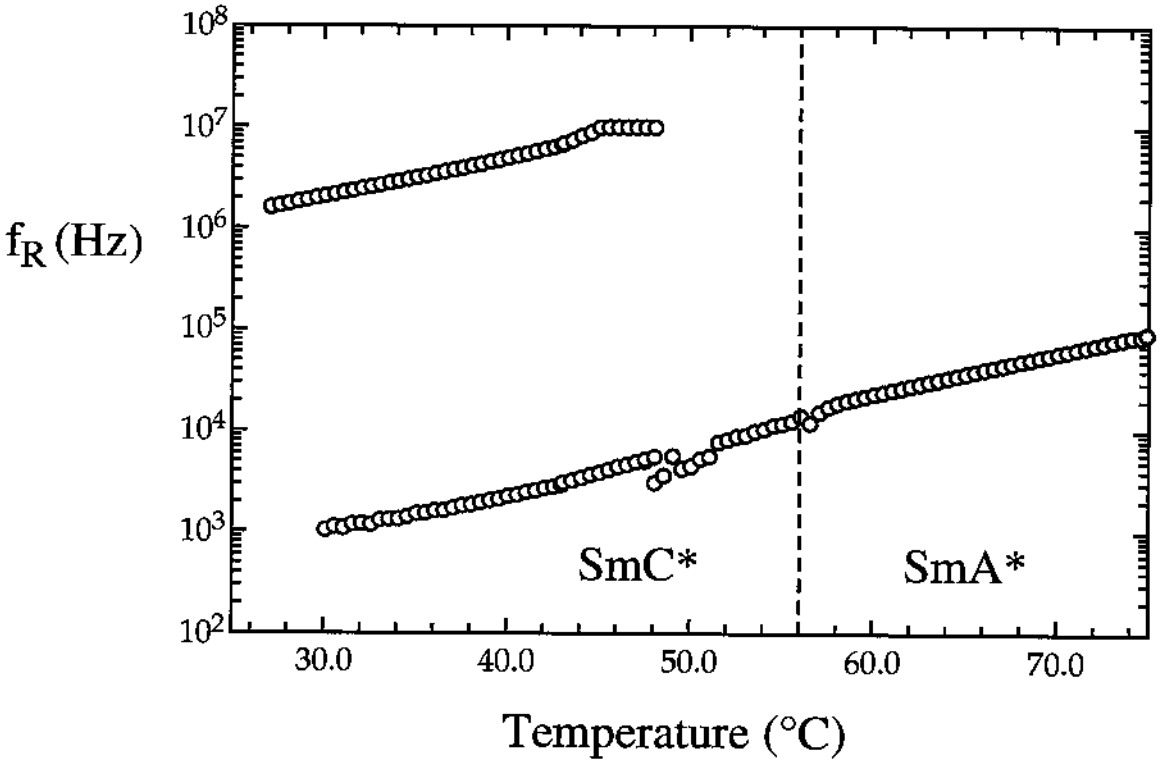

Figure 4.20(a) Temperature dependence of the relaxation frequency in the SmA* and SmC* phases. The data in the temperature range down to 49 °C are obtained by fitting *one* Cole-Cole function. Below this temperature, the spectra was analysed by fitting *two* Cole-Cole function.

The low frequency branch (blue open circles) is attributed to the molecular reorientation around the short axis. The high frequency branch (red open circles) is connected with the molecular reorientation around the long axis. In order to confirm this molecular assignment of

the high frequency branch, we have compared these high frequency values obtained from the homeotropic orientation with those obtained from the planar orientation. Both results are shown in figure 4.20(b) and indicated by the filled red circles. It is obvious that the high frequency values obtained from two different measurements geometries are very close to each other. Moreover, the activation energy in both case, as depicted in Arrhenius plot in figure 4.20(c) are in excellent agreement. The activation energy of the low frequency process is slightly larger that the high frequency mechanism. This is connected with the higher potential for the rotation around the short axis.

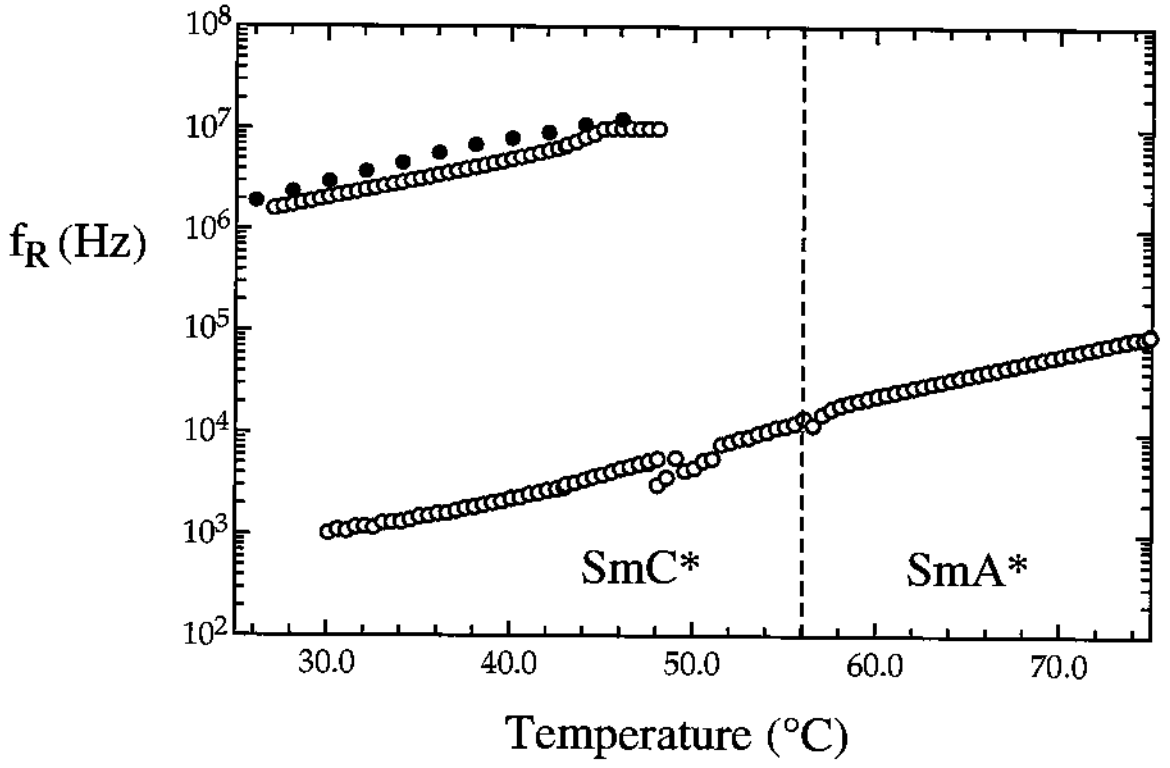

Figure 4.20(b) Temperature dependence of the relaxation frequency in the SmA* and SmC* phases. The open circles (blue and red colours) are the fitted values of from the homeotropic orientation. The filled circles (red colour) obtained from planar orientation.

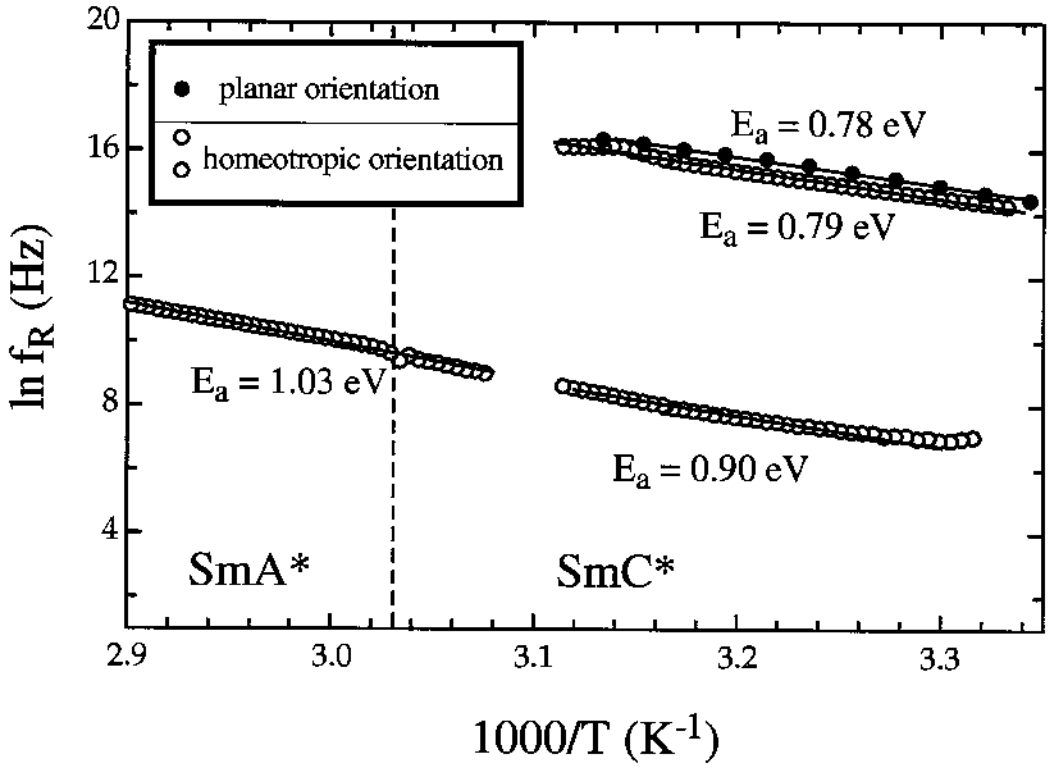

Figure 4.20(c) Arrhenius plot of the relaxation frequency of the molecular rotation around the short axis (blue points) and long axis (red points). Note that in the low frequency branch, the points above 3.29 K^{-1} have not been included in the fitting because of its boor accuracy. Moreover, the points in the range3.28 to 3.12 K^{-1} have been deleted from the plot because they are very scattered.

4.5 *DIELECTRIC SPECTROSCOPY OF THE CRYSTALLINE PHASE (A Comparison with other phases)*

The dielectric spectrum of the isotropic liquid and all liquid crystalline phases is characterized by two main dielectrically active process; fast molecular reorientation around the long axis and hindered reorientation around the short molecular axis. In addition, to these *two non-collective* processes, there are *two collective modes*, i.e. the soft mode and the Goldstone mode, usually observed in chiral smectics.

In the crystalline phase, however, these four collective and non-collective processes are frozen out. Figure 4.21 shows the dielectric absorption spectra obtained on heating the sample from the crystalline phase to the isotropic phase through the smectic A* and C* phases. The border lines between the phases are depicted in the figure. It is obvious that, within the resolution of our measurements, there is no indication of any dielectric absorption in the crystal phase. The onset of absorption peaks could be traced at temperatures above 37 °C, on further heating, the absorption becomes more pronounced with a broad maximum located at 10 kHz. Theses absorption maximum are attribute the Goldstone mode.

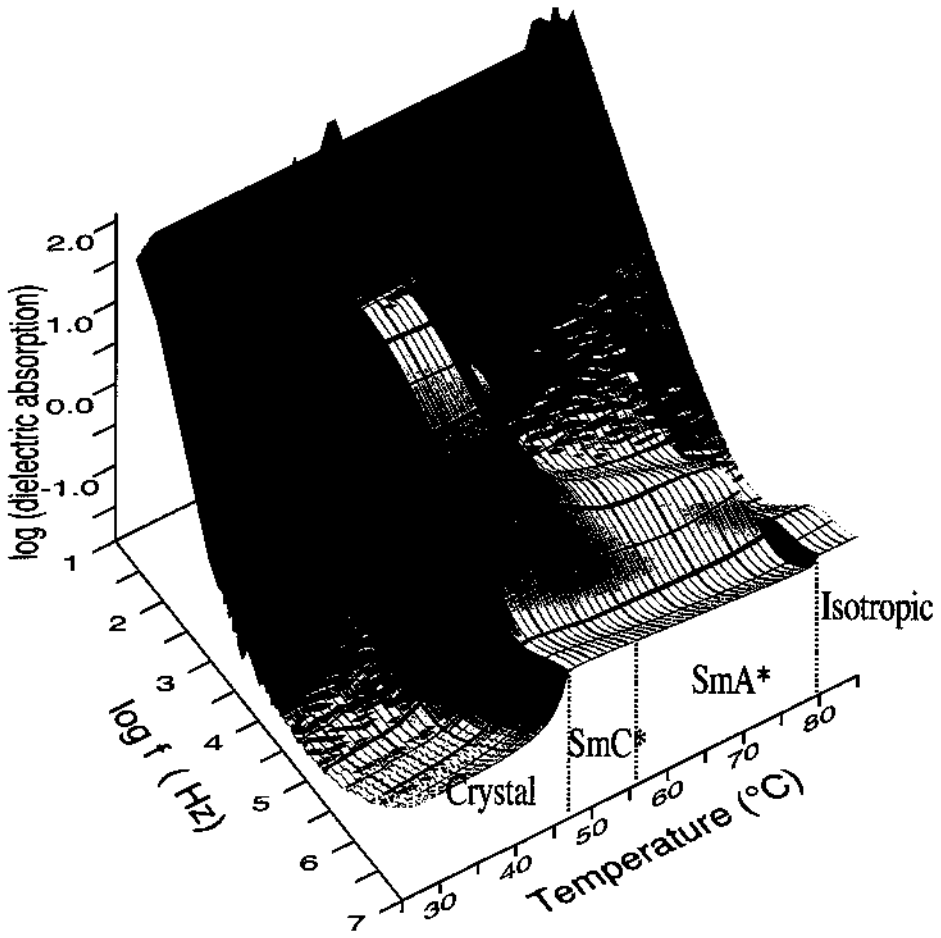

Figure 4.21 Dielectric spectra on heating from the crystalline phase to the isotropic liquid through the liquid crystalline SmC* and SmA* phases.

It may be noted that the transition from the crystal phase to the SmC* phase takes place over a wide temperature interval from 37 °C to 47 °C. The crystal phase has fully changed into the SmC* at 47 °C and extends over seven degrees where we can observe the transition to the SmA* phase. The absorption peaks in the SmA* phase decreases in strength on heating and shifted to the high frequency regime as expected for the soft mode. At higher temperatures, the transition from the SmA* phase to the isotropic phase is observed at about 80 °C. In the isotropic phase the dielectric spectra is characterized by a high frequency absorption located at 1 MHz. A process which could be assigned to the reorientation around the long molecular axis.

CHAPTER 5

EFFECT OF BIAS ELECTRIC FIELD ON THE DIELECTRIC PROPERTIES IN THE SMECTIC A* AND C* PHASES

The complex dielectric permittivity does not depend only on frequency and temperature. A bias electric field is one of the important parameters which strongly affect the dielectric properties of chiral smectic liquid crystals. In this chapter, a detailed studies of the effect of bias field on the dielectric strength and relaxation frequency of the soft mode and Goldstone mode in the smectic A* and C* phases will be presented. This study enables us to investigate the soft mode dielectric behaviour in the smectic C* phase. All the results in this chapter are obtained from measurements carried out on samples of planar orientation of thickness equals to 36 μm.

5.1 EFFECT OF BIAS FIELD ON THE SOFT MODE COMPLEX DIELECTRIC PERMITTIVITY OF THE IN THE CHIRAL SMECTIC A* PHASE

The bias electric field has a strong influence on the complex dielectric permittivity in the smectic A* and C* phases [36-37]. In this section, detailed study of the bias field effect is carried out at different temperatures stating from the vicinity of the SmA* to SmC*

transition and going up in temperature away from the phase transition.

Figure 5.1 shows the dielectric spectrum at bias fields from zero to 34 V over 36 μm at T_C. In general, it can be seen that the dielectric absorption maximum decreases by increasing the bias voltage. Moreover, the relaxation frequency (location of absorption maximum) increases at higher fields. Thus, the bias field acts to block the tilt-fluctuations; i.e. the system becomes "hard" against the tilt-fluctuations. At higher temperatures, as illustrated in figures 5.1(b) to 5.1(h) the effect of bias field on the dielectric absorption maximum and relaxation frequency decreases. At temperatures about one degree above TC, the system becomes field independent.

As clearly observed in all spectra given in figures 5.1, the absorption maximum decreases with bias voltage in a "wavy" fashion. A behaviour which becomes less pronounced at higher temperatures ($T - T_C > 1$ °C). This behaviour is reproducible at different temperatures in the smectic A* phase. It may be noted that bias voltage was left on during all bias field sweeps even it was ON after each frequency scan. The reason for this wavy feature is not clear yet for us.

(i) One of the possibilities is the charge accumulation during application of the DC voltage.

(ii) Since the sample was heated from the SmC* phase, some of surface conditions are inherited into the SmA* phase. These surface anchoring are very strong and could persists to few degrees into the SmA* phase. At higher temperatures this effect diminishes, thus, the

wavy behaviour of the dielectric absorption disappears. In order to check this argument, the same measurements could be repeated on cooling from the high temperature SmA* phase from the isotropic phase where an "isotropic" surface conditions is assumed. If the wavy behaviour disappears then our previous argument about the inherited SmC* surface conditions could be correct. Therefore, further investigations are needed to clarify this point.

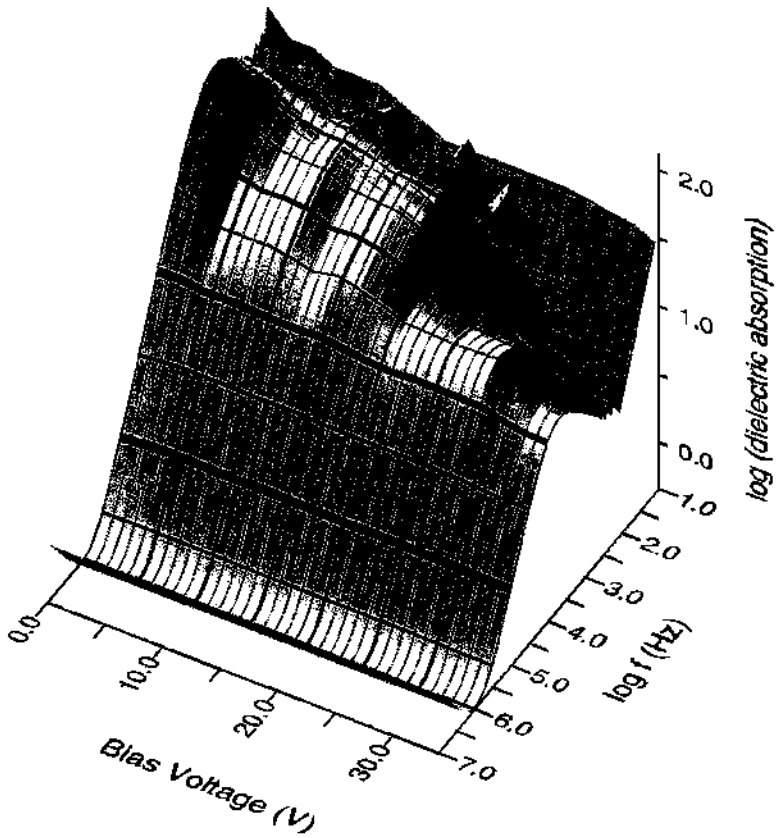

Figure 5.1(a) dielectric spectrum at different bias voltage in at the transition temperature from the smectic A* to C* phase. Sample thickness = 36 μm

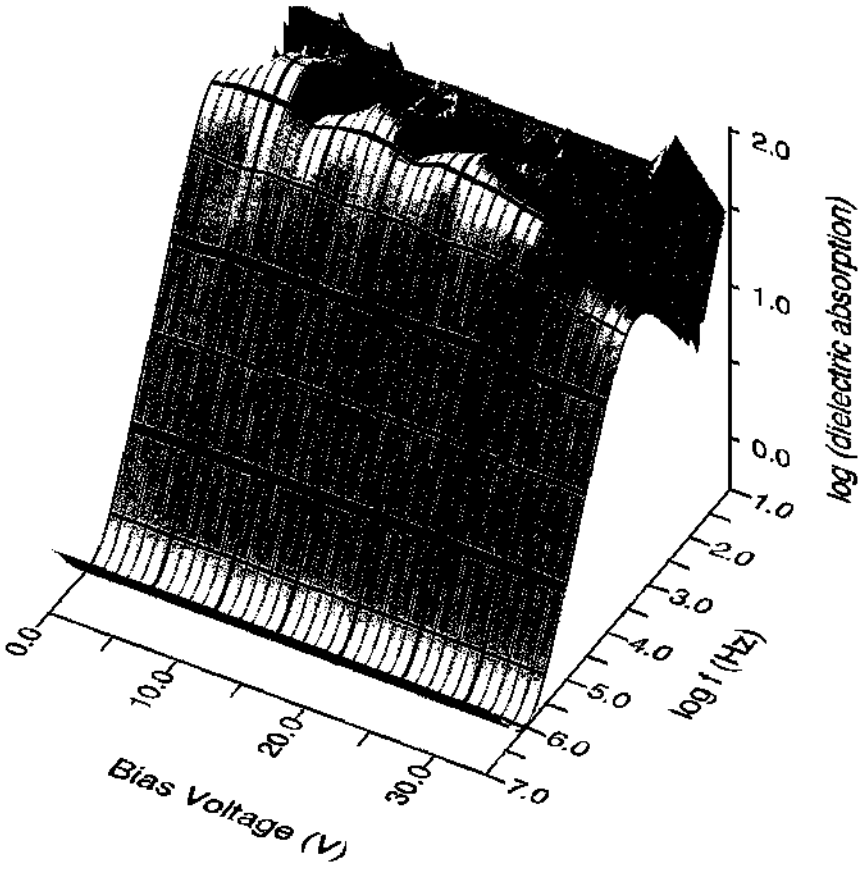

Figure 5.1(b) dielectric spectrum at different bias voltage in the smectic A* phase at T = 56.19 °C. Sample thickness = 36 μm.

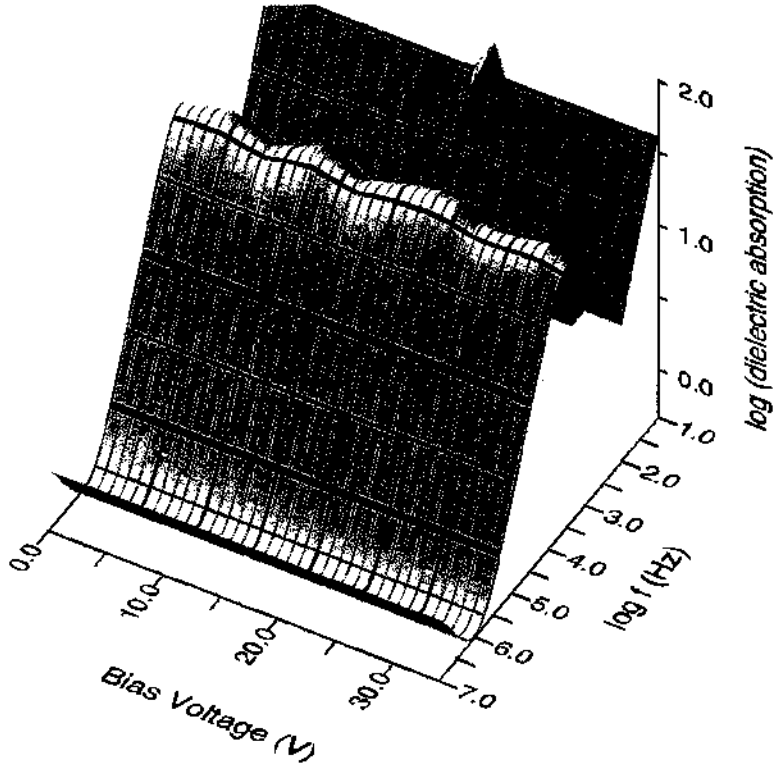

Figure 5.1(c) dielectric spectrum at different bias voltage in the smectic A* phase at T = 56.38 °C. Sample thickness = 36 μm.

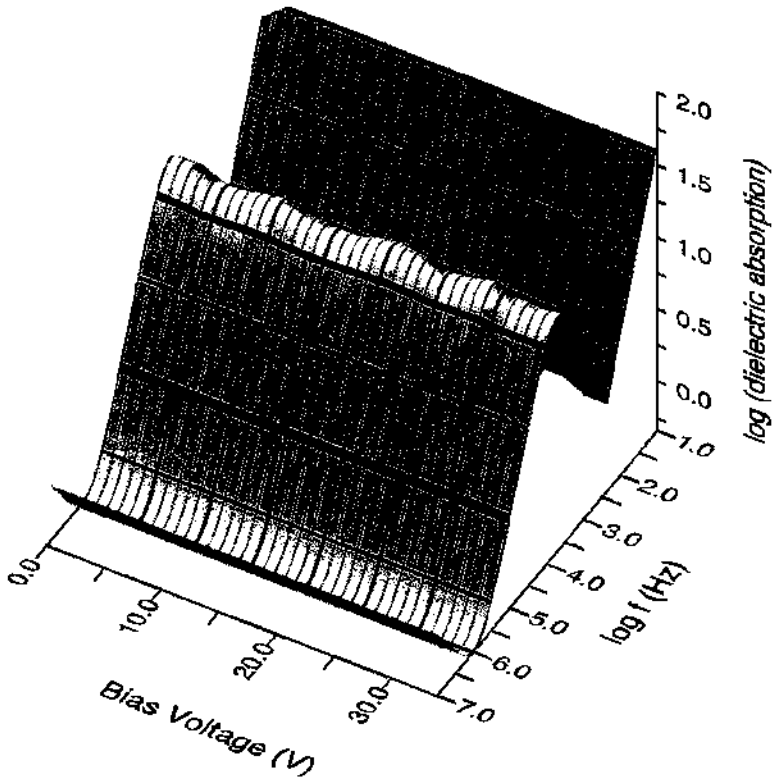

Figure 5.1(d) dielectric spectrum at different bias voltage in the smectic A* phase at T = 56.59 °C. Sample thickness = 36 μm.

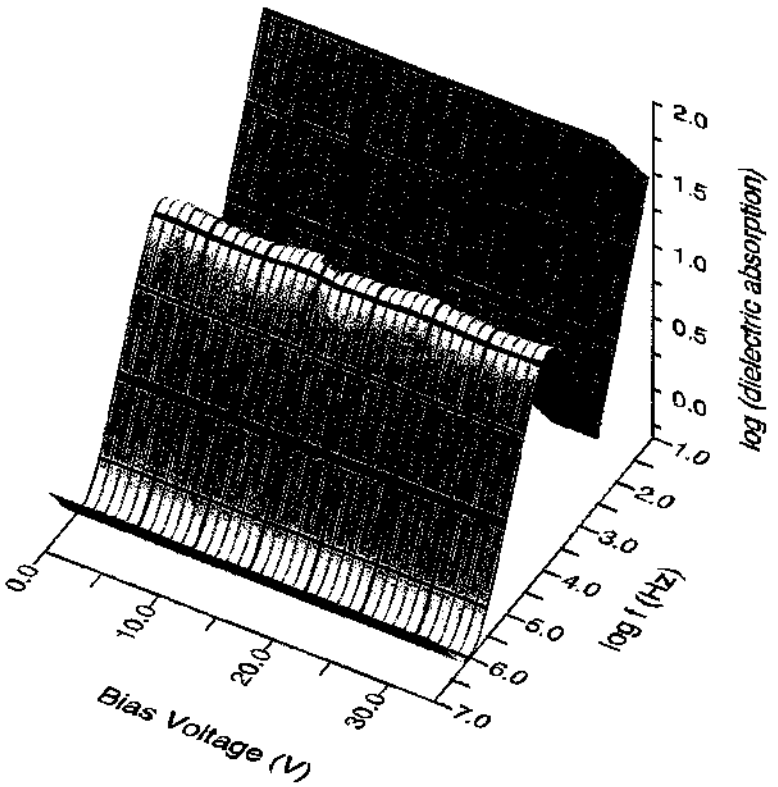

Figure 5.1(e) dielectric spectrum at different bias voltage in the smectic A* phase at T = 56.78 °C. Sample thickness = 36 μm.

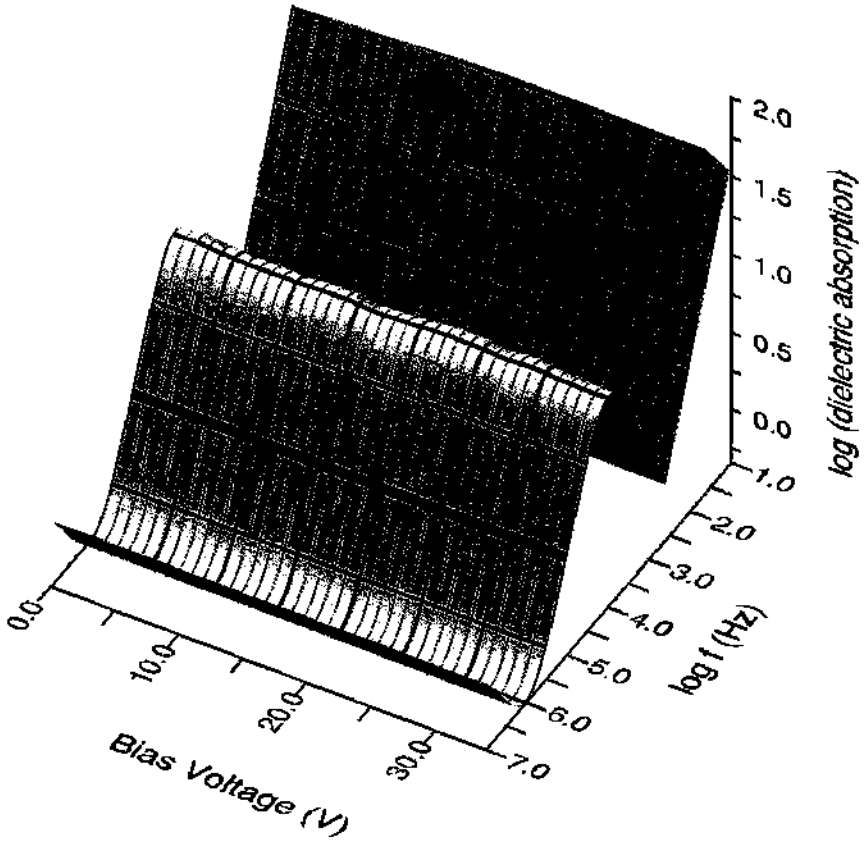

Figure 5.1(f) dielectric spectrum at different bias voltage in the smectic A* phase at T = 56.99 °C. Sample thickness = 36 μm.

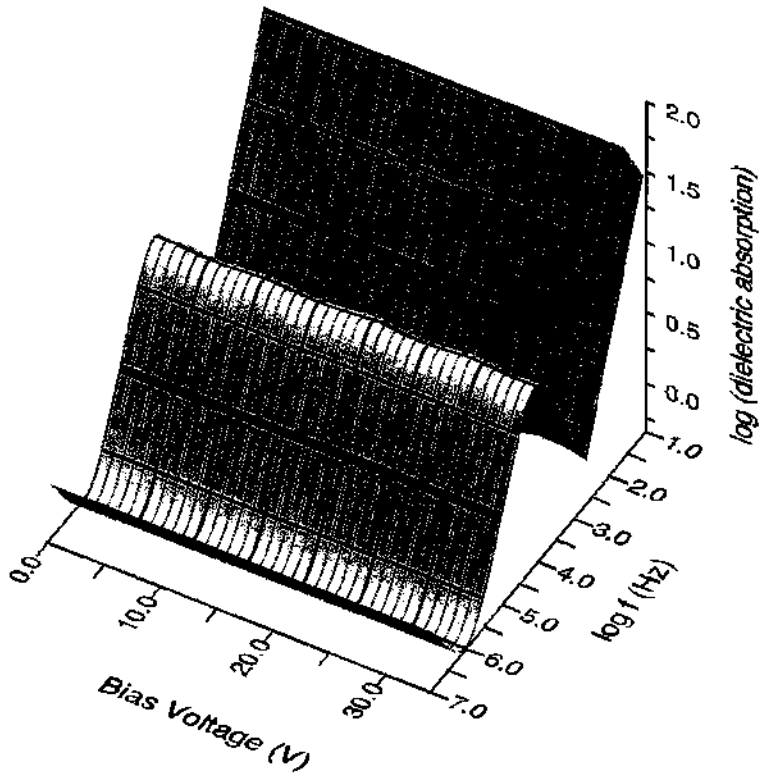

Figure 5.1(g) dielectric spectrum at different bias voltage in the smectic A* phase at T = 57.19 °C. Sample thickness = 36 μm.

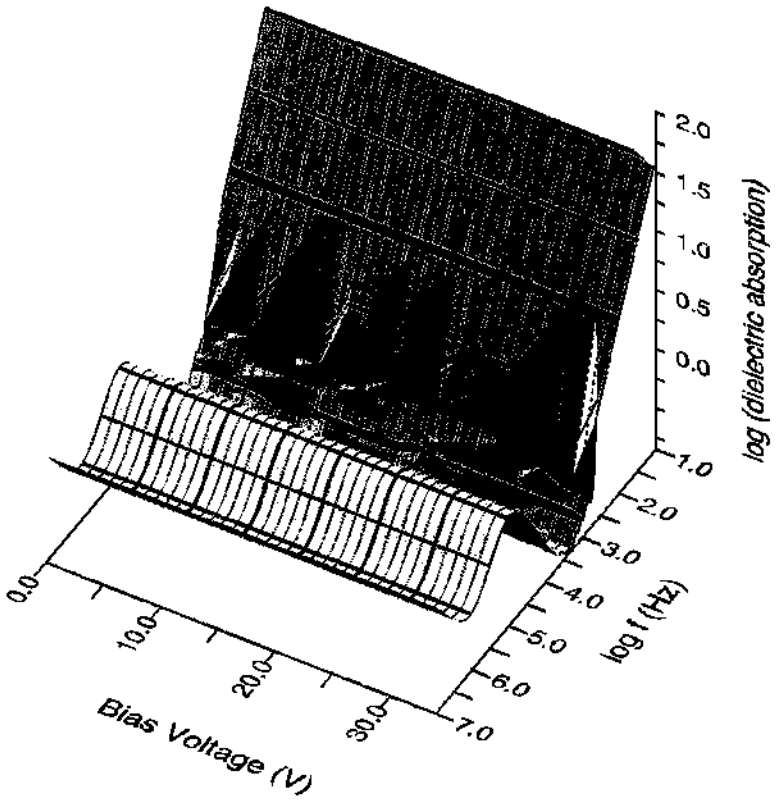

Figure 5.1(h) dielectric spectrum at different bias voltage in the smectic A* phase at T = 61.99 °C. Sample thickness = 36 μm.

The dielectric spectrum of bias field effect on the soft mode dielectric absorption has been fitted at about 0.2 °C above T_C, the fitting results are plotted in figure 5.2. It can be seen that the $\Delta\varepsilon_S$ increase from 180 at zero voltage to 250 at 5 volt, this is about 30 %. At higher voltages $\Delta\varepsilon_S$ decrease to almost 150 followed by a less increase. The relaxation frequency varies in an opposite fashion. The average trend is that $\Delta\varepsilon_S$ decrease and f_S increases with increasing the bias voltage. As pointed out earlier, the bias field effect persists over a temperature interval of about one degree above the transition. At higher temperatures the soft mode dielectric behaviour is field independent. This result is important and of great interest to study the soft mode in the SmC* phase.

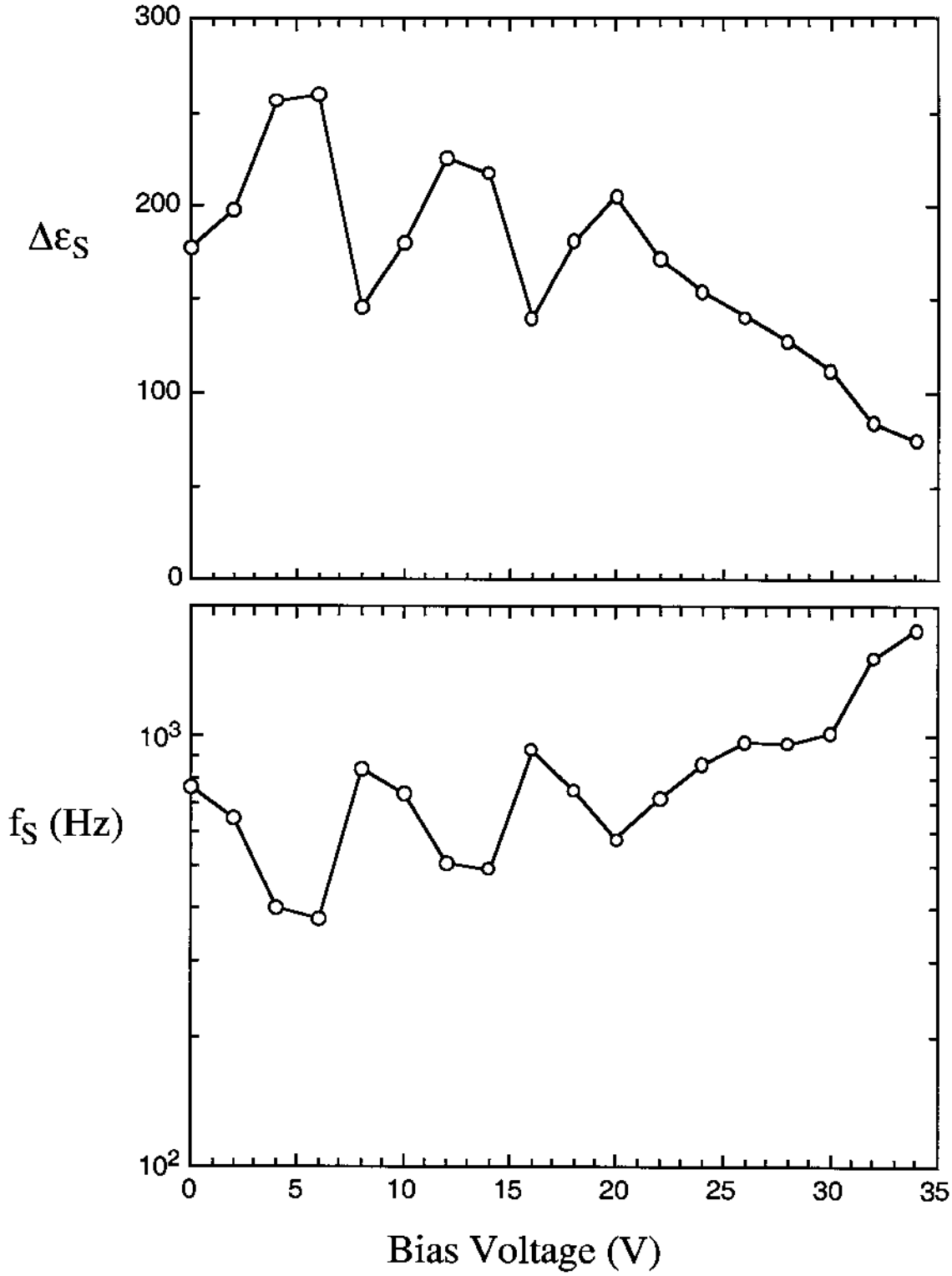

Figure 5.2 Bias voltage dependence of the soft mode dielectric contribution ($\Delta\varepsilon_S$) and relaxation frequency (f_S) at T = 65.19 °C in the smectic A* phase.

5.2 THE INFLUENCE OF BIAS FIELD ON THE GOLDSTONE MODE IN THE CHIRAL SMECTIC C* PHASE

An interesting phenomena takes place when a SmC* material is subjected to an external electric field ($\boldsymbol{E}$) provided that $\boldsymbol{E}$ is perpendicular to the helix axis. Due to the ferroelectric coupling between $\boldsymbol{E}$ and the polarisation $\boldsymbol{P}$, the permanent dipoles of each smectic layer tends to align in the field direction. Thus, resulting in a helix distortion which in the high field regime the helix disappears and the SmC* phase becomes unwound. The field at which the helix is completely unwound is called the critical E_C. In fact there are different external forces that strongly affect the liquid crystal molecular alignment, among these the interactions between liquid crystal molecules and boundaries. In many cases, the influence of the boundary opposes the response to the electric field.

In the present section, a detailed study of the bias electric field effect on a thick SmC* material is investigated. The measurements have been carried out at different temperatures and bias field in the SmC* as shown in figure 5.3(a) where the measurements are carried at 16 °C deep in the SmC* phase, the absorption maximum ε''_{max} is field independent 18 V_{DC}. At higher voltages, ε''_{max} decreases in a *two-step* fashion; i.e. in the voltage range 18.5 V_{DC} to 20.5 V_{DC} there is a steep decrease and in the range above 21.0 V_{DC} ε''_{max} decreases with a lower slope. At T = 44.0°C, generally, ε''_{max} exhibits a similar bias field dependence at the previous temperature, however, the onset of

the sudden decrease in ε'_{max} is observed at lower voltage; V_{DC} = 15 V. At higher temperatures, the decrease in ε'_{max} starts at lowers bias fields. At T = 46 °C, the dielectric spectrum has been fitted to get more a fine behaviour of the bias field dependence of $\Delta\varepsilon_G$ which is proportional to ε'_{max} and the results are plotted in figure 5.4. It is obvious that the behaviour is complicated and its interpretation is non-trivial.

As we have pointed out earlier, the bias field acts to unwind the helical structure which is opposed by the strong boundary effects. In our case, the thickness of all investigated samples equal to 36 μm. By applying a bias voltage over this relatively thick samples, we think that the unwinding process starts at the bulk and the layer close to the

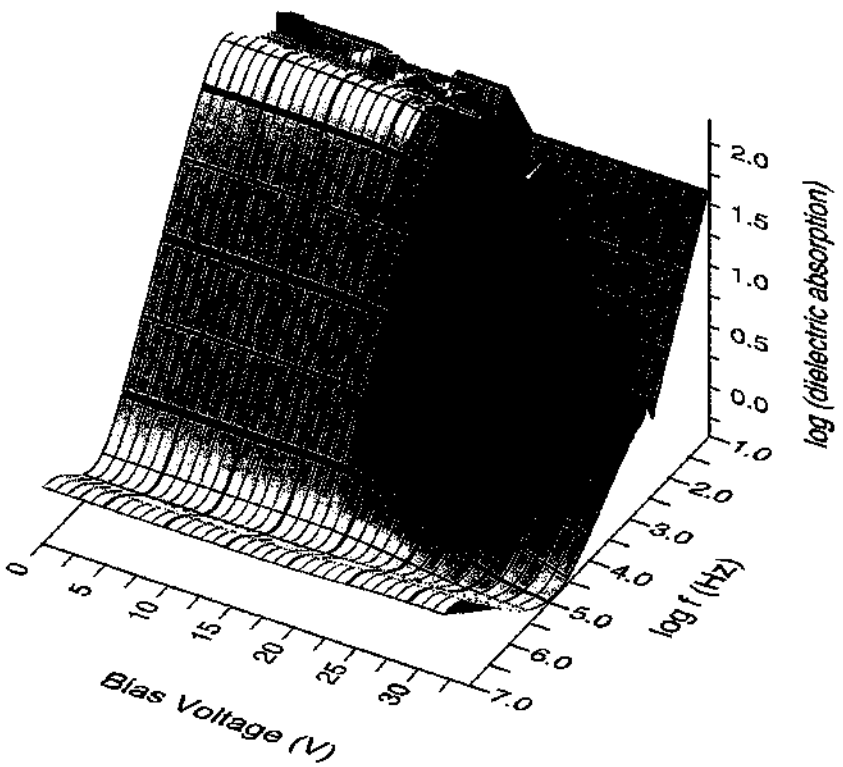

Figure 5.3(a) Dielectric spectra of the Goldstone mode at T = 40.0 °C in the smectic C* phase. Sample thickness = 36 μm

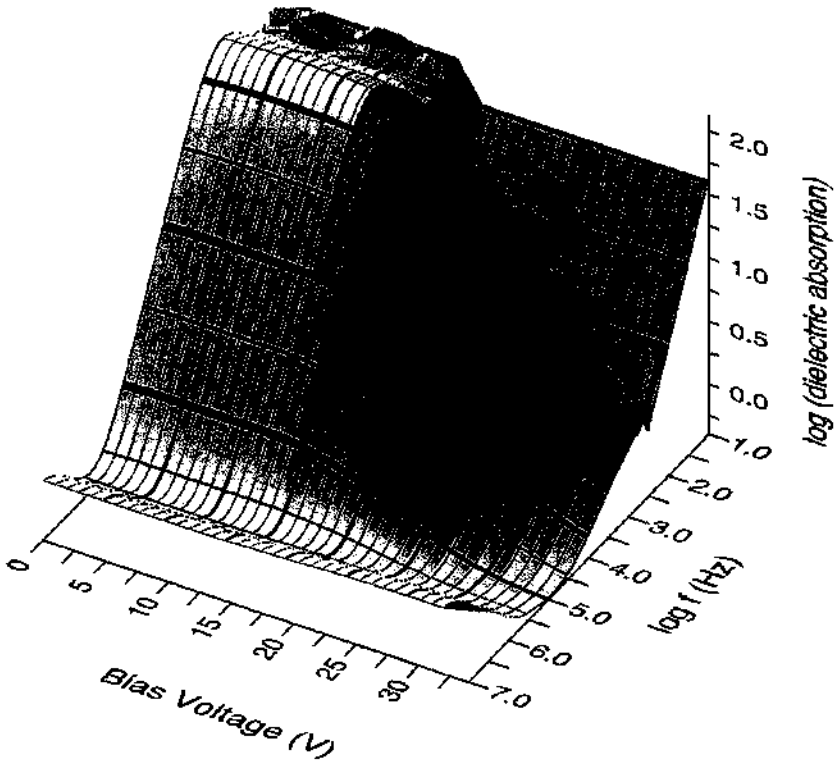

Figure 5.3(b) Dielectric spectra of the Goldstone mode at T = 44.0 °C in the smectic C* phase. Sample thickness = 36 μm

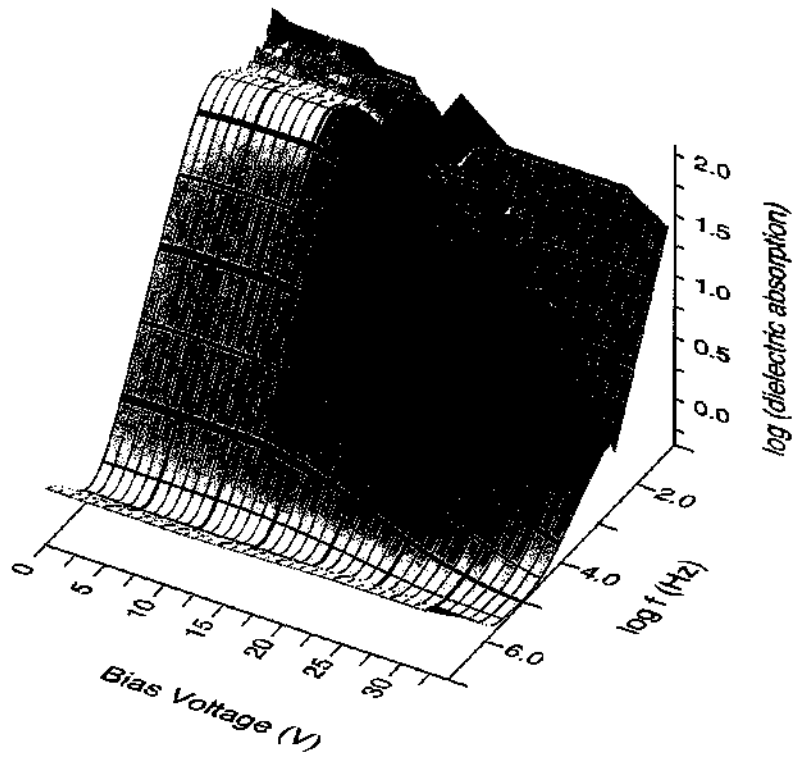

Figure 5.3(c) Dielectric spectra of the Goldstone mode at T = 46.0 °C in the smectic C* phase. Sample thickness = 36 μm

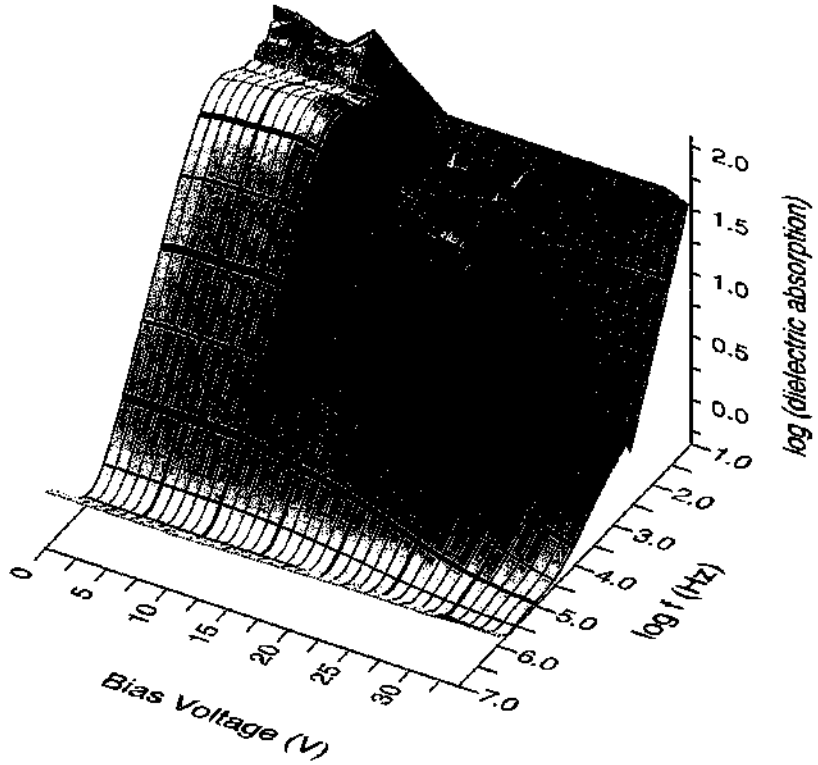

Figure 5.3(c) Dielectric spectra of the Goldstone mode at T = 48.0 °C in the smectic C* phase. Sample thickness = 36 μm

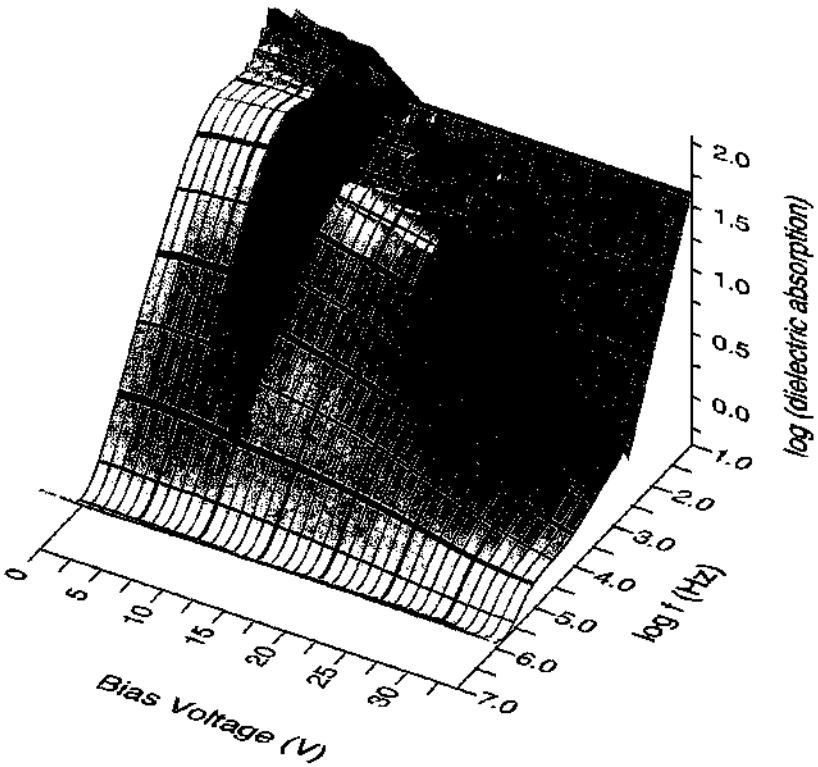

Figure 5.3(d) Dielectric spectra of the Goldstone mode at T = 52.0 °C in the smectic C* phase. Sample thickness = 36 μm

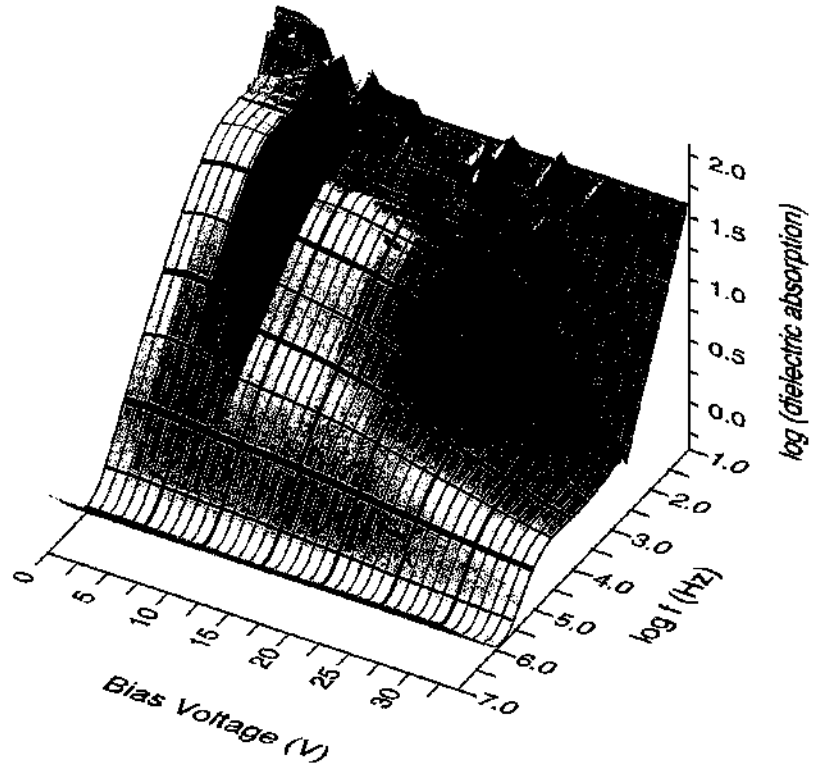

Figure 5.3(e) Dielectric spectra of the Goldstone mode at T = 54.0 °C in the smectic C* phase. Sample thickness = 36 μm

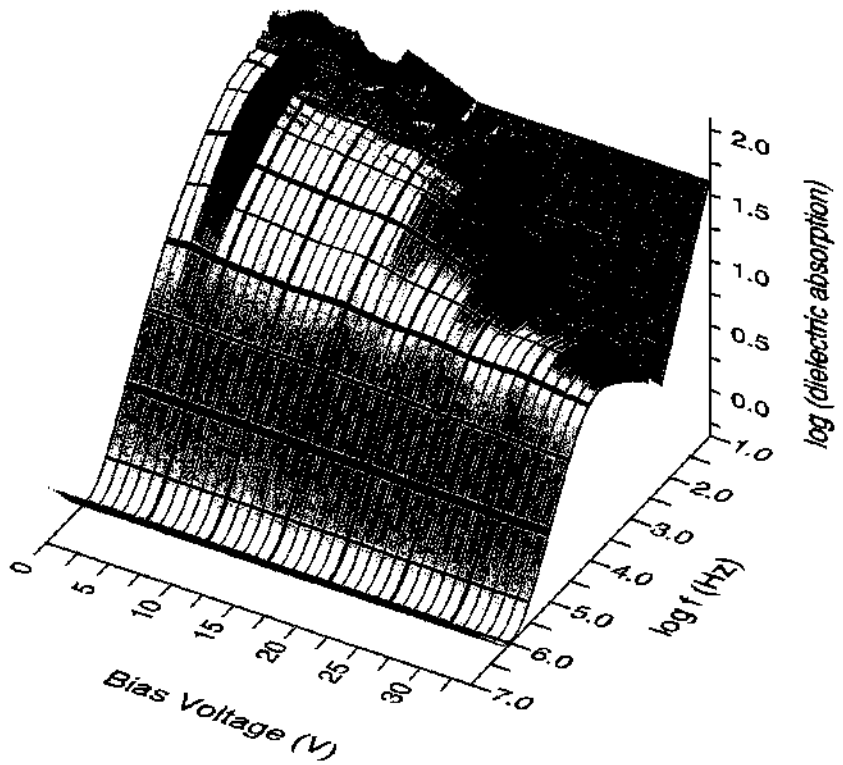

Figure 5.3(f) Dielectric spectra of the Goldstone mode at T = 56.0 °C in the smectic C* phase. Sample thickness = 36 μm

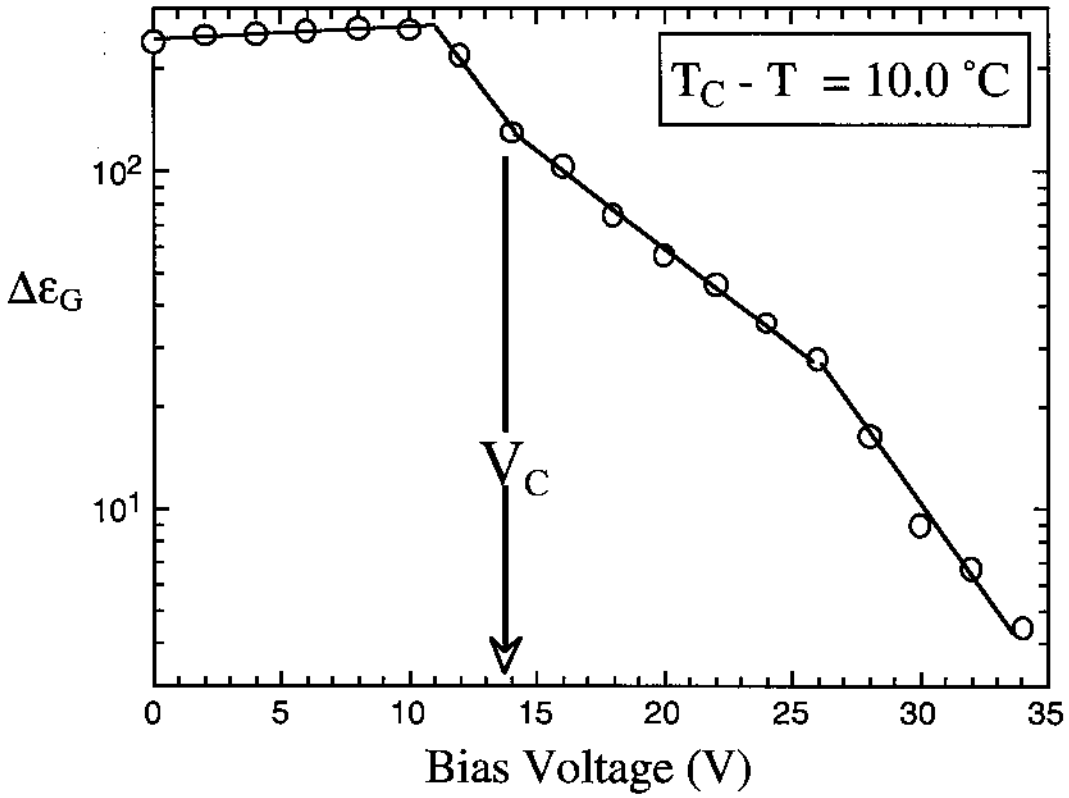

Figure 5.4 Bias voltage dependence of the Goldstone dielectric contribution at 10 °C below the SmA* to SmC* transition temperature.

surface needs much stronger bias field to unwind the helix where the surface conditions plays an important role. Thus, E_C for the bulk is much lower than E_C for the surface layer. In our measurements V_C (or E_C where $E_C = V_C/d$) has been assigned, as depicted in figure 5.4, to the voltage at which the bulk contribution has disappeared. The results in figure 5.5 has been modelled by a power law of the form

$$E_C = a(T_C - T)^{\gamma} \qquad (5.1)$$

where a, T_C and γ are fitting parameters equal to 4.36 [kV/(cmK)], 56.9 °C and 0.54, respectively. The value of exponent γ is very close to the mean field value (0.5).

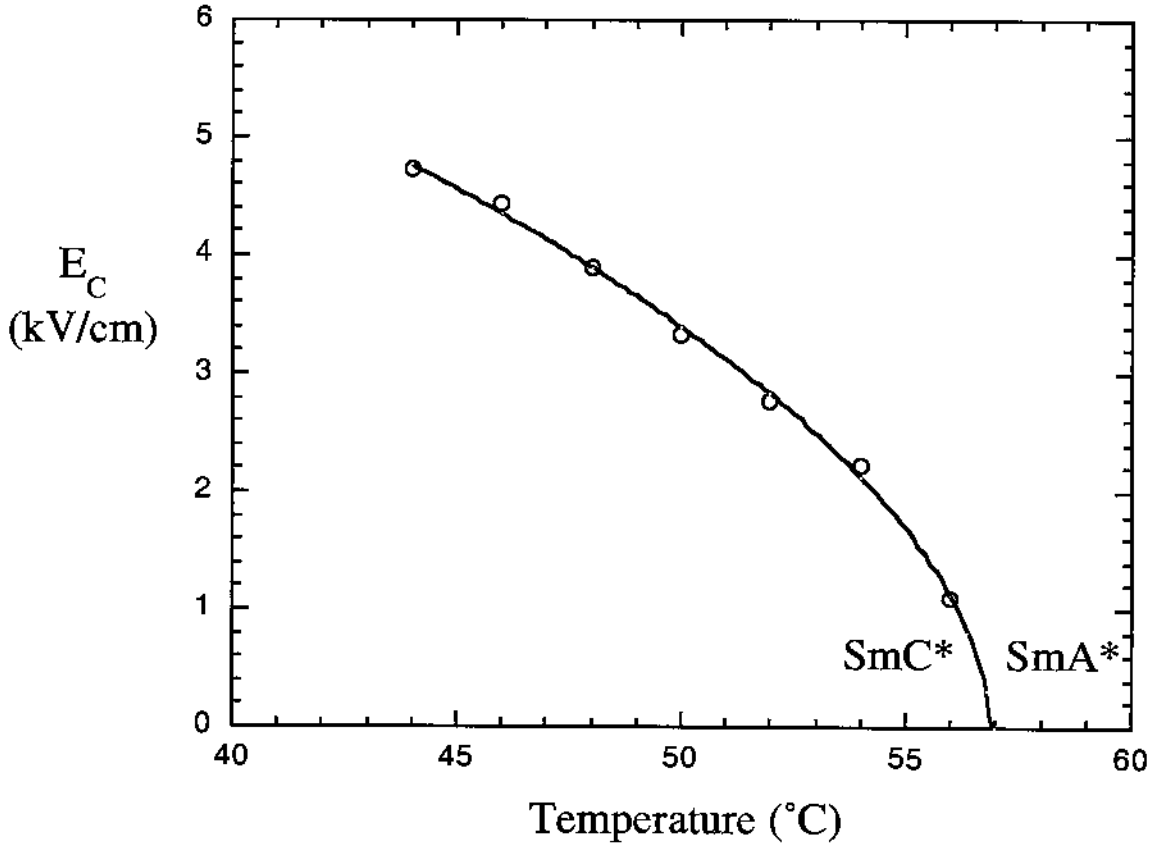

Figure 5.5 Temperature dependence of the critical field for helix unwinding in the smectic C* phase. Sample thickness = 36 μm. The solid line represents the power law fitting.

5.3 THE SOFT MODE DIELECTRIC BEHAVIOUR IN THE SMECTIC C* PHASE

Due to its huge contribution in the SmC* phase, the Goldstone mode overwhelms the relatively weak contribution of the soft mode. Thus, the only possible way to study the soft mode dielectric contribution is to apply a bias electric field in the SmC* phase which unwound the helical structure, thus, quenching the contribution of the Goldstone mode.

Figure 5.6 shows a dielectric spectrum at 1.41 °C below T_C in the presence of a bias voltage of 35 V_{DC}. By fitting this spectrum to two Cole-Cole function, the fitting parameters of the Goldstone (low frequency absorption) and the soft mode (high frequency absorption) are determined. The fitting results are depicted in figure 5.6. There are two overlapped absorption peaks at low and high frequencies attributed to the Goldstone mode and soft mode, respectively.

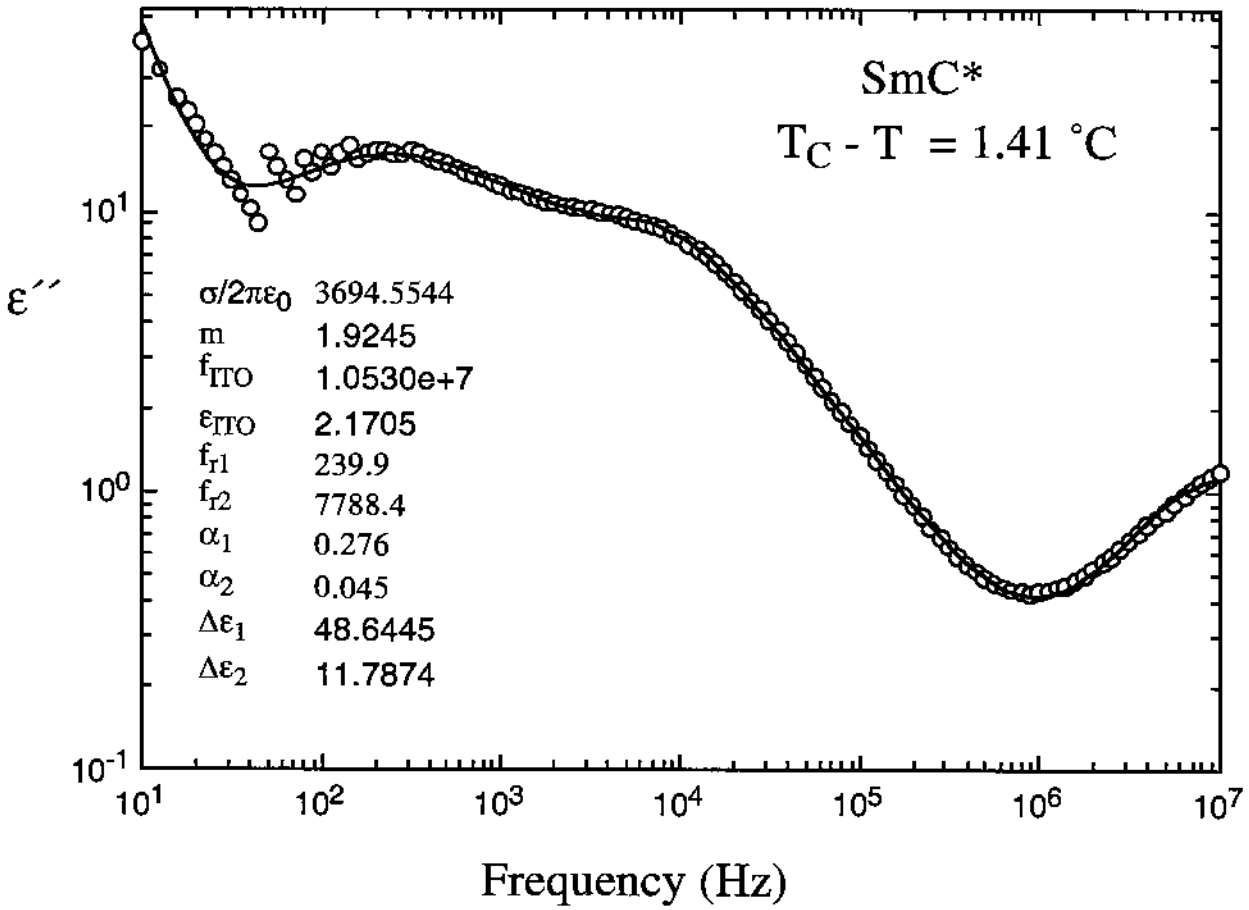

Figure 5.6(a) The dielectric spectrum in the SmC* phase in the presence of a bias voltage of 35 V_{DC}. The solid line is obtained from the fitting of two Cole-Cole equation with low and high frequency backgrounds. The fitting parameters are listed in the figure.

At lower temperature, see figure 5.6(b), the dielectric spectrum contains three peaks. The first two peaks (below 10^6 Hz) are the same

as those in figure 5.6(a), namely, the Goldstone mode and the soft mode. The third peak at high frequency is attributed to the molecular reorientation around the long axis. Note that the dielectric strength of the soft mode $\Delta\varepsilon_S$ (denoted $\Delta\varepsilon_2$ in figure 5.6(b)) is much less than $\Delta\varepsilon_S$ at higher temperature and its relaxation frequency is shifted from 7.7 kHz at T_C-T=1.4 °C to 74.5 kHz at T_C-T=5.9 °C. This is typical for a soft mode.

The temperature dependence of the dielectric dispersion and dielectric absorption in the presence of bias field is shown in the 3D representation in figures 5.7(a) and 5.7(b), respectively.

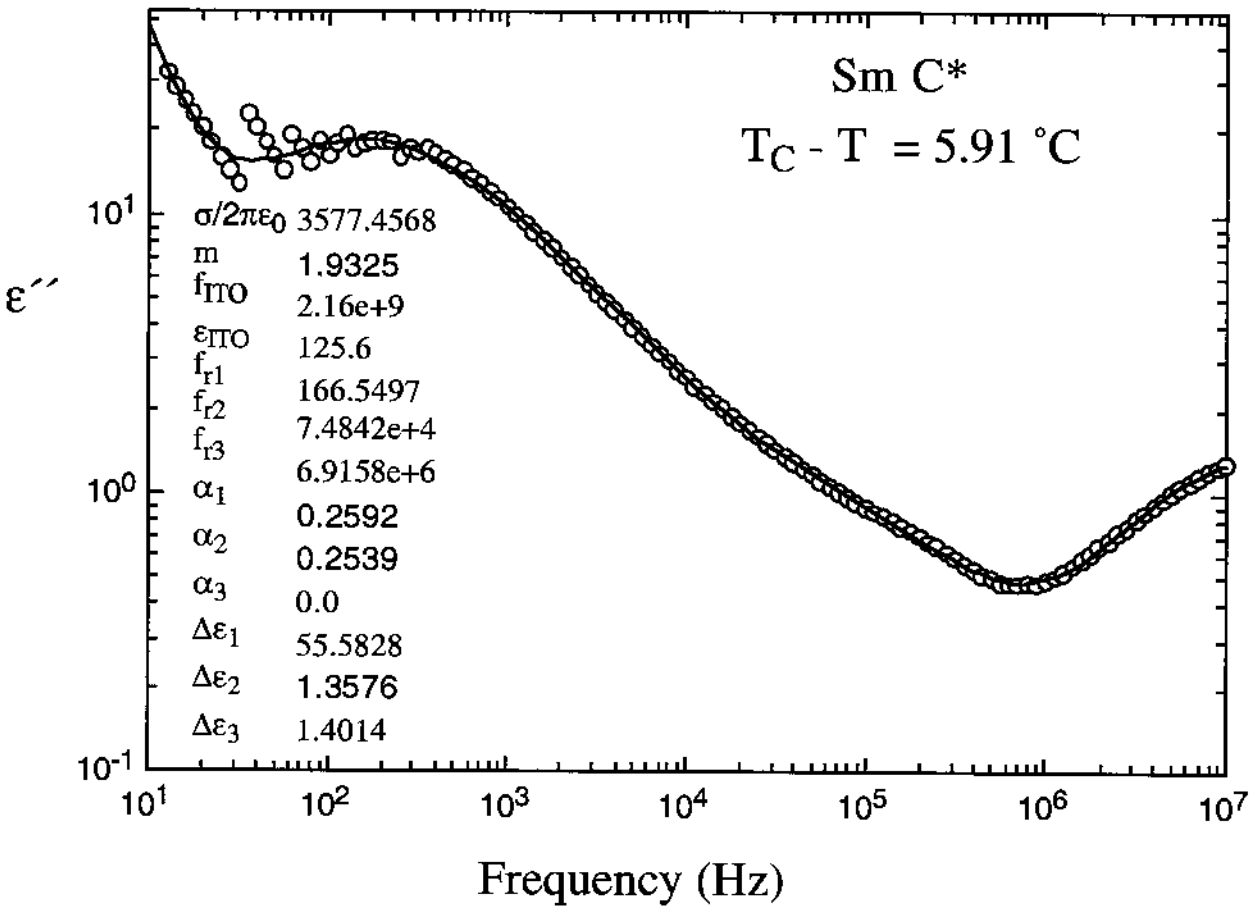

Figure 5.6(b) The dielectric spectrum in the SmC* phase in the presence of a bias voltage of 35 V_{DC}. The solid line is obtained from the fitting of two Cole-Cole equation with low and high frequency backgrounds. The fitting parameters are listed in the figure.

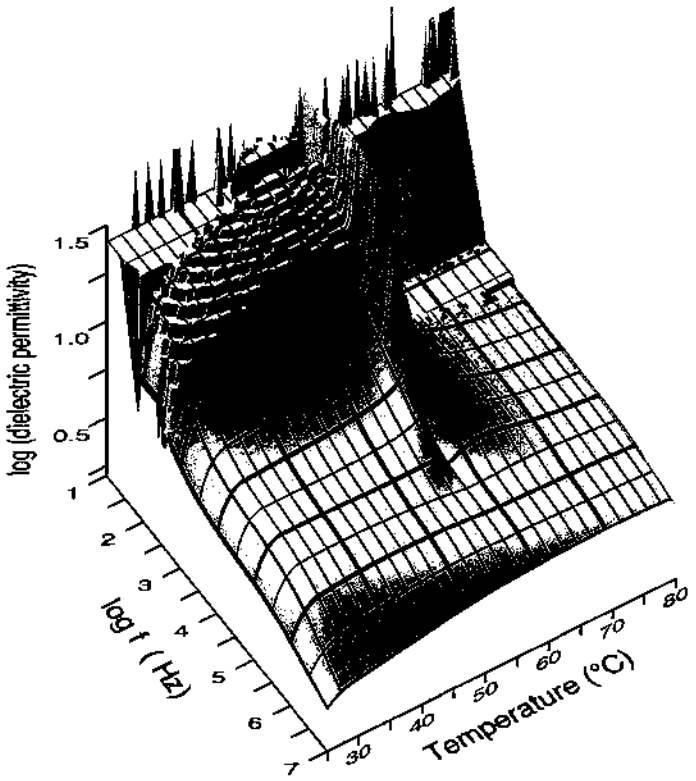

Figure 5.7(a) Dielectric dispersion in the smectic A* and C* phases in the presence of bias voltage of 35 V over 36 μm.

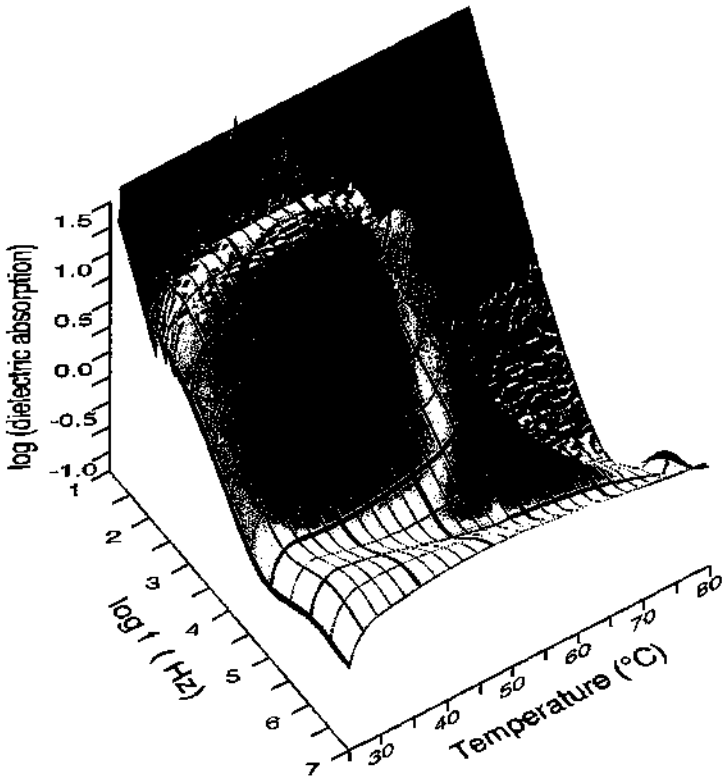

Figure 5,7(b) Dielectric absorption in the smectic A* and C* phases in the presence of bias voltage of 35 V over 36 μm.

The measurements have been carried out in the temperature interval from 70.0 °C to 30.0 °C. The dielectric absorption data have been fitted and the results are plotted in figure 5.8.

In the SmA* phase, the dielectric spectra (see figure 5.6(a)) has been fitted by *one* Cole-Cole function. The values of $\Delta\varepsilon_S$ and f_S have been determined and plotted in figure 5.8. In the SmC* phase, in a temperature interval of two degrees below T_C, the spectrum contains two peaks and the results have been analysed by *two* Cole-Cole function. At lower temperatures from 54.0 °C to 43.0 °C, the dielectric spectrum contains three peaks (see figure 5.6(b); the first two absorptions (below 1 MHz) are connected with the soft mode and the Goldstone mode, and a third peak (above 1 MHz) is related to the molecular rotation around the long axis. A *three* Cole-Cole function has been used to fit the dielectric spectra, and the dielectric parameters of the Goldstone mode ($\Delta\varepsilon_G$ and f_G), the soft mode ($\Delta\varepsilon_S$ and f_S) and the high frequency mode ($\Delta\varepsilon_h$ and f_h) have been determined as shown in figure 5.8. At temperatures below 43.0 °C, the soft mode dielectric contribution is very weak and shifted to higher frequencies and practically difficult to resolve. Therefore, the dielectric spectrum could only be fitted to *two* Cole-Cole function and the extracted values of $(\Delta\varepsilon_G, f_G)$ and $(\Delta\varepsilon_h, f_h)$ are depicted in figure 5.8. It may be noted that the values of $\Delta\varepsilon_G$ are less than $\Delta\varepsilon_S$. This is due to the bias field which partially unwound the helix and diminish the Goldstone mode dielectric contribution.

To further analyse the results in figure 5.8, the temperature dependence of $\Delta\varepsilon_S$ has been fitted by equation (4.3) which is a slight

modification of the Curie-Weiss law. In Curie-Weiss law γ =1, and the cut-off term kq_0^2/α = 0. In figure 5.9, the values of $1/\Delta\varepsilon_S$ are plotted against temperature. Both branches exhibit a slight deviation from linearity. From the fitting (of equation 4.3) in the SmA* phase, the exponent γ = 1.16 which is slightly deviated from one as predicted by mean field theory. In the SmC* phase, the behaviour follows a linear behaviour. The points at temperatures below 50.0 °C have not been included in the fitting because of its poor accuracy. It may be noted that according to the mean field approach, the ratio of the slopes of the soft in the SmC* and SmA*;

$$\frac{\left[\frac{d(1/\Delta\varepsilon_S)}{dt}\right]_{C^*}}{\left[\frac{d(1/\Delta\varepsilon_S)}{dt}\right]_{A^*}} = 2 \qquad (5.2)$$

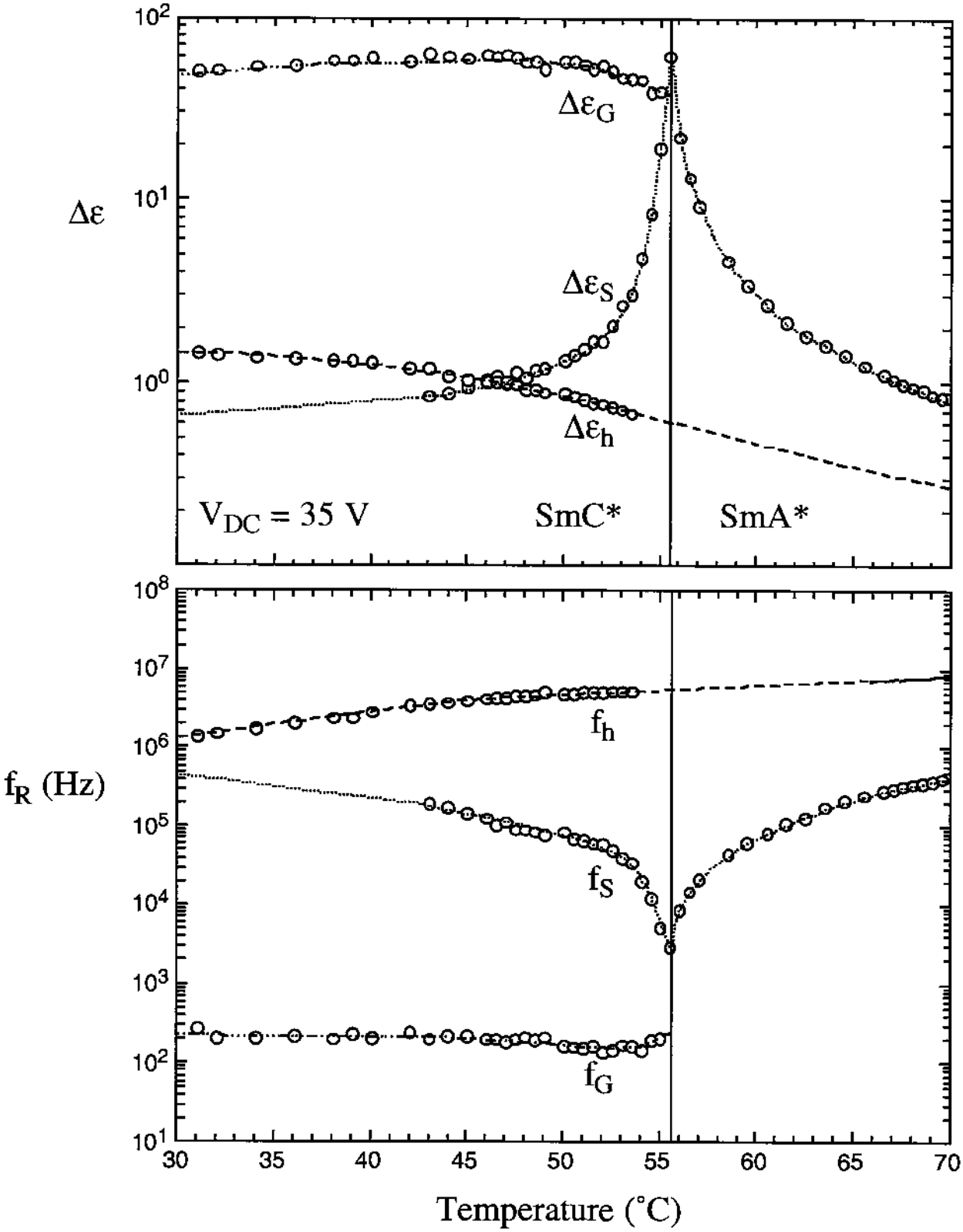

Figure 5.8 Temperature dependence of the dielectric strength and relaxation frequencies of the soft mode ($\Delta\varepsilon_S$, f_S), the Goldstone mode ($\Delta\varepsilon_G$, f_G) and the high frequency mode ($\Delta\varepsilon_h$, f_h) connected with the molecular reorientation around the long axis. The dotted lines are plotted for eyes guiding.

As can be estimated from figure 5.9 (if we ignore the non-linearity) this ratio is about 1.8, a value close to the mean field prediction.

Figure 5.9 shows the temperature dependence of the soft mode relaxation frequency in the SmA* and SmC* phases in the presence of a bias field of 35 V/36 μm. It may be noted that on approaching the SmA* to SmC* phase transition, f_S in the SmA* phase decreases to a finite value (see also figure 5.8-lower part) (cut-off value) about 2 kHz. The values of $f_S(T)$ have been fitted by equation (4.5). As discussed in details (in Chapter 4), the strong non-linear functional dependence of $f_S(T)$ is attributed to the soft mode temperature dependence of the rotational viscosity. In the Landau theory (mean field approach) the soft mode and Goldstone mode rotational viscosities are considered *temperature independent* parameters in the Landau-Khalatnikov equation of motion. This point will be discussed in details in the next chapter.

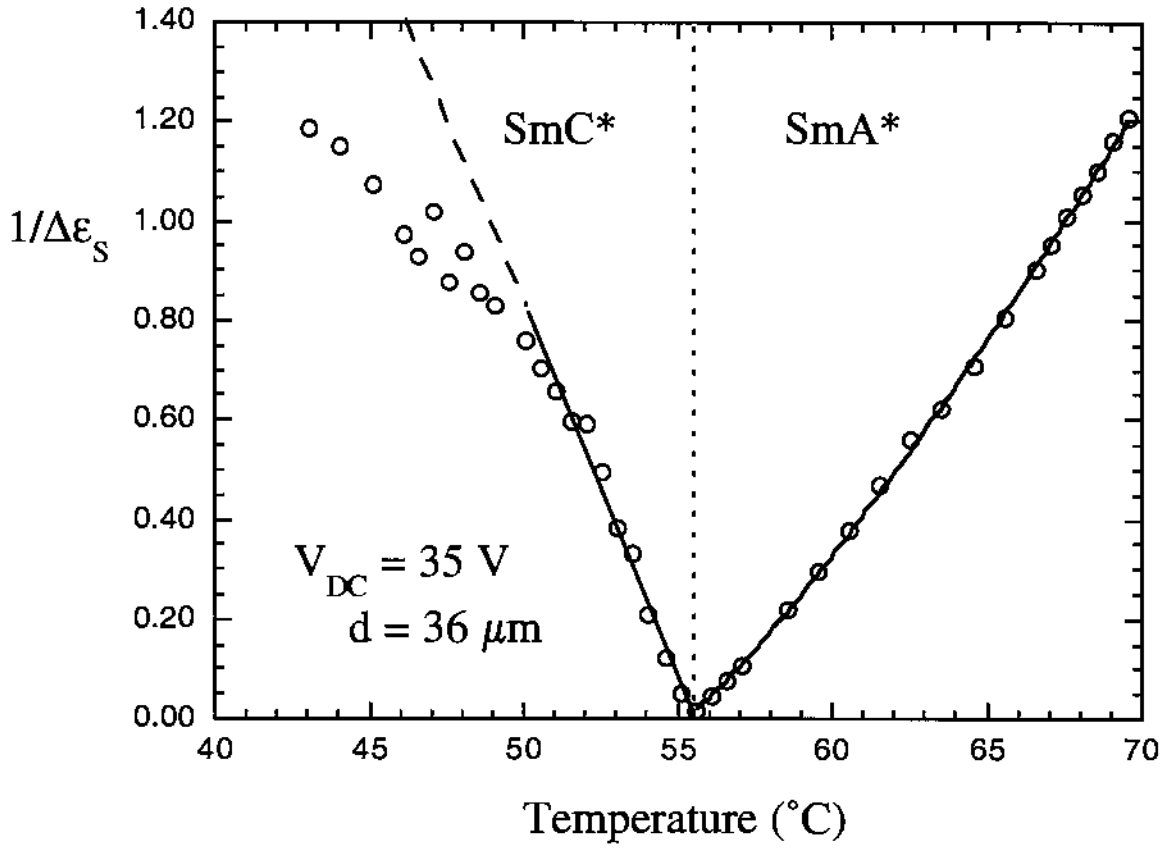

Figure 5.9 Temperature dependence of the inverse of soft mode dielectric contribution in the SmA* and SmC* phases. The measurements are carried out under bias field. The solid lines are obtained by fitting equation (??) to the experimental results.

Let us close up this chapter by comparing the two *collective* excitations in the SmA* and SmC* phases. Figure 5.11(a) shows the dielectric contribution of the soft mode in the SmA* and SmC* phases, and the Goldstone mode dielectric contribution in the SmC* phase. If we ignore the values of $\Delta\varepsilon_S$ at the vicinity of T_C, it is obvious that $\Delta\varepsilon_G$ is larger than $\Delta\varepsilon_S$ by two orders of magnitude. This makes the study of the soft mode in the SmC* phase non trivial.

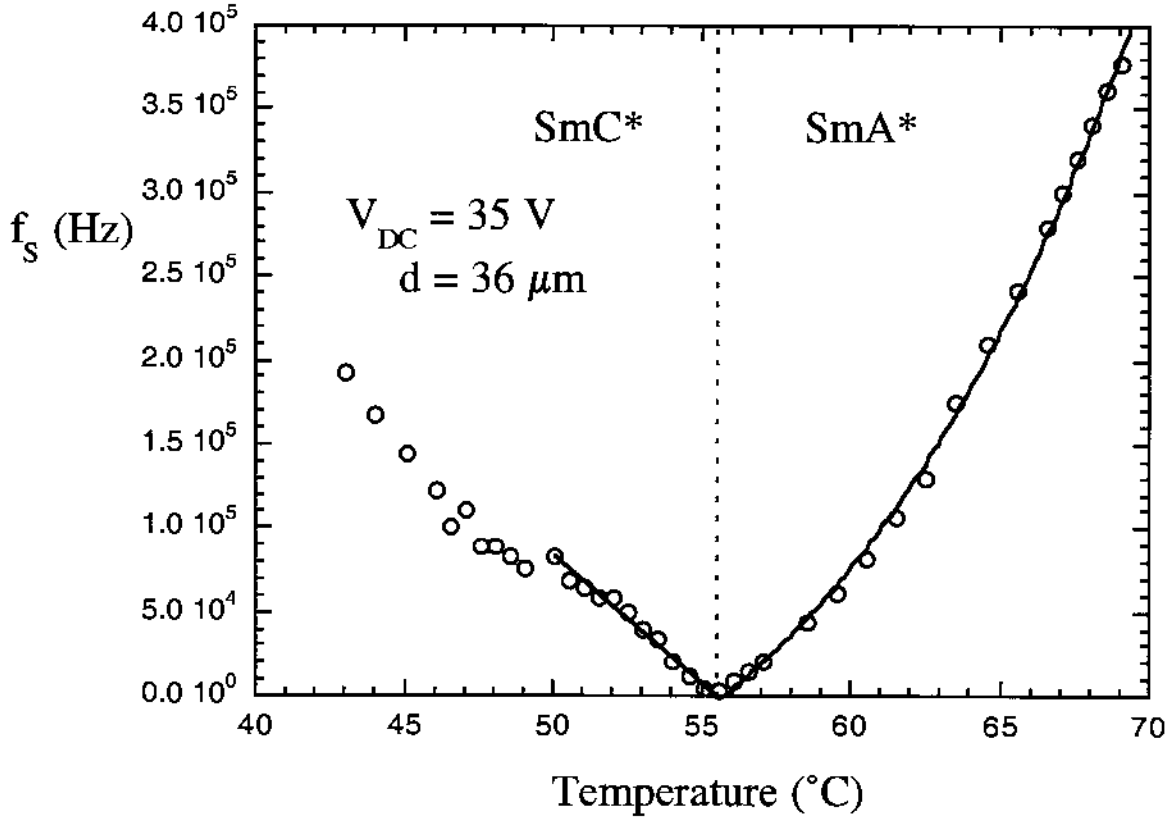

Figure 5.10 Temperature dependence of the soft mode relaxation frequency in the SmA* and SmC* phases. The measurements are carried out under bias field. The solid lines are obtained by fitting equation (??) to the experimental results.

As explained earlier, the only way to resolve the marginal contribution of the soft mode, compared with the Goldstone mode, is by applying a bias electric field. The large contribution of the Goldstone mode is connected with the fact that it does not cost energy to excite the Goldstone mode. However, the soft mode (tilt fluctuations) a way from T_C, it costs energy for the director to deviate from the layer normal because of the large elastic constant controlling the tilt fluctuations, except close to T_C, is very large. This large value of the soft mode elastic constant is the reason for the large values of

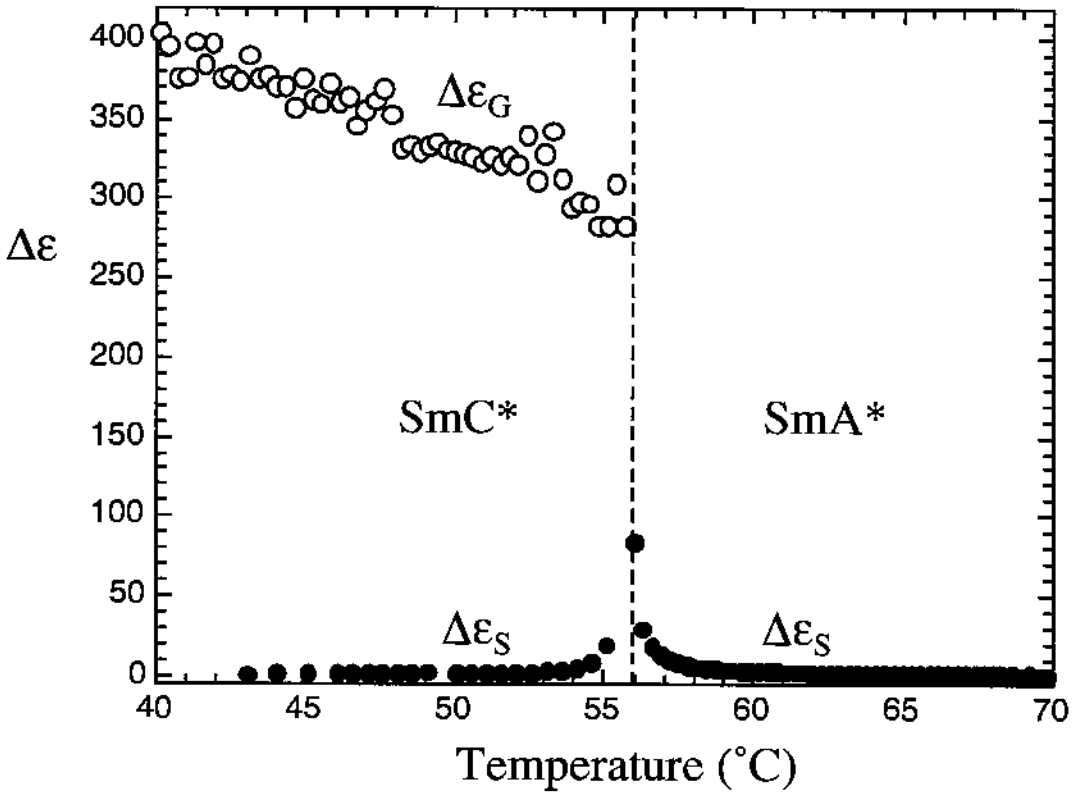

Figure 5.11(a) Temperature dependence of the soft mode and Goldstone mode dielectric contribution in the smectic A* and smectic C* phases, respectively.

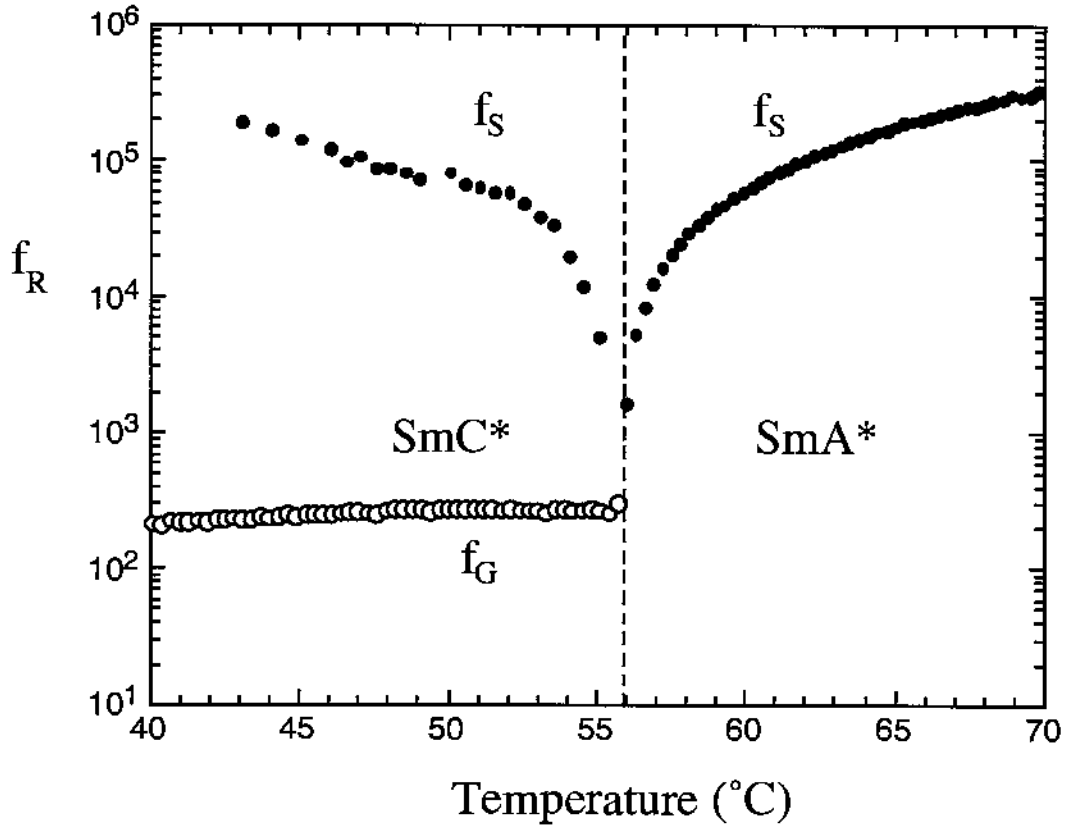

Figure 5.11(b) Temperature dependence of the soft mode and Goldstone mode relaxation frequency in the smectic A* and smectic C* phases, respectively.

the relaxation frequency of the soft mode in both SmA* and SmC* phases as illustrated in figure 5.11(b). Contrary to this behaviour, the Goldstone mode relaxation frequency is low and equals to 200 Hz. This value is less than the soft mode frequency by at least two orders of magnitude.

At the end of this section, it worth pointing out that the Landau theory predicts that both f_S and f_G should degenerate at T_C. However, as shown in figure 5.11(b) it is clear that there is a gap between f_S and f_G by almost one frequency decade. This will be discussed in the next chapter, this contradiction is related to the rotational viscosities of the soft mode and the Goldstone mode, especially, at the SmA* to SmC* transition.

CONCLUSIONS

In the present work, dielectric spectroscopy measurements have been carried out in the frequency range 10 Hz to 10 MHz in order to study the dipolar ordering and molecular motion in the isotropic, smectic A*, smectic C* and crystalline phases.

While in the isotropic phase, the molecular rotations around the short and long axis are active, these main molecular processes are completely frozen in the crystalline phase. There is no indication of any intramolecular rotation in the crystalline phase as seen from the absence of any finite difference between the permittivity and the square of the refractive index.

The molecular dynamics of the liquid crystalline phases exhibits molecular processes of collective and non-collective aspects. In the smectic A* and smectic C* phases, the dielectric spectrum contains two absorption peaks in the kHz and MHz regions which have been assigned to the non-collective motions. These are related to the molecular rotation around the *long axis* (*high frequency* peak) and the rotation around the *short axis* (*low frequency* peak). From the values of distribution parameter α of these two peaks, it is concluded that while the molecular rotation around the short axis (with $\alpha = 0$) the molecule is rotating like a

rigid body, the rotation around the long axis (with $\alpha \approx 0.3$) the molecule is rotating as a *flexible* body.

Besides these two main processes, the dielectric spectrum of the smectic A* and smectic C* phases contains two additional peaks considered as a "finger print" of the chiral phases. In both phases, when approaching the transition temperature T_C, from both sides, the elastic constant controlling the director tilt fluctuations gets *soften* (therefore this is called a *soft mode*) thus, the relaxation frequency f_S strongly falls down with $|T-T_C|$ accompanied with a divergence in its dielectric contribution. In the smectic C* phase, due to the helicoidal structure, the dielectric spectrum contains an absorption peak, large in its intensity and low in its frequency. This is the *Goldstone mode* of the smectic A* to C* transition excited to retain the spontaneously broken continuous symmetry when crossing the transition from the high symmetry smectic A* phase to the low symmetry smectic C* phase.

The bias field effect on both the dielectric contribution and relaxation frequencies of the soft mode and Goldstone mode has been studied in details. It is found that, in the smectic A* phase, the bias field has a remarkable effect on the soft mode *only* over a limited temperature interval (of about one degree) close T_C. In the smectic C* phase, due to the ferroelectric coupling, the bias field has strong influence on the dielectric response and relaxation frequency of the Goldstone mode. At relatively weak field (of about 3 kV/cm) the bias field unwounds the

helical structure, thus removing the dominating Goldstone mode contribution to the total dielectric contribution. Thus, permitting the study of the soft mode over a wide temperature interval. It may be noted that the observed "wavy like" behaviour of dielectric contribution with bias field in the smectic C* phase can not be explained clearly at the present stage, therefore, further investigations are needed to understand the reason of this effect.

Finally, the rotation viscosity coefficients of the soft mode γ_θ and Goldstone mode γ_φ have been determine. While the temperature dependence of γ_θ is modelled by a modified Arrhenius law, the temperature dependence of γ_φ follows a power law.

Thus, it is concluded that the dielectric spectroscopy is a powerful technique not only to investigate the fundamental properties of these phases, however, it provides important material parameters that plays an important role in the electro-optic device application of this fascinating state of matter that has changed our way of in the era of information technology.

REFERENCES

[1] G. W. Gray and P. J. Winsor, Liquid Crystals and Plastic Crystals, Ellis Horwood, Chichester, 1974.

[2] S, Chandrasekhar, Liquid Crystals, Cambridge University (1992).

[3] P. G. de Gennes and J. Prost, The Physics of Liquid Crystals, Clarendon Press, Oxford (1993).

[4] J. W. Goodby and G. Gray, Handbook of Liquid Crystals, Vol. 1, (Eds., D. Demus, J. W. Goodby. G. Gray, H. W. Sprees, V. Vill), Wiley-VCH, pp. 17-23 (1998).

[5] I. Hargittai and M. Margittai, Symmetry Through the Eyes of a Chemist, VHC, New York (1989).

[6] J. W. Goodby and G. Gray, Handbook of Liquid Crystals, Vol. 2B, (Eds., D. Demus, J. W. Goodby. G. Gray, H. W. Spress, V. Vill), Wiley-VCH, pp. 17-23 (1998).

[7] S. Garoff, R. B. Meyer, Phys. Rev. Lett., **38**, 848-851 (1977).

[8] R. B. Meyer, L. Liebert, L. Strzlecki, and P. J. Keller, J. Phys. Lett., Paris, **36**, L69 (1975).

[9] N. A. Clark and S. T. Lagerwall, Appl. Phys. Lett., **36**, 11, pp. 899-90 (1980).

[10] G. Andersson, I. Dahl, P. Keller, W. Kuczynski, S. T. Lagerwall and B. Stebler, Appl. Phys. Lett., , **51**, 640 (1987).

[11] C. J. F. Bötscher, P. Bordewijk, Theory of dielectric polarisation, Volume 1, Elsevier Scientific Publishing 1973.

[12] O. F. Mossotti, Bibl. Univ. Modena, **6**, (1847) 193 ; Mem. di matem. e fisica Modena, 2411 (1850) 49.

[13] R. Clausius, Die mechanische Wärmtheorie, vol II, Braunschweig (1879) 62.

[14] L. Onsager, Journal of the American Chemical Society, **58**, 1486 (1936).

[15] P. Debye, Polar Molecules, Chemical Catalogue Co., New York, NY(1929), see also P. Debye, Polar Molecules, Dower Publications Inc, New York, NY(1945).

[16] W. Maier and G. Meier, Z. Naturforsch., **16a**, 262 (1961).

[17] K.S. Cole and R.H. Cole, J. Chem. Phys., **9**(1941) 341.

[18] R. B. Meyer, Mol. Cryst. Liq. Cryst., **40**, 33 (1977).

[19] T. Carlsson, B. Zeks, C. Filipic and A. Levstik, Phys. Rev, A, **42**, 877 (1990).

[20] F. Gouda, K. Skarp and S. T. Lagerwall, Ferroelectrics, 113, 165, (1991).

[21] C. J. F. Bötscher, P. Bordewijk, Theory of dielectric polarisation, Volume 2, Elselvier Scientific Publishing 1973.

[22] M. Davies, R. Moutran, A. H. Price, M. S. Beevers, G. Williams, J. Chem. Soc., Faraday Trans. II, **72**, 1447 (1976).

[23] H. Kresse, Fortsch. der Physik, **30**, 507 (1982).

[24] W. H. de Jeu, Physical Properties of Liquid Crystalline Materials, Gordon and Breach, New York, (1980).

[25] M. F. Bone, A. H. Price, M. G. Clark and D. G. McDonnell, Liquid Crystals and Ordered Fluids, (Eds., A. C. Griffin and J. F. Johnson) Vol. 4, Plenum Press, New York, pp.799 (1984).

[26] G. Meier, Dielectric and Related Molecular Processes, (Eds., M. Davies), Spec. Period. Reports, Vol. 2, The Chem. Sco. (London, p. 183 (1975).

[27] L. Bata and A. Buka, Molec. Cryst. and Liq. Cryst., **63**, 307 (1981).

[28] C. Druon and J. M. Wacrenier, Molec. Cryst. and Liq. Cryst., **98**, 201 (1983).

[29] A. Buka and A. H. Price, Molec. Cryst. and Liq. Cryst., **116**, 187 (1985).

[30] See Data Sheets and Information Booklets on Liquid Crystal Materials from BDH (England), E. Merck (Germany) and Hoffmann La Roche (Switzerland).

[31] A. Levstik, B. Zeks, C. Filipic, R. Blinc and I. Levstik, Ferroelectrics, **58**, 33 (1984).

[32] Ch. Bahr and G. Heppke, Phys. Rev. A, **44**, 3669 (1991).

[33] Ch. Bahr and G. Heppke, and N. K. Sharma, Ferroelectrics, **76**, 151 (1987).

[34] A. M. Birdar, S. Wrobel and W. Hasse, Phys. Rev. A, **39**, 2693 (1989).

[35] M. Glogarova and J. Pavel, Liq. Cryst., **6**, 325 (1989).

[36] F. Gouda, G. Andersson, S. T. Lagerwall, K. Skarp, B. Stebler, T. Carlsson, B. Zeks, C. Filipic and A. Levstik, Liq. Cryst., **6**, 219 (1989).

[37] Yu. P. Kalmykov, J. K. Vij, H. Xu, A. Rappaport and M. D. Wand, Phys. Rev. E, **50**, 2109 (1994).

[38] K. Hiraoka, Y. Sugano, K. Monzen, Y. Uematsu, M. Tokita, J. Watanabe and T. Furukawa, Mol. Cryst. Liq. Cryst., **299**, 229 (1997).

[39] S. S. Roy, T. P. Majuder and S. K. Roy, Mol. Cryst. Liq. Cryst., **302**, 13 (1997).

[40] S. Havriliak and J. K. Vij and M. Ni, Liq. Cryst., **26**, 465 (1999).

[41] S. K. Kundu, E. Okabe, W. Hasse and B. K. Chaudhuri, Phys. Rev. E, 64, 51708 (2001).

[42] G. Andersson, I. Dahl, W. Kuczynski, S. T. Lagerwall, K. Skarp and B. Stebler, Ferroelectrics, **84**, 285 (1988).

[43] K. Skarp and G. Andersson, Ferroelectrics Lett. **6**, 67 (1986).

[44] W. Kuczynski, Ber. Bunsenges. Phys. Chem. 85, 234 (1981).

[45] C. Escher T. Geelhaar and E. Bohm, Liq. Cryst., **3**, 469 (1988).

[46] S. Kimura, S. Nishiyma, Y. Ouchi, H. Takezoe and A. Fukda, Jpn. J. Appl. Phys. **26**, L255 (1987).

[47] I. Dahl, S. T. Lagerwall and K. Skarp, Phys. Rev. A. **36**, 4380 (1987).

[48] F. Gouda, K. Skarp, G. Andersson, H. Kresse, and S. T. Lagerwall, Jpn. J. Appl. Phys. **28**, 1887 (1989).

[49] H. Sun, H. Orihara and Y. Ishibashi, J. Phus. Soc. Jpn, **62**, 2066 (1993).

[50] S. S. Roy, S. Kundu, N. Ghosh, T.P. Majumder, S. K. Roy, Mol. Cryst. Liq. Cryst., 328, 161 (1999). J. M. Gonnet, J. Guillet, I.

Sirakov, R. Fulchiron and G. Seytre, Poly. Eng. Sci., **42(6)**, 1159 (2002).

[51] T. P. Majumdar, S. S. Roy, S. K. Roy and M. Mitra, , Mol. Cryst. Liq. Cryst., **265**, 577 (1995).